

# Experience on the preparation of HPMC viscous fluid for physical modeling in the geocentrifuge

T.O. Quinten

Additional thesis committee

Dr. Sc. A. Askarinejad  
Prof. dr. K. Gavin

TU Delft  
TU Delft

The logo for TU Delft, featuring a stylized white flame or leaf icon above the text "TU Delft" in a bold, white, sans-serif font.

**TU Delft**

# Contents

<b>1</b>	<b>Abstract</b>	<b>1</b>
<b>2</b>	<b>Introduction</b>	<b>3</b>
2.1	Scaling of diffusive processes in the centrifuge . . . . .	4
2.2	Scaling of dynamic processes in the centrifuge . . . . .	4
2.3	Diffusive-dynamic time discrepancy . . . . .	5
<b>3</b>	<b>(Hydroxypropyl) Methylcellulose</b>	<b>7</b>
3.1	Chemistry. . . . .	7
3.2	Properties. . . . .	7
<b>4</b>	<b>(HP)MC type selection</b>	<b>9</b>
<b>5</b>	<b>Problem statement</b>	<b>13</b>
5.1	(HP)MC fluid preparation . . . . .	13
5.1.1	Hot/cold technique. . . . .	13
5.1.2	Static dispersion technique . . . . .	14
5.2	Shear rate dependency of viscosity . . . . .	14
5.3	Temperature dependency of viscosity . . . . .	15
5.4	Effect of aging on viscosity. . . . .	15
<b>6</b>	<b>Research methodology</b>	<b>17</b>
6.1	Fluid preparation. . . . .	17
6.1.1	Recipe drafting . . . . .	18
6.1.2	Solution preparation . . . . .	19
6.2	Rheological measurements . . . . .	21
<b>7</b>	<b>Results</b>	<b>23</b>
7.1	Global trend identification . . . . .	23
7.1.1	Detailed analysis . . . . .	26
7.1.2	Data fitting . . . . .	30
<b>8</b>	<b>Conclusions</b>	<b>35</b>
8.1	Conclusions with regard to the preparation process. . . . .	35
8.2	Conclusions regarding the rheological results and generic fit. . . . .	36
<b>9</b>	<b>Recommendations</b>	<b>39</b>
	<b>Bibliography</b>	<b>41</b>
<b>10</b>	<b>Appendix</b>	<b>43</b>



# Abstract

Investigating soil response before, during and following large scale, dynamic events like slope failure or impact hammering of monopiles, is challenging. Full scale research into these processes is often conducted in the field, as laboratories don't offer the required space to conduct these experiments. Apart from the monumental costs related to full scale experiments, it is often impossible or impractical to define or portray all boundary conditions, which increases uncertainty. As an alternative to full scale field tests, centrifuge tests on a scaled model are often carried out. When conducting research in the centrifuge, the decrease in geometry is compensated by through the acceleration of the model to  $N$  times gravity  $g$ . In this way, full scale stress conditions are imposed on the sample. Consequently, the model offers an accurate representation of full scale soil behavior. However, artificial 'gravity' enhancement impacts a broad range of physical quantities. Scaling laws dictate how physical quantities are affected by conditions in the centrifuge and require careful observation. Yet, the use of scaling laws introduces a discrepancy between the timescale related to dynamic events and diffusive processes. The latter is of particular importance to build-up and dissipation of deviatoric pore fluid pressures.

Decreasing the permeability of the soil is generally the best option to eliminate the aforementioned discrepancy. Consequently, instead of water, viscous fluid is used for the centrifuge tests, where the viscosity is increased  $N$  times with respect to water. Over the years, various fluids have been developed and utilized in centrifuge experiments. A widely used fluid, consists of aqueous solutions (Hydroxypropyl) Methylcellulose or (HP)MC in short. HPMC molecules form polymeric chains which increase viscosity while largely maintaining the density of the solvent, water. These favorable properties make it a highly sought-after substitute for water in centrifuge experiments. Experience with the fabrication and use of (HP)MC solutions is limited at the centrifuge facility of Delft University of Technology. As part of an initiative to develop in-house knowledge relating to the aforementioned points for physical modeling purposes, this research presents a robust fabrication methodology and maps the viscous properties of HPMC solutions, fabricated using Methocel<sup>®</sup> F4M, at various concentrations.

Results indicate that advocated preparation methodology enables the fabrication of viscous fluids in the range of 10 to 100  $mPa \cdot s$  of consistent quality. However, overall, the viscosities of the fluids created along the lines of the presented methodology are consistently more viscous than anticipated. Several hypotheses aimed explaining the discrepancy are drafted. However, the nature of the underlying cause remains a topic of debate. Furthermore, it is observed that the HPMC fluids express a substantial degree of shear thinning at high shear rates. The relative decrease in viscosity increases with concentration, causing the viscosities of fluids of different concentration to gradually converge at high shear rates. The latter stresses the importance of quantifying expected shear rates beforehand to prevent behavioral inconsistencies between model and prototype. However, under

some circumstances, it is doubtful whether the use of viscous fluids created from Methocel<sup>®</sup> F4M is suitable to study prototype behavior.

In an attempt to facilitate drafting of appropriate recipes for the fabrication of viscous fluid, a general expression is presented to calculate the required concentration, provided the desired viscosity and anticipated shear rate. This generic expression provides adequately describes the experimental data, but requires further tuning in order to fully fulfill its intended purpose. Nonetheless, it provides a valuable indication of the required concentration to obtain a fluid with sought-after properties; thereby shortening the time spent on drafting the ideal fluid recipe.

# 2

## Introduction

During both installation offshore structures, pore water pressures in the direct vicinity are altered as a result of soil-structure interactions. As a direct result, the effective stress regime in the soil body surrounding the structure is affected, thus altering soil behavior. These pore fluid pressure (PFP) fluctuations are of interest in the light of optimizing the installation time of foundations (monopiles) for offshore wind farms, while using impact hammering techniques. Recent research gives reason to believe that (under the right conditions) impact hammering of monopiles can result in the built up of excess PFP, resulting in a temporal decrease of effective stress regime and thus lowering soil resistance during installation [21].

Over the past years, offshore wind turbines and their respective foundations have grown significantly. Simultaneously, the share of the total energy requirement accounted for by (offshore) wind energy has increased. Prognosis indicate that both trends will continue when extrapolating into the foreseeable future [18]. Currently, the dimensions of monopiles lie in the order of 30 *m* (length), 6-8 *m* (diameter) and  $\approx 0.1$  *m* wall thickness [5]. Given the scale of this type of structure, it is imaginable why full scale tests involving monopile installation and simultaneous monitoring of the PFP are nearly non-existent. Additionally, for most large scale processes or endeavors it is difficult to conduct experiments in a controlled lab environment. The latter makes that field experiments are often more cumbersome as not all boundary conditions can be controlled and quantified. For these cases, it often more (economically) sensible employ a different research methodology. Moving back to the topic of dynamic monopile installation, and simultaneous monitoring of PFP in the adjacent soil body; centrifuge experiments are a prime contestant as a substitute for full scale tests. For centrifuge experiments, the full scale geometry (prototype scale) is reduced to a manageable laboratory scale (model scale). This model is subsequently used of testing under high centrifugal accelerations, which artificially enhance the stresses in the soil body. The required centrifugal acceleration is computes such that soil stress regime in the model accurately represents the prototype. The latter is of vital importance to the representativity of the results as soil behavior is governed by a (non-linear) stress-strain relationship. This notion also highlights the prime advantage of centrifuge experiments, namely: the ability to conduct true-to-nature geotechnical research in a controlled environment while using a scale model.

Generally, the amplification of gravity in the centrifuge is denoted as  $N$ . However, the artificial enhancement of gravity influences a range of physical quantities much wider than solely linear dimension. The precise way in which different physical quantities are influenced has been extensively researched, in example by Garnier *et al.* ([13]). For the inteded type of research, the influence on gravitational enhancement on: (I) the processes underlying the generation of deviatoric PFPs (either tensile or compressive pressures); (II) the subsequent reinstatement of a hydrostatic pressure distribution. The nature of the two aforementioned processes is distinctly different as the generation of

deviatoric PFP is classified as a dynamic process; whereas the dissipation of generated pressures is driven by a diffusion. At 1g conditions, the timescales on which the two aforementioned processes play out coincide. However, in the centrifuge, where tests are executed at  $Ng$  instead of 1g, dynamic and diffusive events take place at two evidently different timescales. This discrepancy is demonstrated by means of a derivation. In order to do so properly, a distinction between model and prototype scales and associated parameters is made. To limit the number of characters in the subsequent expressions, variables relating to the model and prototype, are respectively indicated by subscripts  $m$  and  $p$ . Additionally, for clarity, the scaling of diffusive processes (dissipation of deviatoric PFPs) and dynamic processes (generation of deviatoric PFP) is discussed separately, respectively in 2.1 and 2.2.

## 2.1. Scaling of diffusive processes in the centrifuge

The decay of (excess) PFP is coupled to soil deformation through the consolidation process. Under constant total stress conditions, this process describes the increment of volumetric strain related to the simultaneous dissipation of excess PFP and concentration of load borne by the soil structure. The degree of consolidation  $T_v$ , describing the extend to which the consolidation process is complete, is a function of time ( $t$ ), drainage length ( $D$ ) and the consolidation coefficient ( $c_v$ ):

$$T_v = \frac{c_v \cdot t}{D^2} \quad (2.1)$$

If it is required for the degree of consolidation to be the same in both model and prototype, the following should hold:

$$T_{v,m} = T_{v,p} \implies \frac{c_{v,m} \cdot t_m}{D_m^2} = \frac{c_{v,p} \cdot t_p}{D_p^2} \quad (2.2)$$

If the same soil is used in the model as is present in the prototype, it can be reasonably stated that  $c_{v,m} = c_{v,p}$ . Now, provided the scaling law for linear dimension:

$$d_m = \frac{1}{N} \cdot d_p \quad (2.3)$$

Where  $d_m$  and  $d_p$  represent a linear dimension at model and prototype scale respectively. Combining Equation 2.2 and 2.3 yields:

$$\frac{c_v \cdot t_m}{1/N^2 \cdot D_p^2} = \frac{c_v \cdot t_p}{D_p^2} \implies t_m = \frac{1}{N^2} \cdot t_p \quad (2.4)$$

## 2.2. Scaling of dynamic processes in the centrifuge

The scaling law for dynamic time is obtained by considering the centrifuge scaling law for acceleration:

$$a_m = N \cdot a_p \quad (2.5)$$

Where,  $a_m$  and  $a_p$  represent acceleration levels in model and prototype respectively. In agreement with the recommendation of the SI-standard with respect to the denotation of dimensions, acceleration can be expressed as  $L/T^2$ . Combining the latter notion with Equation 2.5, yields:

$$\frac{L_m}{T_m^2} = N \cdot \frac{L_p}{T_p^2} \quad (2.6)$$

Lastly, by incorporating the scaling law for linear dimension (Equation 2.3) into Equation 2.6, it is obtained:

$$\frac{1/N \cdot L_p}{T_m^2} = N \cdot \frac{L_p}{T_p^2} \implies T_m = \frac{1}{N} \cdot T_p \quad (2.7)$$

### 2.3. Diffusive-dynamic time discrepancy

Form the derivations discussed in 2.1 and 2.2, it can be inferred that by using the centrifuge, a discrepancy between dynamic and seepage time is introduced as (at model scale) the former physical quantity is scaled by  $1/N^2$ , against  $1/N$  for the latter respectively. This implies that the dissipation of PFP and associated consolidation happen  $N$  times faster in the model than in the prototype. To overcome the aforementioned issue, it is possible to increase the coefficient of consolidation  $c_v$  by  $N$  times. Formally,  $c_v$  is defined as follows:

$$c_v = \frac{k}{m_v \cdot \rho_f \cdot g} \quad (2.8)$$

Where  $m_v$ ,  $k$  and  $\rho_f$  respectively denote soil compressibility, soil permeability and fluid density. In term of practicality, scaling down  $k$  by a factor of  $N$  is most manageable. Soil permeability is calculated in accordance with the following expression:

$$k = \frac{\kappa_s \cdot \rho_f \cdot g}{\mu_f} = \frac{\kappa_s \cdot g}{\nu_f} \quad (2.9)$$

Where  $\kappa_s$ ,  $\mu_f$  and  $\nu_f$  respectively express intrinsic soil permeability, dynamic viscosity and kinematic viscosity. Substituting Equation 2.9 into Equation 2.8, it is found:

$$c_v = \frac{\kappa_s}{m_v \cdot \rho_f \cdot \nu_f} \quad (2.10)$$

Form Equation 2.10 it follows that two ways exist to ensure proper coupling between dynamic time and seepage time (by scaling  $c_v$  by factor  $N$ ) [15]:

1. Decreasing the intrinsic impermeability  $k_s$  of the medium  $N$  times, in example by using smaller grain sizes. See in example Kutter & Bruce (1992) ([14]);
2. Increasing the dynamic viscosity  $\nu_f$  in the saturated medium  $N$  times while maintaining a similar the fluid density  $\rho_f$ . An approach analogous to that advocated by in example Askarinejad *et al.* (2013) ([4]).

The process of decreasing the  $k_s$  can be tedious as changing the particle size, affects the density, stiffness and strength, thus altering the soil's constitutive behavior. Hence, it is generally preferred to use viscous fluid to decrease soil permeability. However, it should be noted that any increase of  $\rho_{f,m}$  with respect to  $\rho_{f,p}$  is detrimental based on Equation 2.10. Hence, ideally, the viscous substitute for water in the centrifuge experiments should retain a density similar to the density of water. The latter also ensures that there are no noteworthy alterations to the effective stress profile in the sample, as the density of the pore fluid affects the buoyant force exerted on the soil matrix. All aforementioned criteria with respect to characteristics of the ideal viscous fluid are summarized by Equation 2.11.

$$\mu_m = N \cdot \mu_p \leftrightarrow \begin{cases} \nu_{f,m} = N \cdot \nu_{f,p} \\ \rho_{f,m} = \rho_{f,p} \end{cases} \quad (2.11)$$

Literature provides several candidates when it comes down to suitable water substitutes for centrifuge testing. Within the Geo-Engineering research group at Delft University of Technology, experience with the use of two different fluids has recently been gathered, specifically: (I) Van Zeben (2017) ([21]) describes the use of a water based viscous fluid developed and fabricated by Deltares with a dynamic viscosity of  $52.3 \text{ mPa}\cdot\text{s}$  (at  $20^\circ\text{C}$ ) for pile driving experiments at 50g; (II) Askarinejad *et al.* (2013) ([4]) discusses the use of a 79% v/v glycerin-water solution with a dynamic viscosity of  $50.231 \text{ mPa}\cdot\text{s}$  to asses the stability of slopes subjected to heavy rainfall. However, both alternatives were marked unsuitable. Despite of the satisfactory results obtained by Van Zeben (2017), the

outsourced water based viscous fluid is costly and subject long leadtime. Contrastingly, the 79% v/v glycerine-water solution was disqualified based on the observations of Askarinejad *et al.* (2017) with regard to disturbances in the distribution (and generation) of (excess) PFP. The latter manifested itself through an alteration of the mechanical response of the slope. The observed effect was chiefly attributed to the elevated density of the solution ( $1205.3 \text{ kg/m}^3$ ) with respect to water ( $1000 \text{ kg/m}^3$ ). Consequently, the search shifted towards the use of aqueous solutions of Methylcellulose (MC) or Hydroxypropyl Methylcellulose (HPMC).

The first research into the suitability of MC or HPMC as a binding agent for water to obtain viscous solutions for centrifuge experiments dates back about two decades. Zeng *et al.* (1998) ([22], demonstrated that HPMC fluids have no noticeable influence on soil behavior during centrifuge testing. Moreover, (HP)MC solutions (in contrast to many existing alternatives, like glycerin-water mixtures), have almost the same density as water. Consequently, HPMC fluids have been employed in centrifuge research throughout the past years successfully. In example by Dewoolkar *et al* (1999) [10] and Coelho *et al* (2006) [8], who both investigated the response of saturated sand deposits to earthquakes while employing HPMC viscous fluids in their models. Despite the rather widespread use of HP(MC) solutions for centrifuge experiments, experience with fabrication and use within Delft University of Technology is limited. This research is part of an initiative to enlarge the knowledge base regarding (HP)MC fluids, specifically its viscous properties and the associated solution manufacturing process.

# 3

## (Hydroxypropyl) Methylcellulose

Cellulose ethers have been used in a large variety of industries, ranging from food to construction products, over the last five decades. Cellulose ethers are derived from cellulose, a abundantly naturally occurring polymer, which is soluble in water. As mentioned before, two different types of cellulose ethers can be distinguished based on chemistry, namely MC and HPMC. In theory, both types are suitable for use in centrifuge experiments and are seen as equally suitable candidates until further notice. Although cellulose ethers possess many properties which are of interest to different sectors; here, water solubility and thickening properties are most important and consequently lie at the heart of the scope of the is research. To further map the suitability of (HP)MC, its chemical structure and resulting properties are systematically addressed in the following, respectively in 3.1 and 3.2.

### 3.1. Chemistry

Unsurprisingly, MC and HPMC have the same polymeric backbone, which consists of cellulose. In terms of molecular structure, cellulose is predominantly made of anhydroglucose molecules, which chain together to form long polymers. By heating a alkaline solution of cellulose and subsequently treating it with methyl chloride, methylcellulose is obtained as the reaction product. The upper half of Figure 3.1 shows a typical molecular structure of this reaction product. Further purification and grounding are needed to obtain a product suitable for industrial use. In order to produce hydroxypropyl methylcellulose, propeylene oxide is used alongside methyl chloride in the production process. Through substitution, hydroxypropyl molecules merge with the anhydroglucose to form the polymer shown in the lower half of Figure 3.1.

### 3.2. Properties

The degree of substitution (D.S.), the average number of substituted groups per ring [11], of both methyl and hydroxypropyl has an impact on the characteristics of the (HP)MC in therms of organic solubility of aqueous solutions. Consequently, it is of interest to this research. Each of the rings shown in Figure 3.1 has three positions suited for Methoxyl substitution. Hence, the respective D.S. for Methoxyl equals 3.0 at most. It has been proven that a D.S. of 1.64-1.92 optimizes water solubility [11]. Respectively, lower and higher D.S. improve solubility in alkaline conditions and organic solvents, but therefore lie outside the zone of interest. The substitution of Hydroxypropyl has a less pronounced, yet important influence on the properties of HPMC as it raises the hydration temperature of the product (the temperature at which the viscosity of the solution increases). In other words, it determines if a solution is straightforwardly fabricated under laboratory conditions or whether special measures (regarding to temperature; cooling, specifically) are required. Other

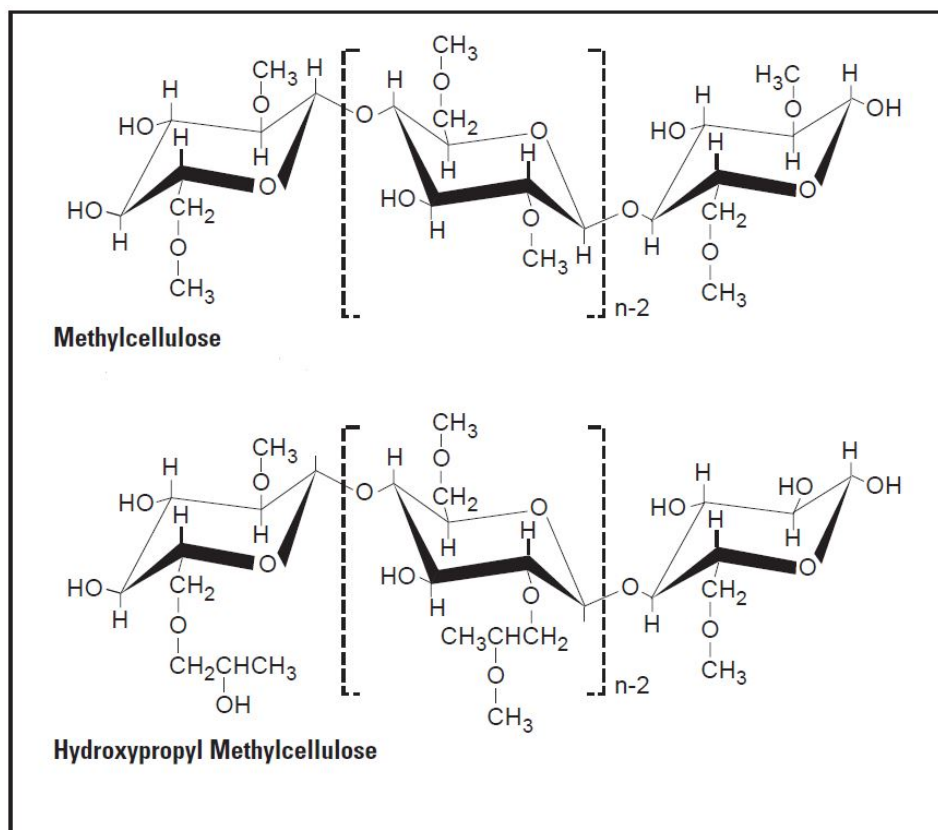


Figure 3.1: Molecular structures of Methylcellulose and Hydroxypropyl Methylcellulose, adapted from [11]

properties which are influenced by the presence of hydroxypropyl include organic solubility and the thermal gelation temperature of aqueous solutions. However, both properties lie outside the scope of this research.

# 4

## (HP)MC type selection

The first challenge regarding the use of (HP)MC in aqueous solutions, is selection of the most suitable type of powder. In terms of manufacturers of (HP)MC products, two companies were identified, namely:

- Ashland Inc., a chemical company operational in >100 countries worldwide, founded in the US in 1924. Ashland<sup>®</sup> offers (HP)MC products under the name Benecel<sup>®</sup>.
- DowDuPont Chemical Company, one of the largest chemical companies in the world offering (HP)MC products known as Methocel<sup>®</sup>.

Although the use of Benecel<sup>®</sup> based viscous fluid for centrifuge experiments is slightly more widespread than the use of Methocel<sup>®</sup>, solutions based on either of the two compounds behave largely similar. The latter gave rise to the selection of the compound exclusively on its availability in the European continent. Therefore, it was established that this research would focus on Methocel<sup>®</sup> products.

Methocel<sup>®</sup> are divided into categories or brands. Specifically, brand A, E, F, J, K and 310 series are distinguished. The main differentiators between the different brands concern: (I) powder composition, which (depending on the intended use) consists of methylcellulose or hydroxypropyl methylcellulose. For hydroxypropyl methylcellulose, differentiation continues based on the ratio between its two respective components; (II) the intended sector of application, in example pharmaceutical or industrial use. Within each of the brands, further differentiation is carried out in terms of nominal dynamic viscosity values at a concentration of 2%, which are also denoted as viscosity grades. To narrow down the whole range of Methocel<sup>®</sup> products to a comprehensive selection of suitable products, the following functional requirement was used:

*A (HP)MC compound suitable for manufacturing viscous fluids between 1 and 100 mPa·s while causing a minimal (<2%) increase in density with respect to that of the employed solvent: water, respectively.*

Based on the criterion mentioned above, the final selection of Methocel<sup>®</sup> products includes: F50, K100, A4C, E4M, A4M, F4M, E4M, E10M. Relevant properties of the aforementioned products are shown in Table 4.1. As can be observed, for most brands instead of a single value, a viscosity range is specified for 2M% aqueous solutions at 20°C. The latter is due to tolerances in the fabrication process, which may cause fluctuations in the amount of active component per reference volume. Therefore, the required concentration at 2M% varies accordingly. Of the candidate brands listed in Table 4.1, types K and E were eliminated. Respectively because the degree of Methoxyl substitution, which plays a key role in water solubility (see 3.2), is significantly lower for the K brand than other candidates. The E brand, despite having the largest degree of Methoxyl substitution, is a pharmaceutical grade brand and therefore significantly more costly to acquire. Therefore it is also eliminated.

	<b>F50</b>	<b>K100</b>	<b>A4C</b>	<b>E4M</b>	<b>K4M</b>	<b>F4M</b>	<b>A4M</b>	<b>E10M</b>
<b>Type</b>	HPMC	HPMC	MC	HPMC	HPMC	HPMC	MC	HPMC
<b>Methoxyl D.S.</b>	1.8	1.4	1.8	1.9	1.4	1.8	1.8	1.9
<b>Bulk density</b>	341	341	276	341	341	341	276	341
<b>Specific volume</b>	0.734	0.717	0.725	0.767	0.717	0.734	0.725	0.767
<b>Specific density</b>	1.36e3	1.39e3	1.38e3	1.30e3	1.39e3	1.36e3	1.38e3	1.30e3
<b>Fluid density <math>\rho_f^*</math></b>	1.02e3	1.02e3	1.02e3	1.02e3	1.02e3	1.02e3	1.02e3	1.02e3
<b>Lower bound <math>\mu_f^*</math></b>	50.0	80.0	3.50e2	2.70e3	2.70e3	3.50e3	4.00e3	7.50e3
<b>Lower bound <math>\mu_f^*</math></b>	0.0500	0.0800	0.350	2.70	2.70	3.50	4.00	7.50
<b>Upper bound <math>\mu_f^*</math></b>	na	1.20e2	5.50e2	5.04e3	5.04e3	7.00e3	na	1.40e4
<b>Upper bound <math>\mu_f^*</math></b>	na	0.120	0.550	5.04	5.04	7.00	na	14.0
<b>Lower bound <math>\nu_f^*</math></b>	0.0000490	0.000784	0.000343	0.00265	0.00265	0.00343	0.00392	0.0735
<b>Lower bound <math>\nu_f^*</math></b>	49.0	78.4	343	265	265	3.43e3	3.93e3	7.35e4
<b>Upper bound <math>\nu_f^*</math></b>	na	0.000118	0.000540	0.00495	0.00495	0.00687	na	0.0137
<b>Upper bound <math>\nu_f^*</math></b>	na	1.18e3	5.40e3	4.95e3	4.95e3	6.87e3	na	1.37e4

\* for a 2M% aqueous solution at 20°C

Table 4.1: Summary of relevant properties of (HP)MC candidates, adapted from [11]

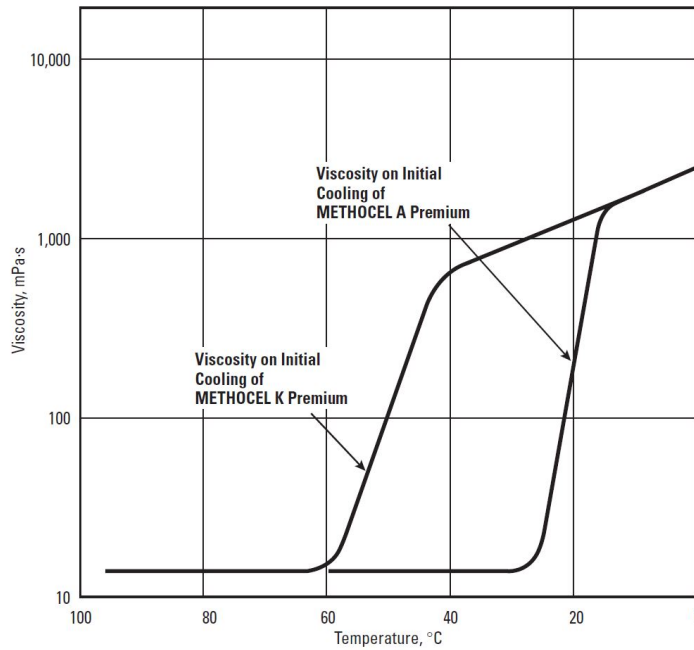


Figure 4.1: Viscosity development of Methocel<sup>®</sup> MC brands (A) and HPMC brands (K) dispersed in aqueous solution at 2M% concentration, retrieved from [11].

from the list of candidates. The remaining brands, A and E, are (in theory) equally soluble in water. The absence of Hydroxypropyl in type A however has negative implications on the hydration temperature for aqueous solutions, which is also illustrated by Figure 4.1. As is demonstrated by Figure 4.1, the presence of Hydroxypropyl molecules in brand K (but also brands E and F), drastically raises the hydration temperature of hot water slurries at 2M% concentration. This is beneficial to the fabrication process as the need for cooling, either indirect, through temperature control; or direct, through the addition of cold water or (potentially) ice, is (partially) omitted. As the presence of Hydroxypropyl molecules in the fluid is irrelevant for the intended application in the centrifuge, the decision was made to use Methocel<sup>®</sup> F. Within the F brand, two different viscosity grades form the final candidates, namely: (I) F50; (II) F4M. The definitive decision between either of the two remaining candidates, is based on the density of the obtained fluid  $\rho_f$  at a reference dynamic viscosity of  $100 \text{ mPa}\cdot\text{s}$ . Considering this hypothetical solution, the use of F50 would yield a fluid where  $\rho_f \approx 1.04 \cdot \rho_w$  whereas for F4M the following would hold:  $\rho_f \approx 1.00 \cdot \rho_w$ . Implicitly, the latter also illustrates that (for the same viscosity) F4M is more efficient in terms of dosage per reference volume of water. Hence, it is also the most economical alternative. Consequently, F4M was marked as the best candidate for the preparation of viscous fluids for physical modeling in the centrifuge.



# 5

## Problem statement

The desire to start manufacturing viscous fluid for centrifuge experiments in-house, is accompanied by several practical challenges, which mainly arise from a general lack of experience with regard to the preparation of (HP)MC fluids at Delft University of Technology. The main challenges include:

- a limited understanding of practical implications of the advocated method of production for (HP)MC aqueous solutions;
- uncertainties with regard to the shear rate dependency of viscosity;
- uncertainty with respect to the correlation between temperature and viscosity;
- aging effects expressed by aqueous solutions of HPMC.

The perceived viscosity during centrifuge test is of the utmost importance to limit the chance of obtaining untrustworthy experimental results. Research carried out by Chian and Madabhushi (2010) ([6]), supports the prior statement. While reviewing the response of a tunnel embedded in liquefiable soil, Chian and Madabhushi (2010) ([6]) found that the use of pore fluids with poorly modeled viscosity resulted in soil behavioral inconsistencies between the model and prototype. This issue is especially relevant given the modest experience with the fabrication and use of HPMC viscous fluid, and further strengthens the call to look into the aforementioned issues to envision a reliable production method. The next sections provide further background on the subject of fluid preparation, shear rate dependency of viscosity, the influence of temperature on viscosity and aging effects. Respectively, these topics are addressed in sections 5.1, 5.2, 5.3 and 5.4.

### 5.1. (HP)MC fluid preparation

Choosing the best-suited method of preparation to craft aqueous HPMC solutions, depends on whether the powder is chemically treated to bring about a temporal insolubility in cold water. If this is the case, the resulting product is categorized as surface treated HPMC. Moreover, the nature of the solvent (in this case water) also plays a role of importance. As the preparation process, which is done in the laboratory, is not subjected to boundary conditions inhibiting the use of warm water, the use of surface-treated (HP)MC is not mandatory. Therefore, solely untreated (HP)MC is considered here. For aqueous solutions created from untreated (HP)MC, two preparation methods exist, namely: (I) the 'hot/cold technique'; (II) static dispersion techniques in cold water. Both are separately discussed below, respectively in 5.1.1 and 5.1.2.

#### 5.1.1. Hot/cold technique

The most common way to prepare aqueous solutions from untreated (HP)MC formulas is by employment of the 'hot/cold technique'. Principally, this technique is based on the insolubility of (HP)MC in hot water. The method itself is comprised of four steps [11]:

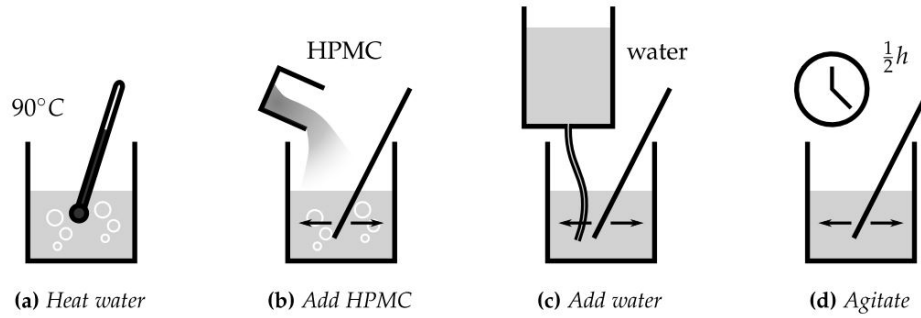


Figure 5.1: The 'hot/cold method' for viscous fluid preparation using (HP)MC, retrieved from [1].

1. Heat anywhere between 1/5 and 1/3 of the total amount water to approximately 90°C.
2. Under continued agitation, add the powder to the hot water to obtain a homogeneous suspension, where all particles are evenly wetted. The influx of powder should be adjusted such that lumps are not formed, as this will prevent even wetting of particles and therefore inhibit full viscosity development.
3. Gently add the remainder of the water as cold water (<10°C) or ice and allow the mixture to gradually reach hydration temperature while continuously stirring. It is important to note that the hydration temperature depends on the type of (HP)MC product used. Hence, it is wise to consult reference manuals provided by the manufacturer to ensure full viscosity development;
4. Maintain agitation for 30 minutes after reaching the hydration temperature.

Figure 5.1 provides illustrations to visually explain the procedure described above.

### 5.1.2. Static dispersion technique

Statically dispersing (HP)MC powder through water forms another preparation alternative. This technique entails gradually pouring (HP)MC powder onto the water surface. The powder subsequently dissolves in the water, causing the viscosity to develop without any interference. The main benefit of this technique is that it is not required to heat or cool volumes of water. Therefore, all water can remain at room temperature. However, the use of this technique does require a steady hand to evenly scatter the powder over the water surface. Additionally, static dispersion is significantly more time consuming than the 'hot/cold method'. Alternatively, if circumstances impede the use of hot and/or cold water, the use of surface-treated products might be of interest as active dispersion through the water is in this instance allowed and shortens the preparation time. However, as surface treated powders are not considered in this research, the hot/cold technique possesses several clear advantages over the static dispersion technique and is therefore the preferred method of preparation.

## 5.2. Shear rate dependency of viscosity

Ideally, a fluid expresses what is called ideally viscous or Newtonian flow behavior when sheared. In this case, the shear stress  $\tau$  is linearly dependent shear rate  $\dot{\gamma}$  and the dynamic viscosity  $\mu_f$  is merely a scaling constant. The aforementioned relationship is known as the Newtonian law of viscosity, and is shown as Formula 5.1.

$$\tau = \mu_f \cdot \dot{\gamma} \quad (5.1)$$

One of the best known examples of a Newtonian fluid (to which Formula 5.1 applies) is water, but other examples include honey and a variety of organic solvents. Newtonian law of viscosity implies that a fluid will retain its viscous properties, regardless of how quickly it is sheared. Or, in other words:  $\mu_f$  is independent of  $\dot{\gamma}$ .

However, in reality most fluids express non-Newtonian flow behavior. Both shear thickening and shear thinning, also known as dilatant and contractive flow behavior, exemplify non-Newtonian flow characteristics. Shear-thickening, concerns cases where  $\mu_f$  is positively correlated to  $\dot{\gamma}$ . Hence, viscosity increases with increasing shear rate. A well-known example solution which expresses shear thickening behavior is oobleck (solution of cornstarch in water). The most common variant of non-Newtonian behavior is however shear-thinning. In this case,  $\mu_f$  is negatively correlated to  $\dot{\gamma}$ . Hence, viscosity decreases with increasing shear rate.

As mentioned before, the pore fluid in the prototype (water) is a prime example of a Newtonian fluid. However, (HP)MC solutions are known to express contractive behavior when sheared. The extent to which this takes place, depends on the fluid concentration and the type of (HP)MC used. Because both are unknown at this stage, it is imperative to investigate the non-linear shear behavior of (HP)MC solutions. Additionally, due to the nature of impact pile hammering, large spatial shear rate gradients can be expected in the surrounding soil body. Knowing that (HP)MC fluids express non-linear flow behavior, this implies the presence of a similar spatial gradient for viscosity, which could negatively impact the observations. Therefore, in addition to characterizing the non-linearity of viscosity, it is mandatory to define a normative shear rate for the centrifuge tests. The latter should ensure that viscous fluid is optimally configured to conduct research in specific shear zones of the soil body.

### 5.3. Temperature dependency of viscosity

Under ideal circumstances, the temperature within the testing facility is maintained at 20°C while testing, which is equal to the temperature standard for rheological experiments. Unfortunately, the centrifuge room at Delft University of Technology is not equipped with any climate regulatory tools. This means that tests are executed in an environment with naturally fluctuating temperature. Due to the dependency of viscosity on temperature (viscosity decreases with increasing temperature), fluctuations can occur. However, it is debatable to which extent an ambient temperature above 20°C influences the viscosity of pore fluid in soil samples. Particularly when samples are large (containing multiple liters of liquid), are stored in a regulated environment prior to testing and are exposed to the elevated temperature in the testing facility for a short period of time; the temperature influence is negligible. For the intended research purpose, all of the aforementioned criteria are met. Hence, the neediness to look into temperature effects is low and therefore completely omitted. However, in all other cases, quantification of the temperature effect is important to determine its respective influence on the fluidity of the pore fluid. In this case, it is advisory to establish whether it is required to increase viscosity to account for the effect of higher ambient temperature. Such a dependency was established by the work of Adamidis & Madabhushi (2014) ([1]) as well as Stewart *et al.* (1998) ([19]). The effect of temperature elevation on fluidity is indicated by Figure 5.2. Although the influence is most pronounced for temperatures below 20°C, higher temperatures cause a substantial decrease in viscosity.

### 5.4. Effect of aging on viscosity

From experience, it is clear that prolonged storage of certain materials initiates deteriorative processes which affect the overall quality and (potentially) the usability of the respective material. Several researchers, amongst which are Adamidis & Madabhushi (2014) ([1]), researched the aging effect of HPMC fluids to determine whether prolonged storage impacts the viscous properties. Adamidis & Madabhushi (2014) measured the viscosity of three HPMC fluids (at different concentrations) over the course of one month. They established that aging did not have any noteworthy effect on viscosity of the solution over the course of the aforementioned period. Hence, it is stated that fluid aging is negligible with respect to the nominal duration of a centrifuge test. Consequently, aging effects are excluded from the scope of this research.

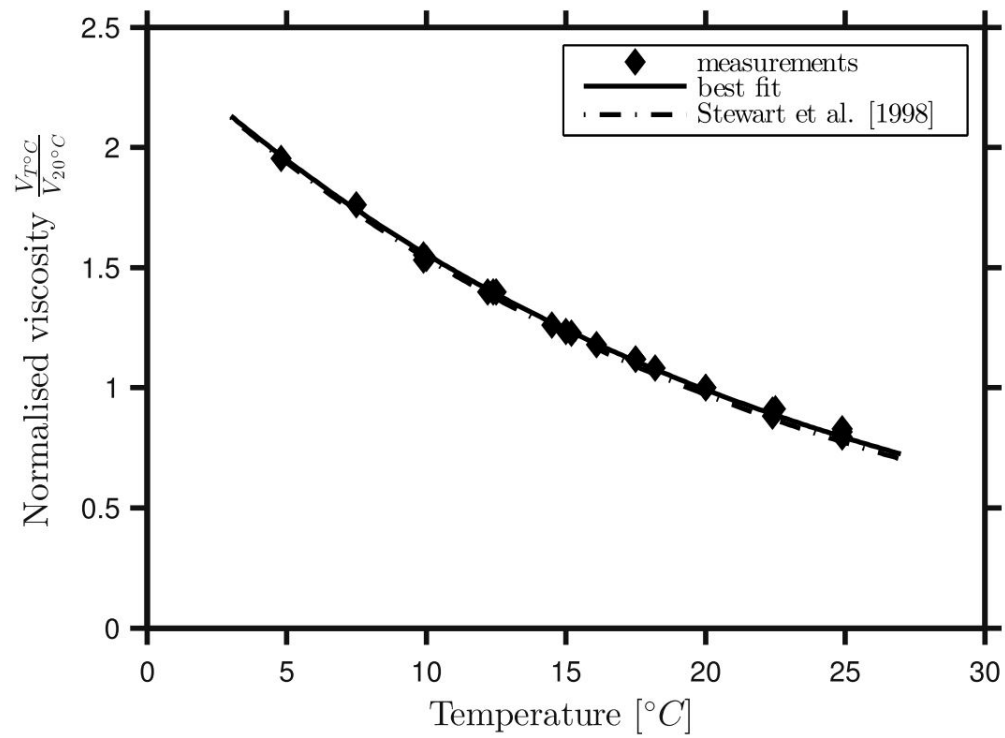


Figure 5.2: Temperature dependency normalized viscosity for aqueous HPMC solutions, after Adamidis & Madabhushi (2014) (11)

# 6

## Research methodology

With regard to the challenges accompanying the use of HPMC fluid for centrifuge experiments, as mentioned in 5, a research methodology is designed aimed at gathering knowledge in the area of: (I) fluid preparation techniques; (II) quantification of the shear rate dependency of viscosity. The research approach with regard to each of the aforementioned points is respectively discussed in 6.1 and 6.2. A total of seven 0.9 l fluid batches were prepared at different concentrations (by mass) to roughly cover the 10 to 100  $mPa \cdot s$  viscosity range. From each batch, 3 samples are taken and tested in a Anton Paar MCR302 rheometer at 20°C. The HPMC powder used to make these batches consists of Methocel<sup>®</sup> F4M and is supplied by DowDuPont Chemical Company. The nominal viscosity range (as provided by the manufacturer) is 3500-7000  $mPa \cdot s$  for a concentration (by mass) of 2% at 20°C. A more elaborate overview of the properties of this Methocel<sup>®</sup> product is provided by Table 4.1.

### 6.1. Fluid preparation

As mentioned before in chapter 5, two ways exist to prepare HPMC-based viscous fluids. Due to the preparation of the aqueous HPMC solution in a laboratory, the process is not inhibited by the unavailability of water of different temperatures. The latter, alongside the fact that non-treated HPMC powder is used, makes the use of the (lengthy) static dispersion technique superfluous. Consequently, use is made of the 'hot/cold method'. Prior to discussing the preparation method, several important remarks are listed below:

- In the following, all concentrations are expressed as the quotient of the effective HPMC (corrected for the moisture content of the powder) over the total solution by mass (in percent [%]).
- Additionally, all quantities mentioned are 'effective quantities'. Hence, any losses due to the transfer of matter (either HPMC powder or water) during the preparation process (in example the pouring of water between containers) are accounted for.
- Due to extensive precautions, evaporation is during preparation is limited to  $\approx 1\%$  by mass. Consequently, solution concentrations presented in the following are not corrected for the effect of evaporation.

The 'hot/cold method' as described by Dow ([11]) but also other researchers, in example Adamidis and Madabhushi (2014) ([1]), lacks practical insights to streamline the preparation process. Hence, the method was initially approached in several ways, yielding mostly unsatisfactory results in the form of:

- Lumpy, cloudy solutions where a gelatinous membrane was formed around clumps of powder, preventing hydration and thus inhibiting full viscosity development. The main cause of

this issue was the use of an unsuitable mixer, incapable of excreting enough shear to ensure full dispersion of the powder.

- Lumpy, clear solutions due to abrupt cooling of the hot (90°C) water after addition of the HPMC powder. The latter resulted in a gelatinous substance which poorly dissolved in the subsequently added cold (10°C) water. This problem was due to a high heat capacity of the container to which the hot water, HPMC powder and cold water were added stepwise. Due to the high heat capacity, the 90°C cooled to a temperature below the hydration threshold, gravely complicating the even dispersion of the HPMC powder in the water.
- Solutions of unrealistically high or low viscosity. These mixture were created from a suspension of HPMC in hot (90°C) water at a fixed concentration. By diluting parts of the fixed concentration mixture by different volumes of cold water, batches of different concentrations should have been obtained. Instead, due to settlement of the suspended HPMC particles, the concentration of the mixture was not constant. The latter caused significant deviations between the anticipated and actual viscosity of the fluid batches obtained after diluting parts of the hot slurry with cold water.

The insights gathered from the unsuccessful attempts at creating HPMC fluid at the right viscosity, were used to professionalize the preparation process and draft a robust methodology. This preparation method, which is based off the 'hot/cold method', is abundantly explained below. First, 6.1.1 discusses the determination of the required volumes and/or masses of HPMC, hot water and cold water. Subsequently, 6.1.2 elaborates upon the preparation procedure of the fluid. Finally, 6.2 goes into the rheological experiments aimed at quantifying the properties of the fabricated aqueous HPMC solutions.

### 6.1.1. Recipe drafting

This section addresses the determination of the required quantities of HPMC, hot water and cold water to obtain a solution at the right concentration by means of step-by-step instructions. Please note that all of the following formulas are mass-based. The latter is due to the appreciable volume fluctuation of a reference mass of water for the temperatures between 10°C and 90°C. Moreover, unlike mass (which is easily and reliably quantified using a scale), the determination of a volume is cumbersome, time-consuming and prone to measurement error.

1. Determine the required amount (of de-aired and demineralized) water to use in the preparation process in kilograms,  $M_w^*$ . Please observe that  $M_w^*$  does not account for the any the moisture content of the HPMC powder.
2. From  $M_w^*$  determine  $M_{w, 10^\circ\text{C}}$  and  $M_{w, 90^\circ\text{C}}$  from Equation 6.1 and 6.2 respectively.

$$M_{w, 10^\circ\text{C}} = 2/3 \cdot M_w^* \quad (6.1)$$

$$M_{w, 90^\circ\text{C}} = 1/3 \cdot M_w^* \quad (6.2)$$

3. Determine the required concentration (by mass) of the viscous fluid. For a rough indication of range of viscosities to expect, Equations 6.3 and 6.4 may be employed to respectively calculate lower and upper bound viscosity estimates [11].

$$\mu_{\text{Lower bound}} = (C \cdot \alpha_{\text{Lower bound}} + 1)^8 \quad (6.3)$$

$$\mu_{\text{Upper bound}} = (C \cdot \alpha_{\text{Upper bound}} + 1)^8 \quad (6.4)$$

Where  $C$  is the concentration (by mass) [%]. Furthermore,  $\alpha_{\text{Lower bound}}$  and  $\alpha_{\text{Upper bound}}$  respectively indicate specific molecular weight constant (calculated in accordance with [11]). For Methocel® F4M, applicable  $\alpha$  values are summarized in Table 6.1.

Type	$\alpha_{\text{Lower bound}}$ [-]	$\alpha_{\text{Upper bound}}$ [-]
F4M	0.88668721	1.01219313

Table 6.1:  $\alpha_{\text{Lower bound}}$  and  $\alpha_{\text{Upper bound}}$  for Methocel<sup>®</sup>, calculated from [11]

4. To readily compute the required amount of powder  $M_p$  to attain the desired concentration, the Equation 6.5 is used. Equation 6.5 follows from the definition of concentration, namely as: the quotient of the effective weight of the HPMC powder (corrected for moisture content) over total mass of the fluid. Unlike other authors, the minor contribution of the HPMC powder to the total mass of the fluid, is accounted for. Hence, after some algebra, the following expression is obtained:

$$M_p = \frac{C \cdot M_w^*}{100 - \theta_p - C} \quad (6.5)$$

Where  $\theta_p$  is the moisture content of the HPMC powder in %. The determination of the moisture content involves the use of a drying oven. As the molecular structure of the HPMC powder is very sensitive to temperature, it is best to dehydrate the powder at a lower temperature for a longer period of time. For this research, samples were dried at both 42°C and 105°C. When dried at 105°C, the apparent moisture content ( $\approx 4\%$ ) was significantly higher than that of the powder dried at 42°C ( $\approx 1\%$ ). However, the upon inspection of the viscous properties of solutions crafted from both powders; it was found that for the same solution concentration, the powder dried at 105°C yielded a viscosity  $\approx 60\%$  lower than the powder dried at 42°C. This gives reason to believe that water incorporated into the crystalline structure of the cellulose molecules was dehydrated, thereby decreasing the degree of polymerization, which governs viscosity development. Consequently, it is advisable to dry HPMC powders at moderate temperatures to safeguard the viscosity development further in the preparation process. To obtain a representative value for  $\theta_p$ , five samples of  $\approx 200$  g were dried at 42°C for 48 hours. Subsequently,  $\theta_p$  was determined as the weighted average of the moisture content of the five individual samples.

### 6.1.2. Solution preparation

In this section, the preparation methodology is discussed. The required steps are listed below:

1. In a beaker, weigh 2/3 of  $M_w^*$  and refrigerate until a temperature of 10°C is reached.
2. In another beaker (heat resistant and large enough to hold  $M_w^*$ ), weigh the remaining 1/3 of  $M_w^*$ .
3. Properly seal the beaker. Possibly by using a steel bowl filled with cold water to aid the condensation and recollection of water vapor, as demonstrated by the left-hand frame of Figure 6.1.
4. Carefully check if any gaps remain between the beaker and its lid. If so, close these gaps to ensure no water vapor is expelled.
5. Using a heated magnetic stirrer, heat the water to temperature of 90°C.
6. Upon reaching 90°C, remove the beaker from the heated magnetic stirrer and add the predetermined amount of HPMC powder to the mixture at once. Practice shows that the latter is helpful to minimize the amount of powder left in the holding container afterwards. Prolonged contact of HPMC powder with water vapor will trigger hydration and thereby decreases manageability, causing a significant amount of powder to stick to the sides of the cup.
7. Using a blender (or preferably high shear mixer) thoroughly disperse the powder through the hot water. Inclusion of air should be minimized as much as possible. If required, a small amount of 10°C water may be added to remove the powder clinging to the mixing device upon removal, following the full dispersion of the powder.

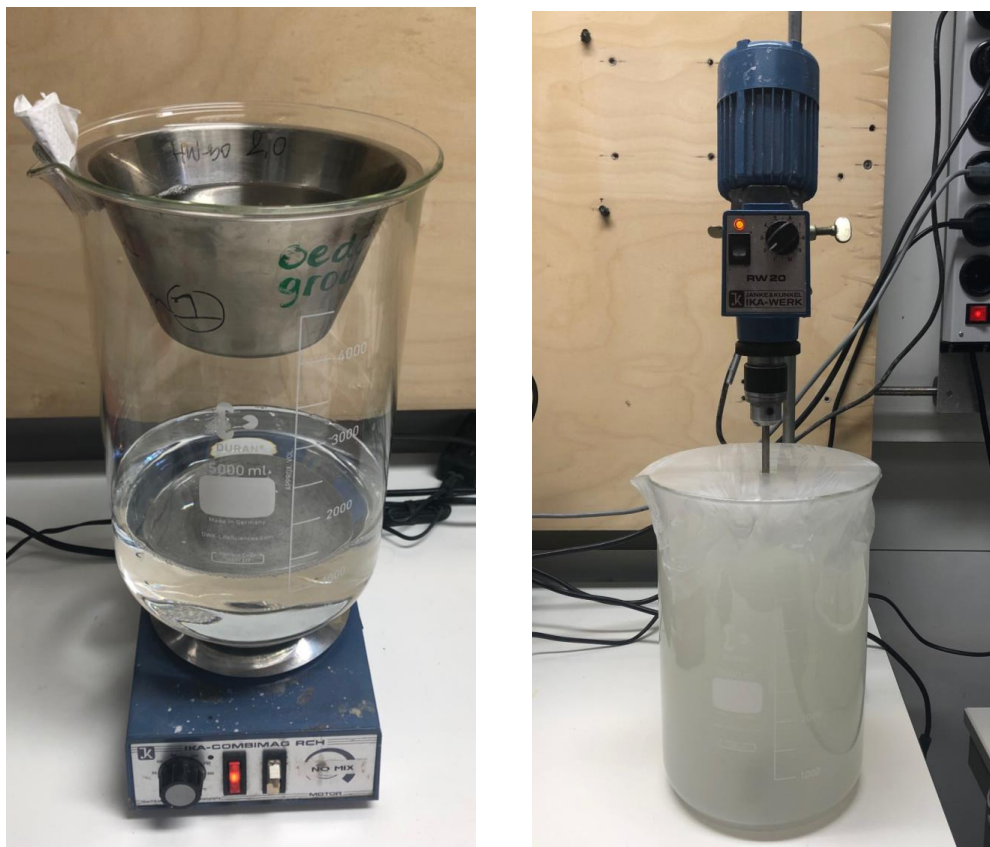


Figure 6.1: (LEFT) Beaker with deaired water on a heated magnetic stirrer. A bowl filled with cold water acts as a condensation device to prevent evaporation during the heating to 90°C. (RIGHT) Agitation of the final solution by a stirrer. The top of the beaker is sealed of with PARAFILM<sup>®</sup> foil to counteract evaporation.

8. Carefully lower a industrial stirrer into the beaker holding the suspension of HPMC and 90°C water and initiate agitation. Make sure to tune the stirrer such that the entire volume of fluid is agitated.
9. Close off the beaker to prevent evaporation during agitation. The lid should have a recess to enable the installation of the stirrer and the addition of the (remainder of) 10°C water. In case a lid is not available the top of the beaker could be sealed with PARAFILM<sup>®</sup> foil.
10. Slowly add the refrigerated (10°C) water to the mix, while agitation continues. The right-hand frame of Figure 6.1 illustrates the result following completion of this step.
11. Continue the agitation process until the temperature is <25°C. This temperature should ensure full powder hydration and thus viscosity development. In case another brand of Methocel<sup>®</sup> product is used, it is advised to look up the appropriate hydration temperature in the reference manual.
12. Maintain the stirring process for at least 30 minutes after the solution reached 25°C.
13. Finally, depending on the quantity, the finished fluid is de-aired the using a vacuum chamber for several hours.

The methodology advocated above yielded uniform, fully translucent viscous fluids as a final product. The inclusion of air through agitation by the stirrer is limited. For viscosities at the lower end of the spectrum, entrapped air was expelled rather quickly under the effects of buoyant forces acting of remaining air bubbles. Although this also happens for higher viscosity solutions, the process is

significantly slower as rising air experiences more drag due to the elevated viscosity. In the latter case it is advisory to place the fluid in a vacuum chamber to accelerate the process as indicated by the last step of the preparation process.

Seven fluid batches were prepared in accordance with the preparation method described above. For these solutions, Table 6.2 shows the idealized masses of: (I) HPMC powder  $M_p$ ; (II) effective HPMC powder (compensated for moisture content)  $M_{p, \text{eff}}$ ; (III) 10°C water  $M_{w, 10^\circ\text{C}}$ ; (IV) 90°C water  $M_{w, 90^\circ\text{C}}$ . Additionally, Table 6.2 depicts the idealized concentration  $C_{\text{ideal}}$  of the solution (based off aforementioned powder and water quantities) as well as the obtained concentration  $C_{\text{actual}}$  (calculated from the actual amount of powder and water used to create the particular batch of fluid) and the expected viscosity range for the actual concentration of the mixture. Similarly to Stewart *et al.* (1998) ([19]), the actual concentrations were verified by means of dry tests.

Batch ID [-]	$M_p$ [g]	$M_{p, \text{eff}}^*$ [g]	$M_{w, 10^\circ\text{C}}$ [kg]	$M_{w, 90^\circ\text{C}}$ [kg]	$C_{\text{ideal}}$ [%]	$C_{\text{actual}}$ [%]	$\mu_{\text{Lower bound}}$ [mPa.s]	$\mu_{\text{Upper bound}}$ [mPa.s]
F4M.35	2.84	2.81	0.600	0.300	0.3500	0.3598	9.16	11.99
F4M.45	3.67	3.62	0.600	0.300	0.4500	0.4582	15.29	21.07
F4M.50	4.07	4.02	0.600	0.300	0.5000	0.4982	18.67	26.23
F4M.55	4.47	4.42	0.600	0.300	0.5500	0.5490	23.87	34.30
F4M.60	4.88	4.83	0.600	0.300	0.6000	0.6023	30.67	45.07
F4M.65	5.29	5.23	0.600	0.300	0.6500	0.6497	38.07	57.00
F4M.70	5.70	5.64	0.600	0.300	0.7000	0.6899	45.53	69.20

\* calculated based on a nominal moisture content  $\Theta_p$  of 1.09 % based on a series of five dry tests at 42°C

Table 6.2: Summary of water and HPMC quantities required to create solutions of specific concentration, complemented by the actual concentration (calculated from the use of water and powder during the preparation process) and the expected viscosity range for this concentration based on Equations 6.3 and 6.4

## 6.2. Rheological measurements

Rheological experiments are preformed to gain insight into the viscous properties of the batches. To this end, use is made of a Anton Paar MCR302 rheometer (a rotational viscometer which operates in accordance with the Searle principle) to obtain the viscosity curve (viscosity  $\mu_f$  as a function of shear rate  $\dot{\gamma}$ ) of the prepared solutions. The rheometer is equipped with smooth cylindrical rotor of type B-CC27 and sample cup of type C-CC27. From each of the seven fluid batches, three 15 ml specimens were randomly extracted from the lot. In order to quantify the effect of prolonged stagnation of the fluid as well as the inclusion of small air pockets on the viscous properties, the samples were extracted at the following instances: (I) prior to agitated of the mixture; (II) following agitation of the solution; (III) following agitation of the deaired fluid. Hence, in total 21 (3x7) rheological experiments are conducted. The employed rheological test protocol has the following key properties:

- When applicable, prior to the extraction of a 15 ml specimen, the entire solution was homogenized by 30 seconds of agitation.
- The fluid was transferred to the measurement cup of the rheometer using a syringe to minimize air inclusions. All samples with bubbles  $>0.1 \text{ mm}$  or multiple visible air inclusions were rejected.
- All viscosity tests are carried out at 20°C ambient temperature, with a tolerance of  $\pm 0.15^\circ\text{C}$ .
- The measurement position of the tip of the concentric bob is set to 0 mm relative to the bottom of the measurement cup. It is important that a single value is used for all measurements as the adjustment of the measurement position has a subtle effect on the apparent viscosity.
- Viscosity is determined for shear rates between 0.1 and 1000 1/s. The author recognizes that the aforementioned range of shear rates is rather wide as shear rates expected to incite from

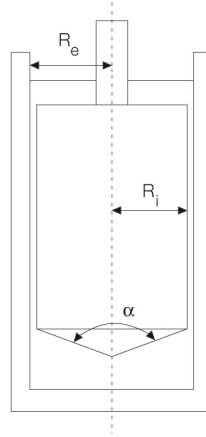


Figure 6.2: Schematic overview of concentric pin used for rheological experiments with relevant geometric annotations, adapted from [3]

impact pile driving range from 10 to 100  $l/s$ . However, due to the ambition to utilize this research for the fabrication of viscous fluid in general, a wider than strictly necessary range of shear rates was settled for. The shear rate is computed as the quotient of the velocity difference between the extremities of the fluid domain  $v_f$  over the physical distance between the extremities of the fluid domain  $d_f$ , as is also shown by Equation 6.6:

$$\dot{\gamma} = \frac{v_f}{d_f} \quad (6.6)$$

Analogous to the definitions used by Figure 6.2; for the concentric cylinder, the width of the fluid domain  $d_f$  is defined as:

$$d_f = R_e - R_i \quad (6.7)$$

Where  $R_e$  is the radius of the measurement cup and  $R_i$  the bob radius.

- The rheometer performs two full shear cycles, where a full cycle consists of the increase of the shear rate from 0.1 to 1000  $l/s$ , followed by the opposite process: the decrease of shear rate from 1000 to 0.1  $l/s$ . (for each cycle) the velocity imposed on one of the boundaries of the fluid domain is increased and decreased logarithmically.
- In every decade (in example 0.1 up to (but excluding) 1  $l/s$ ), ten logarithmically spaced viscosity readings are taken. Amounting to a total of 41 readings per measurement interval, 82 per full shear cycle and 164 per test.
- The measurement intervals for the viscosity readings also follow an inversely logarithmic relationship. Hence, for lowest shear rate (0.1  $l/s$ ), the measurement interval equates to 15 s. Whereas for the largest shear rate (1000  $l/s$ ), the measurement interval equals 1 s. Due to transient effects in the development of laminar flow, it is essential to space measurement intervals in a similar fashion whenever the viscosity is assessed at shear rates below 1  $l/s$ . As a rule of thumb for the required measurement interval, the following expression is used [3]:

$$\Delta t_m = 1/\dot{\gamma} \text{ for } \dot{\gamma} < 1 \quad (6.8)$$

Where  $\Delta t_m$  is the advocated measurement interval provided the shear rate  $\dot{\gamma}$ . For all shear rates larger than 1  $l/s$  it is recommended to set the measurement interval to  $\geq 1$  s.

# 7

## Results

In this section, the rheological results are discussed. As mentioned in 6 a series of 21 experiments was performed to obtain the flow curves for seven batches of solution. Firstly, in 7.1 raw experimental data are presented and global trends are identified. Based on the insights provided by the raw data, the most meaningful data are selected for further analysis in 7.1.1. This includes the derivation of confidentiality intervals, based on a statistical analysis of the rheological data for each batch. Moreover, for several shear rates, viscosity readings are plotted versus concentration; through which a power law is subsequently fitted to obtain a set of continuous expressions, which describe the development of viscosity as a function of concentration (for several shear rates). The fitted curves are subsequently used in the derivation of a generic expression which relates viscosity to shear rate and concentration of two shear rate domains, namely: (I)  $0.1 \leq \dot{\gamma} \leq 10$ ; (II)  $10 < \dot{\gamma} \leq 1000$ .

### 7.1. Global trend identification

As previously mentioned in 6, three 15 *ml* samples were taken from each fluid batch and tested in the rheometer. Each fluid specimen was subjected to two full shear cycles. The latter implies that for each sample, the viscosity at a specific shear rate is recorded four times. Therefore, (for each batch) twelve viscosity readings are available for each shear rate part of the rheological shear cycle. For all batches, the response to monotonic shear cycling of the three specimens is comparable. This shows that agitation and de-airing have a negligible effect on viscosity readings. However, the author recognizes that both actions are an inseparable part of a well thought out test methodology. Yet, due to the largely overlapping results, a single flow chart is presented for each batch; containing twelve individual flow curves. To visualize the variability of the measurements, the same data is also presented as box plot. For batch F4M.45, aforementioned graphs are part of the main report, respectively as Figure 7.1 and 7.2. Figures corresponding to the remaining six batches are included section I of the Appendix.

Figure 7.1 clearly explicates the large coincidence of the twelve flow curves, especially in the domain between 1 and 1000 *1/s*. For shear rates  $< 1$  *1/s*, differences between individual flow curves increase. The observed diversion progressively increases for further decreasing shear rates. Using Figure 7.2, the variability of the viscosity readings is quantitatively assessed. In the shear rate range from 1 to 0.1 *1/s*, the interquartile range (IQR) increases from  $< 0.1$  to  $\approx 3$  *mPa.s*. Despite the increase of IQR, the data remains relatively centered around the median, which implies little fluctuation of the mean viscosity for batch F4M.45. However, as demonstrated in section I of the Appendix, for other batches the data is undeniably skewed towards higher viscosities. Although the viscosity at low lower shear rates is not of interest for the dynamic pile hammering tests, it might be of value for centrifuge experiments of a different nature. If this is the case, the median is arguably the most

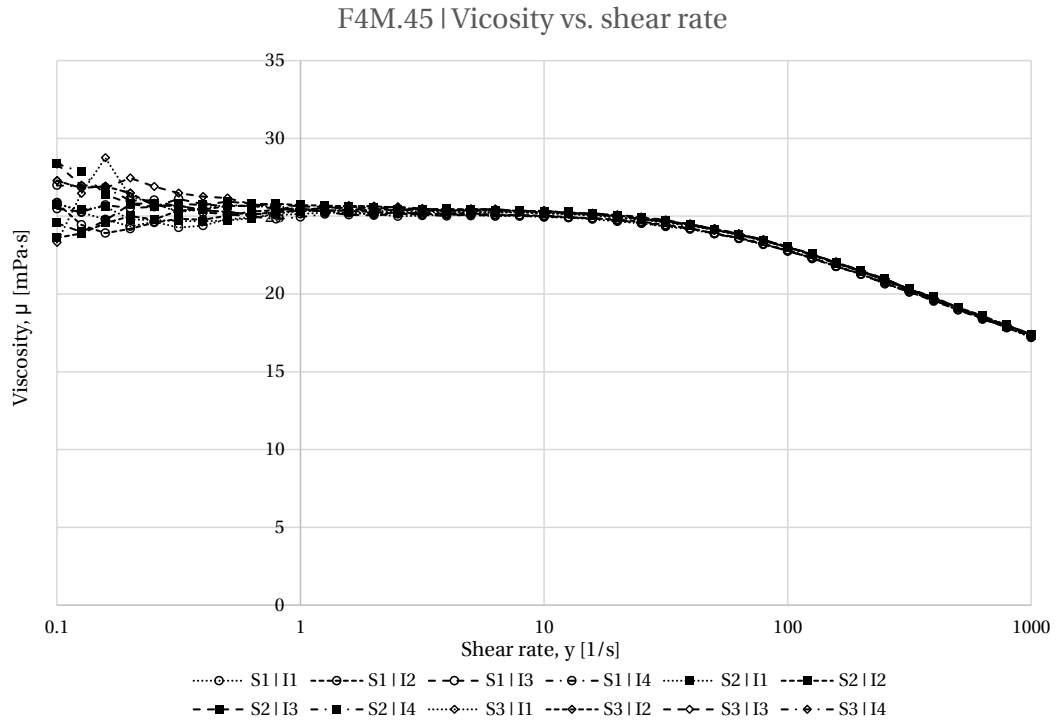


Figure 7.1: Flow curves corresponding to batch F4M.45. Legend entries are presented in the format SX | IY, where X codes for the specimen number (1 - not agitated, not deaired; 2 - agitated, not deaired; 3 - agitated, deaired) and Y corresponds to the shear interval (1-4)

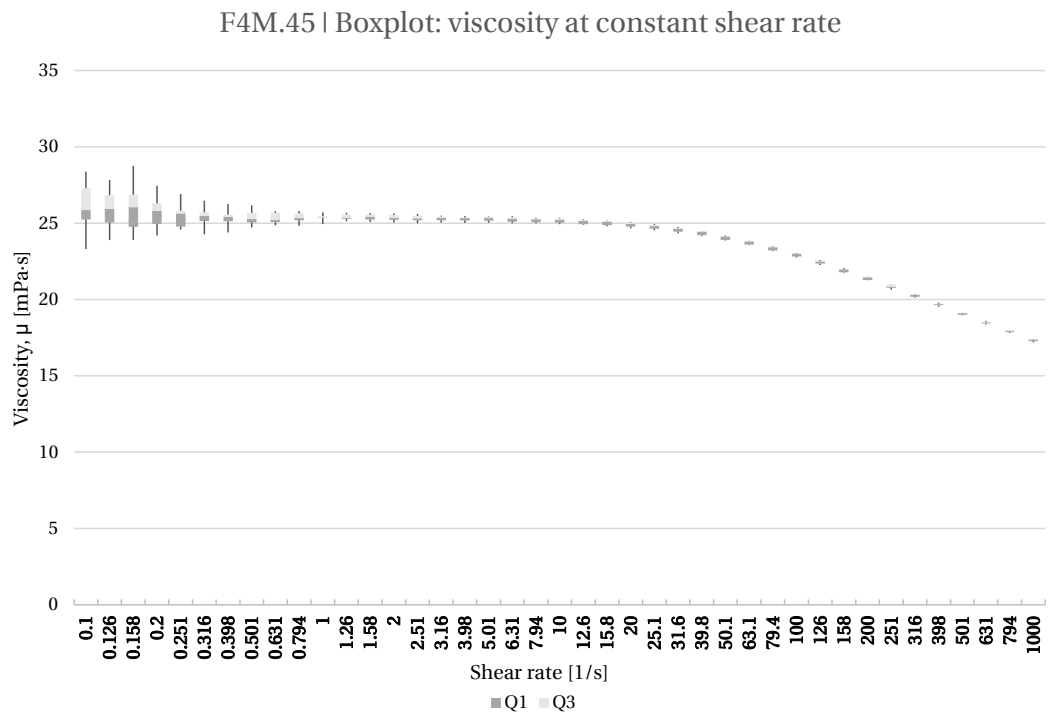
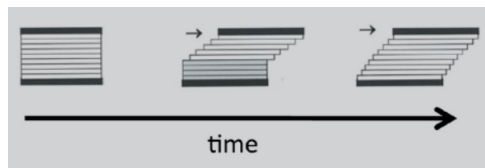
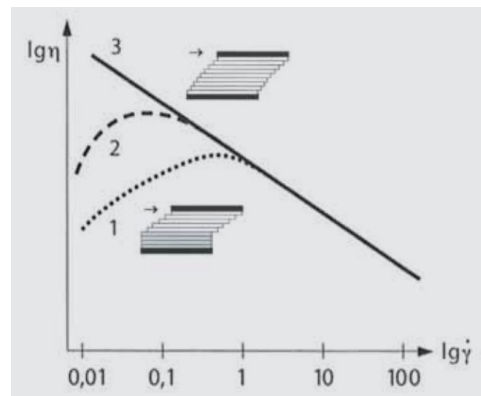


Figure 7.2: Variability of viscosity readings for batch F4M.45 per shear rate



(a) Development of laminar flow during shearing in a rotational viscometer, adapted from [2]



(b) Observed deviation of flow curve due to viscosity measurements at non-laminar flow conditions. Measurement interval is inadequate for curves 1 and 2, but adequate for curve 3. Adapted from [2].

reasonable approximation of data at the lower end of the shear rate spectrum as the mean can be disproportionately influenced by outliers in the data; especially when considering that a mere 12 viscosity readings per shear rate were obtained. Yet, it is arguably preferred to disregard low shear rate measurements entirely and attempt to acquire more reliable data for  $0.1 \leq \dot{\gamma} \leq 1$  1/s. To this end, it is important know the underlying cause(s) of the observed scatter. These, together with plans of mitigation are listed below (arranged by decreasing order of likelihood).

1. *Non-laminar flow conditions.* To guarantee the reliability of the results, laminar flow should have fully developed is the zone adjacent to the rotary bob prior to taking measurements. Failing to meet the aforementioned criterion causes underestimation of true viscosity, an is also illustrated by Figure 7.3b. For shear rates  $< 1$  1/s, the required time to form laminar flow conditions to develop is inversely proportional to the shear rate, corresponding to Equation 6.8. Though the aforementioned criterion was respected while drafting the test plan; the presence of transient flow conditions at the time of measurement cannot be fully ruled out. In this sense, experimentation with the sampling interval  $\Delta t_m$  at low shear rates is possibly the best plan of action.
2. *Surface imperfections on the concentric measurement cylinder.* The used concentric bob had some minor surface imperfections. As a consequence, it is possible that the perceived shear resistance is misleadingly augmented. The latter causes a deviation is the viscosity measurement which is most critical for low shear rates as the added resistance due to surface imperfections is (relatively) the largest. Re-polishing of the measurement cone should in theory solve the aforementioned issue. Alternatively, a new concentric cylinder could be used.
3. *Air inclusions in the test fluid.* Though extensive provisions were taken to prevent the inclusion of air in the test samples, the presence of several bubbles in each specimen was inevitable. Due to the limited sample size of 15 mm, a small number of bubbles can have a real influence on the measured dynamic viscosity. For homogeneous two-phase solutions, several expressions have been introduced to quantify viscosity. Amongst others, authors which contributed to the development of theory to describe the viscous behavior of two-phase solutions include: McAdams *et al.* (1942) ([16]), Cicchitti *et al.* (1960) ([7]) and Dukler *et al.* (1964) ([12]). A commonality between the two-phase viscosity calculated form the relationships proposed by the aforementioned authors, is that they rely on the mass-averaging of viscosities. The latter implies that the presence of air in the sample would decrease viscosity. Although this research found that the differences between ordinary (without visible air-inclusions) and

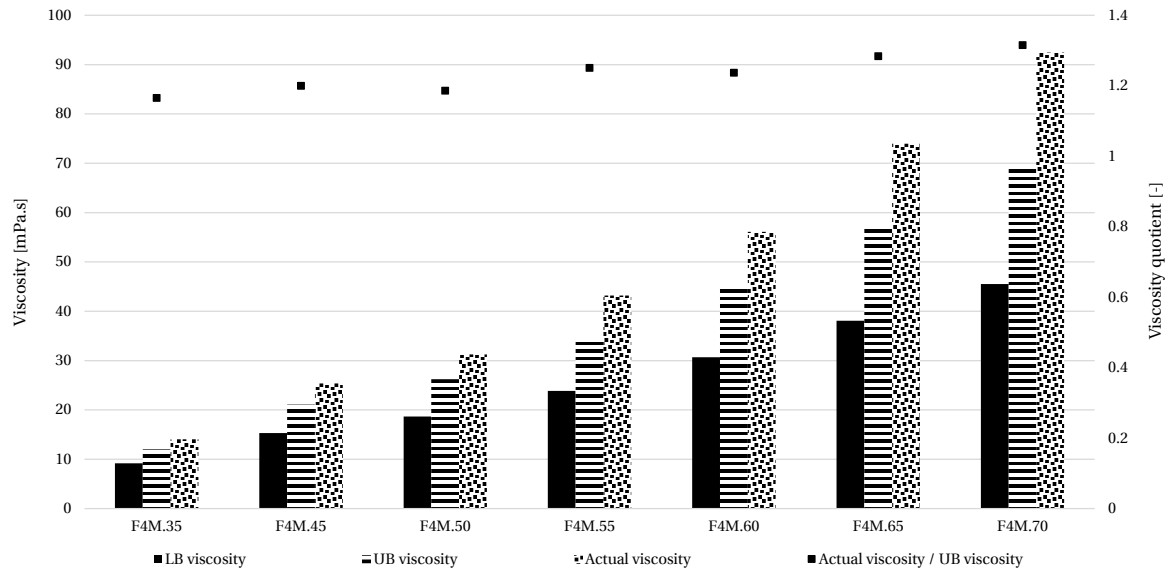


Figure 7.4: Actual, manufacturer lower bound and manufacturer upper bound viscosity. Actual viscosity concerns the mean viscosity for a shear rate of 1  $1/s$ . Additionally, the quotient of actual viscosity over manufacturer upper bound viscosity plotted on the secondary y-axis.

desired samples were negligible, deairing of samples should be part of the sample preparation routine.

Due to time restrictions, it was not possible to re-execute the rheological experiments while accounting for the above recommendations. Besides, as the observed dispersion at lower shear rates is within the acceptable range, the data is not excluded from further analysis.

### 7.1.1. Detailed analysis

To look into the consistency of the fluid preparation method, the obtained viscosity at a certain concentration is compared to the lower and upper bound viscosity provided by the manufacturer (which is respectively calculated in accordance with Equations 6.3 and 6.4). The results of the aforementioned consistency analysis is depicted in Figure 7.4. Please note that the true viscosities shown in Figure 7.4 are the averages obtained at a shear rate of 1  $1/s$ . It is unclear for which shear rate Equations 6.3 and 6.4 have been drafted by Dow. Therefore, some uncertainty remains with respect to Figure 7.4. From Figure 7.4, it follows that the quotient of actual viscosity over manufacturer upper bound viscosity is rather stable and varies between 1.2 and 1.3. The minor increase of the viscosity quotient, is attributed to the modest quantity of powder (3 to 6 *grams* per liter) used to create each batch. Although precautions were taken by mixing the bulk of powder prior to use, the small sample size may give rise to noticeable deviations between mean properties (chiefly regarding water content  $\theta_p$  and reactivity) of the bulk of HPMC and the sampled amount. These effects are more relevant as the size of the specimen decreases, thus for lower concentrations. Measurement and rounding errors contribute to further diversification of viscosity quotient.

Despite a consistent fabrication process along the lines of 6.1.1 and 6.1.2, the viscosity consequently exceeds the upper bound viscosity estimate provided by the Dow. With regard to the latter point, several hypothesis were drafted, aimed at explaining the aforementioned discrepancy: (I) disregarding the effect of evaporation, as mentioned in 6.1; (II) miscalculation of moisture content; provided an overestimation of  $\theta_p$ , the required quantity of HPMC to obtain the desired concentration is overestimated; (III) better than anticipated dispersion of the HPMC particles; (IV) deviation from the powder's nominal composition in the form of more reactive compound per reference vol-

Batch	$\Theta_p$ [%]	Evaporation [%]	$\tilde{C}$ [%]	$\mu_{LB}$ [mPa·s]	$\mu_{UB}$ [mPa·s]
<b>F4M.35</b>	1.0994	0.6777	0.3657	9.4580	12.4216
<b>F4M.45</b>	1.0994	0.6424	0.4650	15.8317	21.8887
<b>F4M.50</b>	1.0994	0.7894	0.5065	19.4460	27.4155
<b>F4M.55</b>	1.0994	0.6924	0.5570	24.8072	35.7664
<b>F4M.60</b>	1.0994	0.5880	0.6100	31.7806	46.8420
<b>F4M.65</b>	1.0994	0.8051	0.6596	39.8016	59.8133
<b>F4M.70</b>	1.0994	0.9740	0.7018	47.9711	73.2272

Table 7.1: Recalculation of solution concentration and lower and upper bound, expected viscosity; assuming  $\Theta_p = 0\%$  and accounting for evaporation.

ume, due to sampling. With regard to the first two points, Table 7.1 depicts both the moisture content and evaporation by weight (as a percentage of the initial fluid weight) for each batch; alongside the updated concentration  $\tilde{C}$  and re-evaluated lower and upper bound viscosity estimates,  $\mu_{LB}$  and  $\mu_{UB}$  respectively. As becomes clear from Table 7.1, assuming  $\Theta_p = 0\%$  as well as accounting for evaporation yields a minimal increase of the expected viscosity. Hence, the first two suggested causes of the discrepancy in actual and anticipated viscosity do not provide a closing explanation. Provided the right equipment, the dispersion of HPMC is water not a highly complex process. Knowing so, chances of significantly improving this process compared to the manufacturer are slim. Hence, the sampling hypothesis is once more advanced as a possible explanation. However, provided the shear rate underpinning Equations 6.3 and 6.4 is  $>10$  1/s, there is a reasonable chance the discrepancy is explained by not observing shear thinning effects at elevated shear rates. For now, as the observed discrepancy is consistent for all concentrations and therefore does not affect the usability of the fluid; the effort to find a closing explanation is seized. Possibly, an explanation is offered by future research.

Despite surpassing the manufacturer's viscosity prognosis, the consistent viscosity quotient as plotted in Figure 7.4 permits further exploration of viscosity development as a function of solution concentration. To this end, average viscosity as function of shear rate is plotted for all seven batches in Figure 7.5. The labels next to the data points in Figure 7.5 show the sample standard deviation  $s_n$  at each shear rate. To validate that the sample standard deviation is the good measure of data variability, histograms were drafted. As the scatter of the viscosity readings is related to the shear rate, data normalization over all shear rates simultaneously would yield ambiguous results. Instead, data normalization is conducted per shear rate. Due to large differences in the viscosity measurements between batches, the aforementioned normalization was carried out for each batch individually. The assassinated process entails the division of each measurement through the mean viscosity for the examined batch at the shear rate of interest. Hence, finally, a sample population of per shear rate consists of (7 x 12) 84 normalized viscosity readings. Due to the large number of shear rates (41 in total), histograms and corresponding distribution functions were exclusively drafted for the following shear rates: 0.1, 0.0316, 1, 3.16, 10, 31.6, 100, 316 and 1000 1/s. For all histograms, bin width is set to 1/4 of the standard deviation  $\sigma_p$  of the population of normalized viscosity measurements for the shear rate of interest. With the exception of Figure 7.6, which depicts the histogram corresponding to  $\dot{\gamma}=316$  1/s, the resulting plots are part of section II of the Appendix. Based on the insight provided by Figure 7.6, the viscosity readings per shear rate are regarded as normally distributed. Therefore, the use of (sample) standard deviation is a reasonable choice to describe the dispersion of data. Additionally, several other observations are made based on the information provided by the histograms and corresponding distribution functions:

- All considered data populations are reasonably fitted by a normal distribution function. This notion is particularly interesting for the histograms corresponding to the lowest shear rates

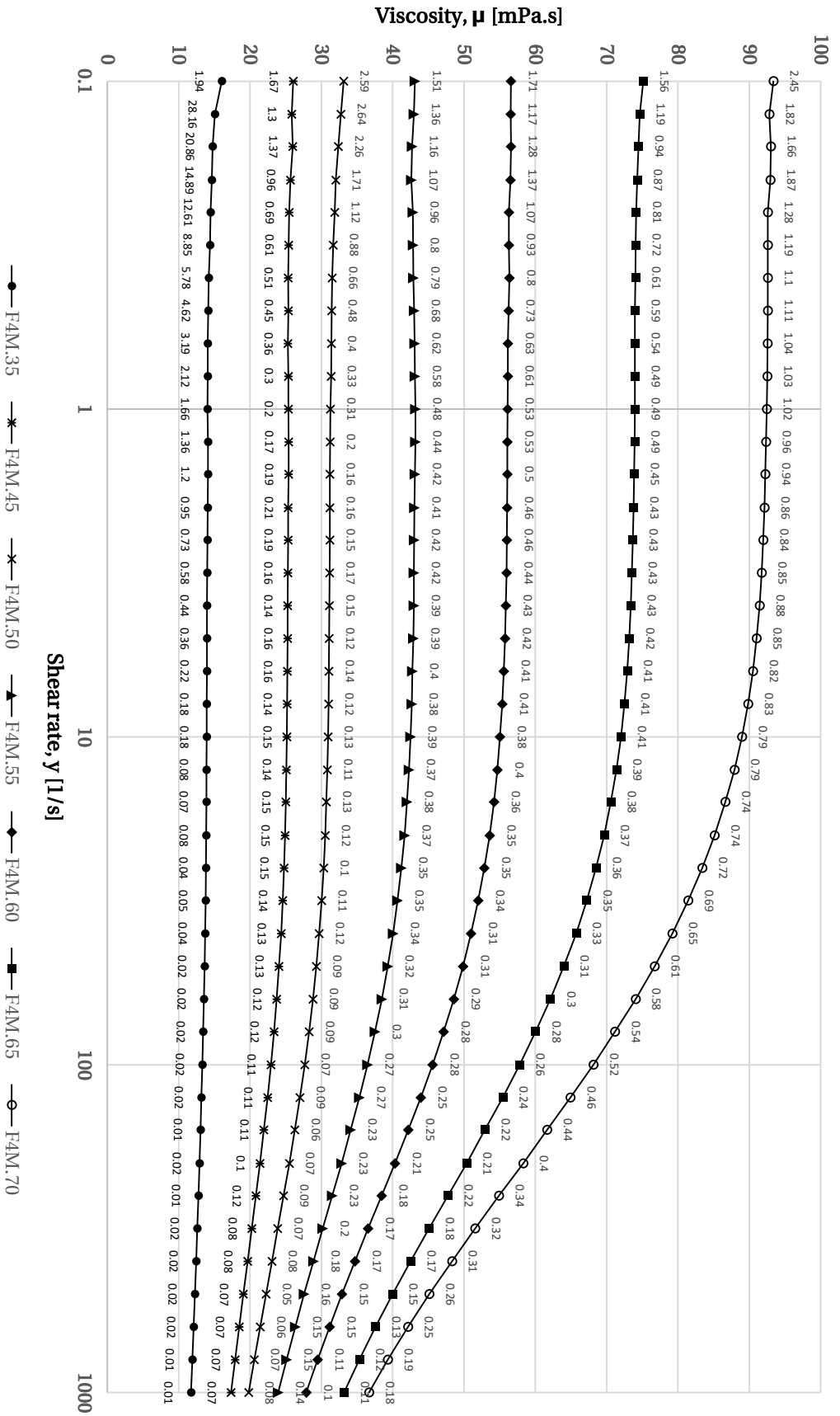


Figure 7.5: 12-point average viscosity as a function of shear rate for each of the seven tested fluid batches. Labels show standard deviation of the data underlying each average shown in the above graph.

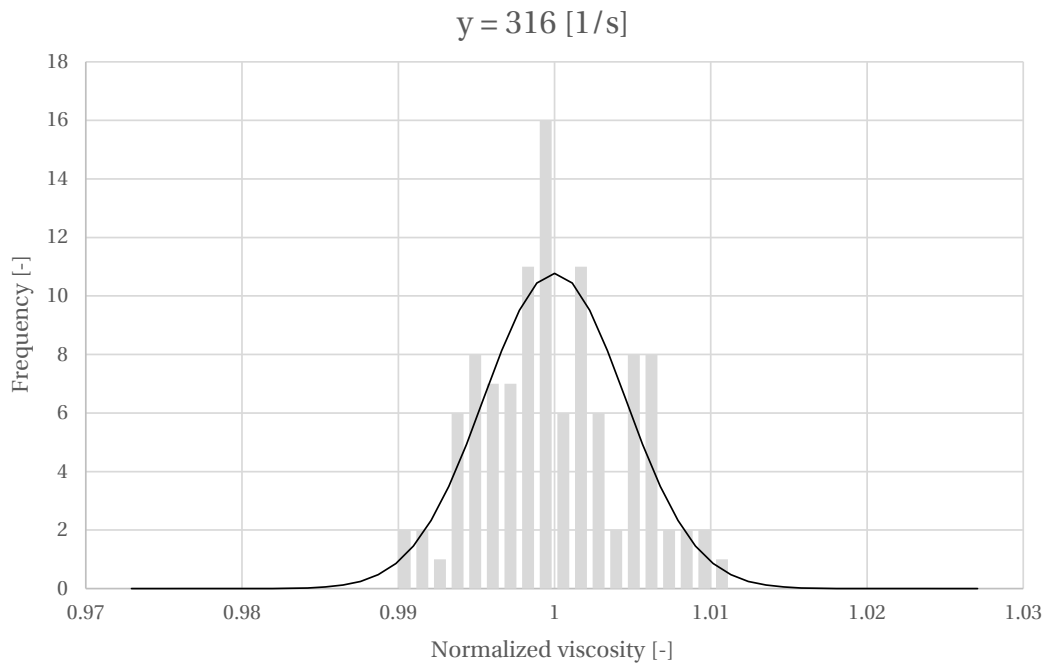


Figure 7.6: Histogram of normalized viscosity readings at  $\dot{\gamma} = 316$  1/s for the ensemble of all seven batches. Binwidth corresponds to  $\sigma_p/4$ , where  $\sigma_p$  is the standard deviation of the aforementioned population of 84 normalized measurements.

(0.1 and 0.316 1/s). Naturally, steepness of the normal distribution function decreases as a result of the increased scatter (and thus larger standard deviation) of measurements, an previously discussed in 7.1. As also indicated earlier, the scatter seems neatly centered around the median value. Consequently, it is concluded that the mean and median are spaced closely together. The latter gives reason to believe that the source of the increased variability at low shear rates is also normally distributed. Therefore it is more likely that the dispersion of data is related to transient flow conditions at the time of measurement, instead of the influence of surface imperfections or air inclusions. As, respectively, the aforementioned two sources would skew the curve, either towards the right and left, respectively.

- The steepness of the normal distribution functions increases with shear rate, indicating improved reliability of the measurements. This observation diminishes the likelihood that the increased variability at lower shear rates is exclusively due to entrapped air, as this influence is independent of the shear rate unlike the causes proposed by the remaining hypotheses.

Upon close inspection of Figure 7.5, several behavioral trends are noticeable. First, for low concentrations the fluid practically behaves as a Newtonian fluid over the entire range of shear rates. For higher viscosity fluids, the shear-thinning behavior at higher shear rates becomes progressively more pronounced. It is unlikely that this is related to the concentration of the fluid, as concentrations are in fact relatively comparable for all batches. Instead, the observation seems it related the viscosity itself, which depends on measure and nominal length cellulose polymers in the solution. Consequently, it is clear that a high non-linear relationship describes the dependency of viscosity on concentration. Which is consistent with the trend proposed by Equations 6.3 and 6.4. However, aforementioned formulas do not explain the progressive non-linearity in the viscous properties. It is hypothesized that this is due to preferential alignment of the polymers in the solution (parallel to the direction of shearing) at higher shear rates. Whereas the distribution of the polymeric chains expresses a higher degree of randomness under stagnant or low shear conditions. The aforementioned hypothesis would also provide an explanation to the convergence of the flow curves for high

shear rates.

The non-Newtonian flow behavior of the tested HPMC solutions could lead to behavioral discrepancies between the model and prototype as the viscosity of water is unaffected by  $\dot{\gamma}$ . Hence, it is advisable to estimate expected shear rates beforehand and assess whether the viscosity decrease is within acceptable limits. Adjusting the viscosity for the anticipated decrease at nominal shear levels can be considered if the shear rate is uniformly distributed over the sample (in example for earthquakes). However, this measure should be approached with caution as is further illustrated by the following example. Assuming the fluid concentration was such that dynamic and diffusive timescales are synchronized at the nominal shear rate during the event; when the vibration ceases and  $\dot{\gamma}=0$  1/s, fluid viscosity reassumes an improperly scaled value. Consequently, the duration of all dissipative processes which play-out in the aftermath of the earthquake is stretched with respect to reality due to the mismatch in viscosity and g-level. The example, illustrates that (depending on the intended goal of the research) viscosity adjustments to account for shear thinning effects can be unjustifiable. In this case another type of viscous pore fluid should be used. Alternatively, the non-Newtonian flow characteristics of other brands of viscosity grades of Methocel<sup>®</sup> can be explored, as these could exhibit more favorable flow behavior at high shear rates.

Another observation with respect to Figure 7.5, considers the reduction of the interval for ideally viscous behavior. For higher concentrations, the left extremity shifts of the aforementioned interval gradually moves towards the left-hand side of Figure 7.5. This behavior is in line with trends indicated by Dow ([11]) for high viscosity grades of Methocel<sup>®</sup> F. Finally, Figure 7.5 demonstrates increase in sample standard deviation  $s_n$  for shear rates  $<1$  1/s. This declaration was first made in 7.1 on the global data analysis. Possible causes relating to last observation are also presented in the aforementioned section.

To provide a comprehensive overview of the uncertainty of the viscosity measurements, section III of the Appendix contains (95%) confidence intervals plotted for viscosity as a function of concentration for the following shear rates: 0.1, 1, 10, 100 and 1000 1/s. The graph corresponding to a shear rate of 0.1 1/s is included in the main report as Figure 7.7. From Figure 7.7 it is clear that, in terms of absolute magnitude, the width of the confidence interval is constant. Hence, the relative error is smaller at higher concentrations. This indicates that high concentration fluids are less sensitive to the noise-inducing sources discussed in 7.1. Unlike prior observations, the latter favors the hypotheses which relates the increased dispersion to imperfections of the concentric bob. Looking at the remaining figures of section IV of the Appendix; at higher shear rates, the width of the confidence interval increases with concentration. Though the absolute error consequently increases, the relative error remains constant. As this observation is in line with anticipated trends, it is not further investigated.

### 7.1.2. Data fitting

To extrapolate the results of this research into a useful guideline for the fabrication of aqueous HPMC solutions, it is attempted to capture the observed viscosity trends in the form of two generic equations, respectively applicable to the following shear rate domains: (I)  $0.1 \leq \dot{\gamma} \leq 10$ ; (II)  $10 < \dot{\gamma} \leq 1000$ . To derive the generic expressions to approximate the data in the aforementioned shear rate domains; viscosity data (as a function of concentration) is fitted by a power law derived from least square regression. To account for the true variability of the data, individual viscosity measurements are used instead of the mean value per batch. Like before, due to the shear rate dependency of viscosity, the analysis is carried out for one shear rate at a time. Viscosity data are fitted using a power law for a section of shear rates. These are presented in Table 7.2 and 7.3, where the former corresponds  $0.1 \leq \dot{\gamma} \leq 10$  and the latter to  $10 < \dot{\gamma} \leq 1000$ . Figures associated with the data fitting procedure are part of section IV of the Appendix. Here, the best fit relationship alongside with determination coefficient ( $R^2$ ) is presented in the bottom right corner. As all of the fitting relationships are of

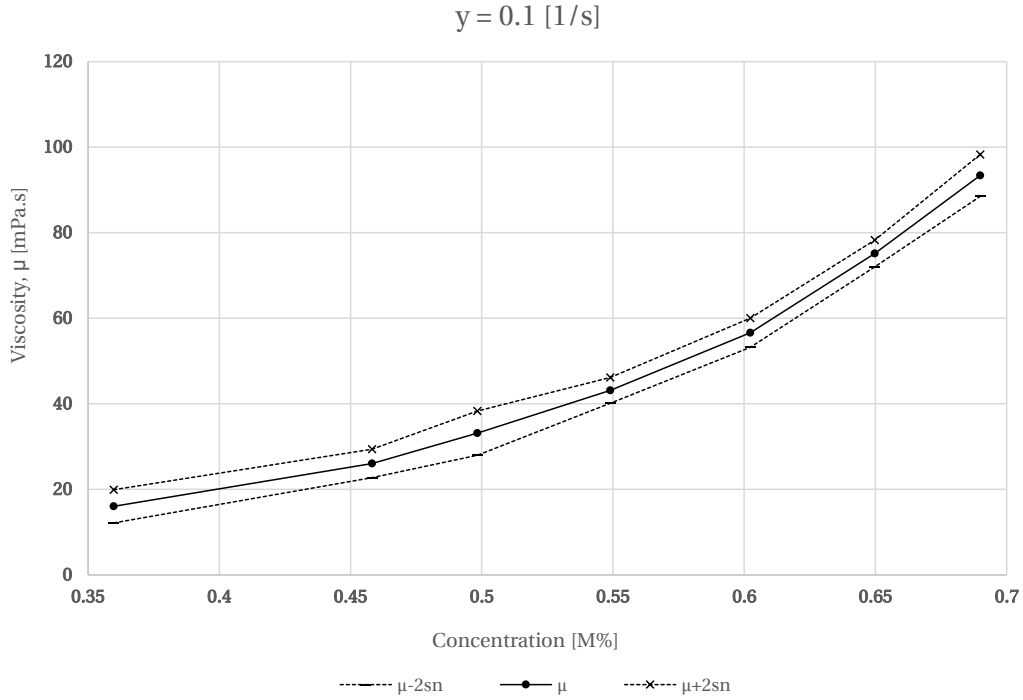


Figure 7.7: Mean viscosity as a function of concentration for  $\dot{\gamma}=0.1 \text{ 1/s}$  and 95% confidence bounds following from the normal distribution of viscosity readings.

the same type, they are represented in a basic form as illustrated by Equation 7.1.

$$\tilde{\mu}_f = A \cdot C^B \quad (7.1)$$

Where  $C$  is the concentration of the fluid by mass and both  $A$  and  $B$  are fitting constants. For a the considered shear rates, constants  $A$  and  $B$  and associated  $R^2$  are conveniently part of Tables 7.2 and 7.3. Based on Table 7.2 and 7.3, approximation of  $\tilde{\mu}_f$  by the general expression provided by Equation 7.1, yields satisfactory results. Moreover, both  $A$  and  $B$  exhibit a clear dependency on the shear rate  $\dot{\gamma}$ . Hence, to obtain a general equation with relates the viscosity  $\mu_f$  to both concentration  $C$  and shear rate  $\dot{\gamma}$ , trends in  $A$  and  $B$  are also approximated by means of a power law. Approximations of the two aforementioned variables are respectively denoted as  $\tilde{A}$  and  $\tilde{B}$ . To ensure that the generic viscosity expression is dimensionally correct, the shear rate  $\dot{\gamma}$  is nondimensionalized through division by the unity shear rate,  $1 \text{ 1/s}$ . In the following, the resulting parameter is referred to as  $\tilde{\gamma}$ . The aforementioned fitting procedure yields the following general expression for  $\tilde{A}$ :

$$\tilde{A} = \begin{cases} 251.51 \cdot \tilde{\gamma}^{-1.500 \cdot 10^{-2}}, & \text{for } 0.1 \leq \tilde{\gamma} \leq 10 \\ 746.80 \cdot \tilde{\gamma}^{-3.360 \cdot 10^{-1}}, & \text{for } 10 < \tilde{\gamma} \leq 1000 \end{cases} \quad (7.2)$$

It should be noted that the approximation provided by Equation 7.2 was drafted on the trends in  $A$  and  $B$  for the following shear rates from table 7.2: 0.631, 1, 3.61, 6.31 and 10  $1/s$ . The to decreased reliability of viscosity measurements for  $\dot{\gamma}=0.1$  and  $\dot{\gamma}=0.316 \text{ 1/s}$ , their respective fitting constants were not considered when drafting the Equation 7.2.

Analysis of the fitting constants for  $10 < \tilde{\gamma} \leq 1000$  as depicted in Table 7.3, yielded the following expression for  $\tilde{B}$ :

$$\tilde{B} = \begin{cases} 2.8929 \cdot \tilde{\gamma}^{-5.000 \cdot 10^{-3}}, & \text{for } 0.1 \leq \tilde{\gamma} \leq 10 \\ 4.1259 \cdot \tilde{\gamma}^{-1.240 \cdot 10^{-1}}, & \text{for } 10 < \tilde{\gamma} \leq 1000 \end{cases} \quad (7.3)$$

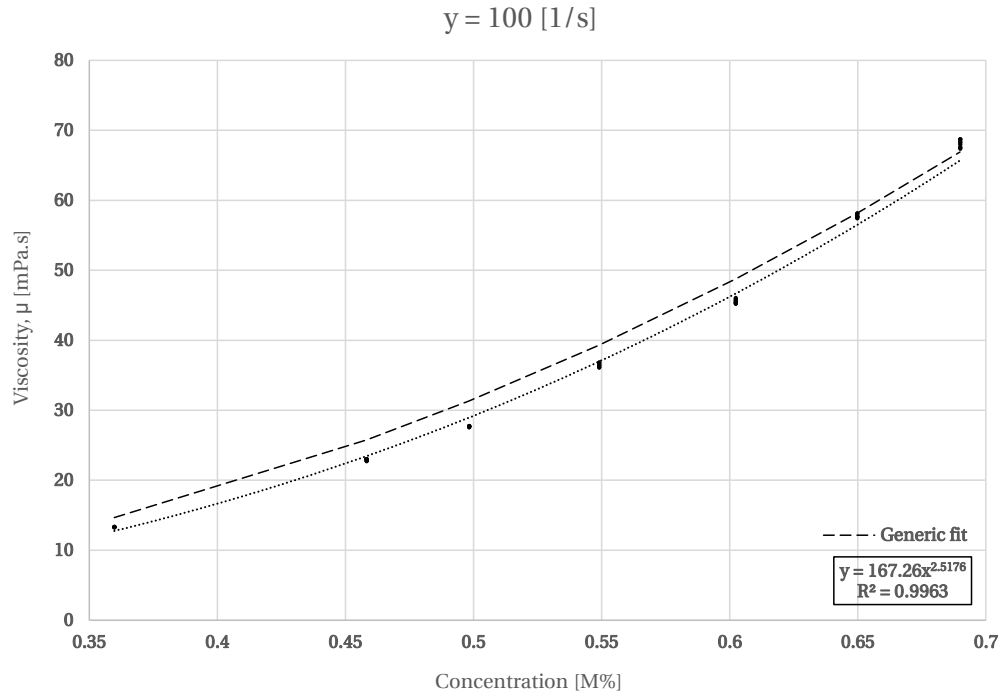


Figure 7.8: Rheological measurements at different concentrations for  $\dot{\gamma} = 100$  1/s, accompanied generic and least square power fit ( $y = Ax^B$ ). For the latter of the two approximations, the corresponding equation and  $R^2$  is depicted in the bottom left corner.

For both Equation 7.2 and 7.3 the leading constant has the unit  $mPa \cdot s$ . Due to its relation to  $\tilde{\gamma}$ , the power coefficient is of undetermined dimension. Provided Equation 7.2 and 7.3 the generic fit for viscosity is provided by Equation has the following general form:

$$\tilde{\mu}_f = \tilde{A} \cdot C^{\tilde{B}} \quad (7.4)$$

Where  $\tilde{A}$  and  $\tilde{B}$  are in determined accordance with Equation 7.2 and 7.3, respectively. For a variety of  $\tilde{\gamma}$ ,  $\tilde{A}$  and  $\tilde{B}$  were evaluated and are part of Table 7.2 and 7.3.

Finally, to determine how well the variation of the measurements is captured by the general approximation as shown by Equation 7.4, the determination coefficient  $\tilde{R}^2$  is computed. Recalling that the approximation is of the form  $\tilde{\mu}_f = \tilde{A} \cdot C^{\tilde{B}}$ , the function is linearized first. This yields the following expression:

$$\ln(\tilde{\mu}_f) = \ln(\tilde{A}) + \tilde{B} \cdot \ln(C) \quad (7.5)$$

Following the application of the least square regression theorem to Equation 7.5,  $\tilde{R}^2$  is quantified. Corresponding values are presented in Table 7.2 and 7.3. Upon inspection of the obtained determination coefficients, it is clear that the generic expression provides an acceptable way to approximate viscosity  $\mu_f$ , provided the concentration  $C$  and non-dimensional shear rate  $\tilde{\gamma}$ . As is logically expected,  $\tilde{R}^2$  is always smaller than  $R^2$  (which corresponds equation 7.1).

To graphically illustrate how accurately the trend in the viscosity data is represented by the generic fit, this comparison is provided by Figure 7.8 for  $\dot{\gamma} = 1$  1/s. From Figure 7.8, it is clear that viscosity values are slightly overestimated by the generic approximation. However, the absolute deviation is more or less constant. As a consequence the relative error is decreased from  $\approx 15\%$  at a concentration of 0.35%, to  $\approx 3\%$  at a concentration of 0.70%. For all other shear rates listed the Table 7.2 and 7.3, the approximation by Equation 7.4, is shown by the figures in section IV of the Appendix; alongside the experimental data and associated least squares approximation by Equation 7.1.

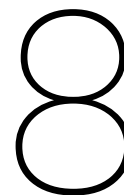
$\tilde{y}$ [-]	A [mPa.s]	B [-]	$R^2$ [-]	$\tilde{A}$ [mPa.s]	$\tilde{B}$ [-]	$\tilde{R}^2$ [-]
<b>0.100</b>	234.70	2.7285	0.9746	260	2.93	0.968
<b>0.316</b>	248.15	2.8626	0.9901	256	2.91	0.990
<b>0.631</b>	251.74	2.8930	0.9921	253	2.90	0.992
<b>1.000</b>	251.77	2.8939	0.9923	251.5	2.893	0.9923
<b>3.160</b>	249.78	2.8882	0.9926	247.2	2.876	0.9926
<b>6.310</b>	245.96	2.8732	0.9932	244.7	2.866	0.9932
<b>10.00</b>	240.73	2.8513	0.9936	243.0	2.860	0.9936

Table 7.2: Fitting coefficients for Equation 7.1 and 7.4, together with determination coefficients  $R^2$  and  $\tilde{R}^2$ ; provided  $0.1 \leq \dot{\gamma} \leq 10$ .

$\tilde{y}$ [-]	A [mPa.s]	B [-]	$R^2$ [-]	$\tilde{A}$ [mPa.s]	$\tilde{B}$ [-]	$\tilde{R}^2$ [-]
<b>31.60</b>	213.78	2.7363	0.9951	234.1	2.689	0.9502
<b>63.10</b>	187.86	2.6196	0.9959	185.5	2.468	0.9695
<b>100.0</b>	167.26	2.5176	0.9963	158.9	2.331	0.9748
<b>200.0</b>	134.15	2.3269	0.9966	125.9	2.139	0.9772
<b>316.0</b>	112.55	2.1751	0.9967	108.0	2.021	0.9767
<b>501.0</b>	92.989	2.0096	0.997	92.48	1.909	0.9753
<b>631.0</b>	84.414	1.9270	0.9971	85.58	1.855	0.9740
<b>794.0</b>	76.590	1.8453	0.9972	79.23	1.803	0.9719
<b>1000</b>	69.468	1.7640	0.9972	73.32	1.752	0.9692

Table 7.3: Fitting coefficients for Equation 7.1 and 7.4, together with corresponding determination coefficients  $R^2$  and  $\tilde{R}^2$ ; provided  $10 < \dot{\gamma} \leq 1000$ .





## Conclusions

For the sake of clarity the conclusions are subdivided into two categories. Firstly, 8.1 addresses concluding remarks with regard to the preparation methodology for aqueous solutions of HPMC. Secondly, 8.2 presents conclusions relating to the obtained rheological results of the seven fluid batches as well as the generic fit which was derived from this data.

### **8.1. Conclusions with regard to the preparation process**

Several important lessons were learned relating to the preparation methodology. During recipe drafting, the moisture content of the HPMC powder is accounted for as prolonged storage of gradually hydrates HPMC molecules and consequently increases the specific weight of the powder. Thereby reducing the quantity of reactive compound per reference mass. When this effect is not appreciated, the viscosity of the resulting solution is likely lower than anticipated. Determination of the moisture content is straightforwardly executed, provided the availability of a suitable heat source. Experience with the determination of the water content indicates that the temperature at which the powder is dried may cause water, which is part of the crystalline structure of HPMC molecules, to evaporate. It seems that this form of dehydration negatively impacts the formation of polymers upon the addition of the powder to water, which consequently has an inhibitory effect on viscosity development. Consequently, solutions which employ HPMC powder dried at elevated temperatures (105°C) do not reach intended viscosity levels. The latter is not true for solutions crafted from powder dried at more moderate temperatures (42°C).

The preparation of HPMC solutions by use of the hot/cold technique, requires the HPMC powder to be added to volume water of sufficiently high temperature (>90°C). The latter ensures optimal exploitation of the insolubility of HPMC in hot water, which promotes the dispersion of particles to obtain a homogeneous hot slurry where all particles are evenly wetted. In case the warm water is transferred between holding cups prior to the addition of HPMC powder, the heat capacity of the mixing container should be appreciated as it decreases the water temperature. Compensatory measures include: (I) further elevation of the temperature of the water; (II) preheating the container. The agitation following the addition of the HPMC to the hot water, should be thorough as sufficient shear needs to be applied to the slurry to prevent the formation of clumps of unhydrated powder. In this respect, the use of a blender or high shear mixer is advisable. During agitation of the slurry, the entrapment of air should be limited to the largest possible extend to suppress the formation of foam on top of the solution. The homogeneous slurry of HPMC in warm water is cooled through the addition of cold (10°C) water. The drop in temperature initiates the dissolution of HPMC particles, thereby marking the start of viscosity development. This process is continued as the solutions cools down further towards the hydration temperature. Once, agitation is terminated, a uniform, fully

translucent fluid emerges. The entrapment of air was shown to be limited for all samples which were prepared in according to the methodology discussed in this research. Any remaining entrapped air is fully expelled over time due to the buoyant force acting on the air bubbles. However, for high viscosity solutions ( $>80 \text{ Mpa}\cdot\text{s}$ ) this process is time intensive due to increased drag on the raising air bubbles, linked to the higher viscosity. In latter case, the elimination of air is aided by the exposing the fluid to a (partial) vacuum.

## 8.2. Conclusions regarding the rheological results and generic fit

Results from the rheological experiments indicate that the advocated method of preparation allows for the production of solutions with homogeneous viscous properties. Viscosity curves corresponding to the three (randomly sampled) 15 ml specimens, effectively coincide. The latter indicates both the effect of prolonged stagnation as well as deairing has no perceivable effect on the viscosity. The former point indicates that it is possible to create viciously saturated samples for centrifuge testing some time in advance. However, although deairing has no observable effect on the recorded viscous behavior at various shear rates; it is ill-advised to use fluid which has not been deaired in centrifuge experiments. This is due to effect of entrapped air on the compressibility of the pore fluid. The latter is particularly important for fully saturated samples which aim to capture undrained soil behavior. Consequently, best practice dictates that the viscous fluid is deaired before use in the centrifuge. However, untreated fluid specimens may be used to infer the viscosity of the solution; provided that the scale and abundance of entrapped air is within reasonable limits.

Another clear observation which follows from the results considers the shear rate dependency of viscosity for the HPMC visocus fluids. With the exception of solutions with a viscosity  $<10 \text{ mPa}\cdot\text{s}$ , non-Newtonian flow behavior in the form of shear thinning is observed at the upper end of the shear rate spectrum. The extend to which this behaviors manifests itself is seemingly related to the viscosity. High viscosity mixtures, significantly express higher degrees of contractive behavior when compared to low concentration solutions. In part, it is logical that low viscosity fluids exemplify (nearly) Newtonian flow behavior due to the lower HPMC concentration. However, as indicated both by the experimental results and Dow, viscosity and concentration are correlated in a highly non-linear manner. As the development of viscosity is related the degree to which individual HPMC molecules form polymeric chains as well as the respective size of these chains, it is hypothesized that these polymeric structures react different to shear than individual HPMC molecules. Under high ( $>100 \text{ 1/s}$ ) shear rates, the polymers have a preferential orientation which coincides with the direction of shearing. The shift towards the aforementioned state from a state of random orientation, is accompanied by a large decrease in apparent viscosity. Although the ultimate shear rate was limited to  $1000 \text{ 1/s}$ , observations point towards the possible convergence of the viscosities for solutions of different concentrations, provided  $\dot{\gamma} \gg 1000 \text{ 1/s}$ .

The effect of shear thinning might have disadvantageous consequences when HPMC solutions (which employ high viscosity grades of Methocel<sup>®</sup> brand F, specifically F4M) are used for centrifuge testing. Unlike water, where the viscosity is independent of shear rate; tested aqueous solutions of HPMC are (especially at higher concentrations) extremely sensitive to fluctuations in shear rate. Based on this observation; arguably, the use of HPMC fluids is exclusively justified when the shear rate is uniformly distributed over the soil sample. Experiments which are characterized by a wide range of shear rates, might yield global results which deviate substantially from reality as the apparent viscosity differs for each shear rate regime. Therefore, provided capturing global soil behavior is the predominant research interest, viscous fluids crafted form Methocel<sup>®</sup> type F4M are arguably disqualified. Alternatively, it is possible to account for anticipated shear thinning effect by increasing the concentration of the solution. In this case, it is important to observe the possible detrimental effects ensuing from this compensatory measure, specifically when the shear rate varies in space and/or time.

When rheological measurement are compared to the formula to estimate (lower and upper bound) viscosity as proposed by Dow [11], it is found that all fluid batches exceed the upper bound viscosity estimate. In an attempt to unite the deviating observation, the concentrations of the tested solutions were corrected for evaporated water during he preparation process ( $\approx 1\%$ ). Additionally, it was assumed that the moisture content of the powder equals 0%. However, The combined set of measures proved insufficient to close the gap between the rheological data and the anticipated viscosity. Consequently, several hypotheses were proposed to unify the experimental results with the theoretical estimates. Alternatively, the validity of Equations 6.3 and 6.4 (as proposed by Dow) is possibly only warranted for a shear rate well above 1  $1/s$  (the shear rate for which Figure 7.4 was drafted. Due to the shear thinning effect, the viscosity decreases which would decrease the viscosity discrepancy. Finally, the representativity of the small quantities of HPMC (used to craft the solutions in this research) with respect the bulk of (25  $kg$ ) HPMC powder is under debate. Due to sampling, the moisture content and amount of reactive material per reference volume could deviate from the mean properties of the entire batch; possibly leading to the observed inconsistencies. Based on the available observations is was proven impossible to confidently point out the source of the discrepancy. Fortunately, the overestimation is consistent over all measurement; enabling the further investigation of apparent viscosity as a function of concentration and shear rate. Hopefully, future research provides a conclusive explanation with regard to elevated viscosities.

Despite the remaining questions surrounding the obtainment of higher than anticipated viscosities, it remains possible to formulate a generic expression for the viscosity as a function of both concentration and shear rate. The proposed fit consists of a power law ( $\mu = AC^B$ ) where  $C$  is the solution's concentration and  $A$  and  $B$  are shear rate dependent scalers. When the generic expression was evaluation for a set of 16 shear rates, satisfactory results are obtained. Compared to the rheological measurements, the generic fitting formula has a determination coefficient of at least 0.9502. The latter illustrates that the fit provides a reasonable estimate of the expected viscosity provided concentration and shear rate. Currently, it seems that the availability of this relationship can accelerate the recipe drafting for HPMC viscous fluids for specific test purposes. However, for now, it is recommended to verify the viscous properties of solutions for which the required concentration was determined using the generic formula.



# 9

## Recommendations

Although the results presented in this research are largely satisfactory, it is possible to further elevate quality and completeness. Areas of interest to which the latter notion applies, are discussed in this section. Firstly, research into the effect of temperature on the fluidity of the solutions was omitted due to a advantageous set of boundary conditions applicable to the research for which the developed viscous fluids are intended (see chapter 2 for more information). However, it is imaginable that the influence of temperature is not negligible for other types of research involving the centrifuge. In this respect, it is advised to look into the influence of the nominal ambient temperature in the centrifuge room on the viscosity of HPMC pore fluid. This would involve rheological research aimed at quantifying the temperature dependency of the viscosity of HPMC solutions at different concentrations. For the sake of completeness, the associated test plan should preferably also include shear rate variations. Additionally, a simplified model, aimed at describing the transfer of heat from the air to a saturated soil sample in the centrifuge room, should be developed. The prime objective of this model would consist of the quantitative assessment of the timescale associated with the (partial) transfer of ambient heat to the specimen, preferably as a function of sample geometry and soil to fluid ratio. Such a model would form a consistent, scientific to determine whether temperature influence should be compensated by augmenting the concentration of the viscous fluid. Alternatively, a climate regulatory system could be installed in the centrifuge room to provide a stable testing environment during testing.

Secondly, as a result of the decision to use a high viscosity grade of Methocel<sup>®</sup> brand F, only very small amounts of powder are required to fabricate viscous fluids in the range of 10-200 *mPa.s*. Although the economical use of the HPMC powder has clear advantages, the sensitivity to dosage and measurement errors is relatively high. The latter diminishes the repeatability of the production process to some extent. Therefore, the option to acquire a lower viscosity grade of Methocel<sup>®</sup> brand F could be considered. Due to the usage of larger quantities of HPMC per reference volume; relatively, the influence of measurement or fabrication errors is reduced. Theoretically, this should benefit the reproducibility of results. The downside of using higher viscosity grade HPMC is the associated increase in density with respect to a fluid of similar viscosity crafted from a high viscosity grade powder. To some extent the increase in density influences the permeability of the soil; causing a larger deviation between model and prototype. Provided that at least Methocel<sup>®</sup> F50 is chosen as an alternative, it is reasonable assumed that this difference is minor and arguably acceptable; as the maximum difference would amount to merely 5%.

Thirdly, in the configuration of the rheometer for this research, the gap between the tip of the concentric bob and the bottom of the sample cup was set to 0 *mm*. Though particularly true for rheometers employing a cone-plate or plate-plate measurement systems (a concentric cylinder measurement system was used for this research), the gap size has a pronounced influence on vis-

cosity readings as is also widely reported in literature by for example [9] and [17]. As reported by Vadodaria (2018) [20], viscosity readings decrease with a decreasing measurement gap. Although it remains unclear as to which measurement gap is considered ideal, it implicates that the configuration of the rheometer influences the viscosity readings to a certain extent. The aforementioned effect has not explicitly been accounted for in this research. Hence, some ambiguity is implicitly present in the obtained results. Future research could seek to quantify the sensitivity of the rheological measurements to changes in the test configuration. Based on this analysis it might be possible to with a higher margin of confidentiality agree of the configuration which yield the most representative measurements.

Finally, as demonstrated by the rheological results, the nonlinear decrease of the viscosity increases for larger shear rates. The observed progressive, shear thinning behavior highlight the importance of a founded understanding of the shear rates exerted on the saturated soil matrix during testing. The latter is specifically relevant when high viscosity fluids are used, in example 100 *mPa·s* fluids for 100g centrifuge experiments. Arguably, the use of HPMC viscous fluid is only warranted in either of the following cases: (I) the soil strains are homogeneously distributed over the entire sample during testing; (II) The research is specifically focuses on capturing the soil behavior associated with a single, precisely defined phenomena. Capturing the global behavior of a system which exhibits strains which are one or several orders of magnitude apart, is virtually impossible provided the observed flow behavior. However, the latter statement only applies to fluids crafted from Methocel<sup>®</sup> F4M. The possibility that flow behavior for aqueous solutions of a different Methocel<sup>®</sup> brands or viscosity grades is distinctly differs from the observations made in this research. In this respect, it is advisable further explore the use of different Methocel<sup>®</sup> products in the future. Additionally, as the analytical quantification of anticipated shear rates is only possible for a handful of scenarios, there is a clear need for a general framework to aid the reliable determination of expected shear rates for centrifuge experiments. It is clear that the development of such a framework from literature and potentially experimental research, would yield an powerful and valuable tool to enforce the prevention of model-prototype discrepancies.

# Bibliography

- [1] O. Adamidis and S.P.G. Madabhushi. On preparation of viscous pore fluids for dynamic centrifuge modelling. Technical report, 2014.
- [2] Anton Paar. Instruction Manual RheoCompass™ Software. .
- [3] Anton Paar. Tips and Tricks on Rotational Measurements. Technical report, .
- [4] A. Askarinejad. *Failure mechanisms in unsaturated silty sand slopes triggered by rainfall*. Phd thesis (no. 21423), ETH Zurich, 2013.
- [5] T De Blaeij. On the modelling of installation effects on laterally cyclic loaded monopiles. 2013.
- [6] S.C. Chian and S.P.G. Madabhushi. Influence of fluid viscosity on the response of buried structures in earthquakes. I. In *Physical Modelling in Geotechnics - Proceedings of the 7th International Conference on Physical Modelling in Geotechnics 2010, ICPMG 2010*, pages 111–115, 2010.
- [7] A. Cicchitti, C. Lombaradi, M. Silversti, G. Soldaini, and R. Zavattarlli. Two-phase cooling experiments – pressure drop heat transfer burnout measurements. *Energia Nucleare*, 7(6):407–425, 1960.
- [8] P.A.L.F. Coleho, S.K. Haigh, and S.P.G. Madabhushi. Effects of successive earthquakes on saturated deposits of sand. *Physical Modelling in Geotechnics - Proceedings of the 6th International Conference on Physical Modelling in Geotechnics 2006, ICPMG 2006*, pages 443–448, 2006.
- [9] GA Davies and JR Stokes. Thin film and high shear rheology of multiphase complex fluids. *Nonnewton Fluid Mechanics*, 148:73–87, 2008.
- [10] M. Dewoolkar, H-Y Ko, A.T. Stadler, and S.M.F. Astaneh. A Substitute Pore Fluid for Seismic Centrifuge Modeling. *Geotechnical Testing Journal*, pages 196–210, 1999.
- [11] Dow Chemical Company. Methocel Cellulose Ethers, Technical Handbook. Technical report.
- [12] A.E. Dukler, W. Moye, and R.G. Cleveland. Frictional pressure drop in two-phase flow. Part A: a comparison of existing correlations for pressure loss and holdup, and Part B: an approach through similarity analysis. *AIChE Journal*, 10(1):38– 51, 1964.
- [13] J. Garnier, C. Gaudin, S.M. Springman, P.J. Culligan, D. Goodings, D. Konig, B. Kutter, R. Phillips, M.F. Randolph, and L. Thorel. Catalogue of scaling laws and similitude questions in geotechnical centrifuge modelling. *International Journal of Physical Modelling in Geotechnics*, 7(3):01–23, 2007. ISSN 1346-213X. doi: 10.1680/ijpmg.2007.070301. URL <http://www.icevirtuallibrary.com/doi/10.1680/ijpmg.2007.070301>.
- [14] Bruce L Kutter. Dynamic centrifuge modeling of geotechnical structures. *Transportation research record*, (1336):24–30, 1992. ISSN 0309051746.
- [15] P.C. Lambe and R.V. Whitman. Scaling for earthquake shaking tests on a centrifuge. In *Conference of Soil Dynamics and Earthquake Engineering*, volume 7, pages 367–378, Southampton, 1982.

- 
- [16] W.H. McAdams, W.K. Woods, and L.C. Heroman. Vaporization inside horizontal tubes II-benzene-oil mixtures. *Transactions of the ASME*, 64(3):193–200, 1942.
- [17] CJ Pipe, TS Majmudar, and GH McKinley. High shear rate viscometry. *Rheologica Acta*, 47: 621–642, 2008.
- [18] Steve Sawyer, Sven Teske, and Morten Dyrholm. The Global Wind Energy Outlook. *Gwec*, 2016.
- [19] Douglas P Stewart, Yie-ruey Chen, and Bruce L Kutter. Experience with the Use of Methylcellulose as a Viscous Pore Fluid in Centrifuge Models. *Geotechnical Testing Journal*, 21(4):365–369, 1998.
- [20] Saumil Sudhir Vadodaria, Amaka J. Onyianta, and Dongyang Sun. High-shear rate rheometry of micro-nanofibrillated cellulose (CMF/CNF) suspensions using rotational rheometer. *Cellulose*, 25(10):5535–5552, oct 2018. ISSN 0969-0239. doi: 10.1007/s10570-018-1963-4. URL <http://link.springer.com/10.1007/s10570-018-1963-4>.
- [21] J. Van Zeben. *Physical modelling of pore pressure development during impact pile driving using geo-centrifuge*. Msc. thesis, Delft University of Technology, 2017.
- [22] X Zeng, J Wu, and B.A. Young. Influence of Viscous Fluids on Properties of Sand. *Geotechnical Testing Journal*, pages 45–51, 1998.

# 10

## Appendix

All relevant figures which were not added to the main report are presented here. For clarity, the appendix is subdivided into four sections to which are referred from the main report, namely:

- I. *Flow curves and boxplots*
- II. *Histograms and normal distribution functions*
- III. *95% confidence intervals for rheological measurements*
- IV. *Rheological measurements plotted alongside least square approximation (power law) and generic fit*

I Flow curves and boxplots

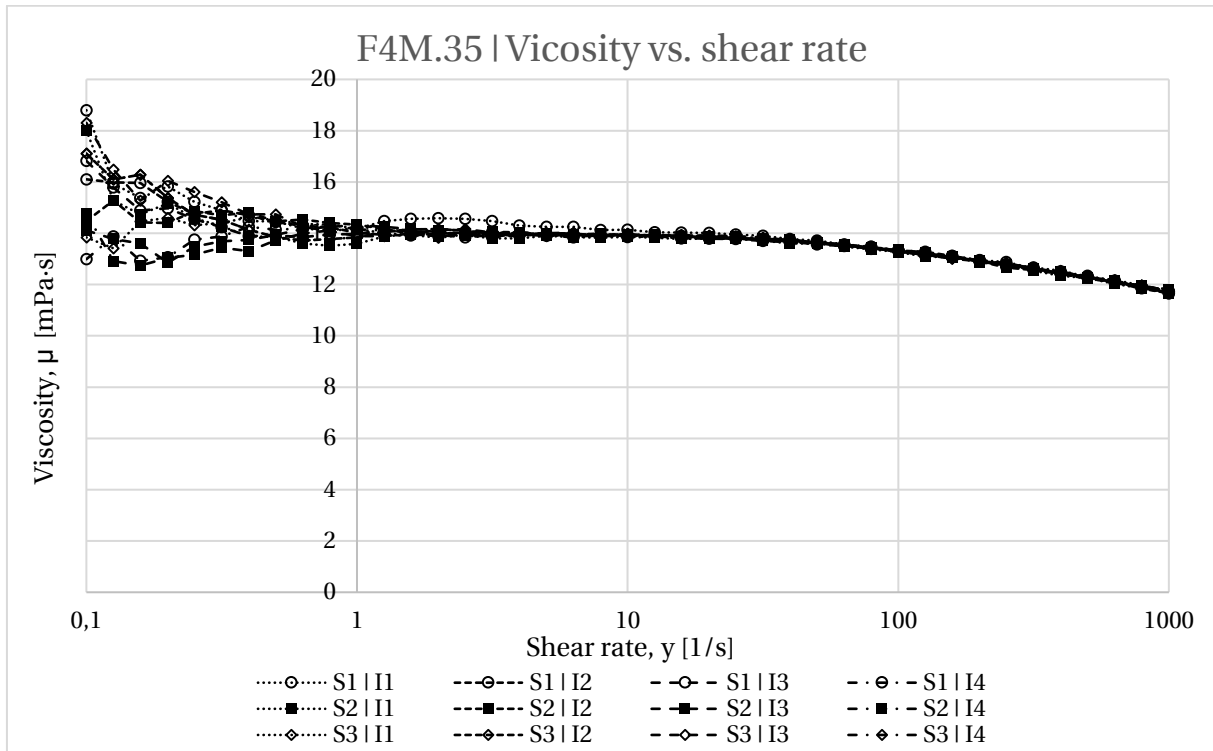


Figure I-1: Flow curves corresponding to batch F4M.35. Legend entries are presented in the format SX | IY, where X codes for the specimen number (1 - not agitated, not deaired; 2 - agitated, not deaired; 3 - agitated, deaired) and Y corresponds to the shear interval (1-4)

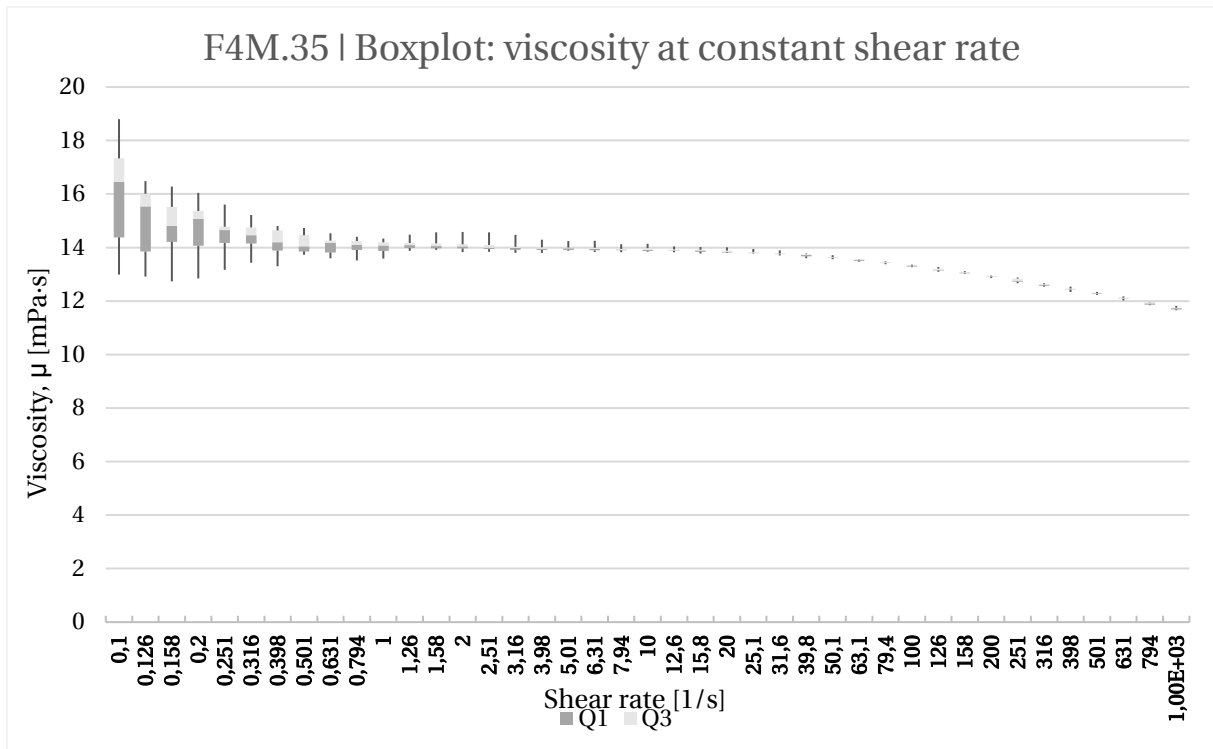


Figure I-2: Variability of viscosity readings for batch F4M.35 per shear rate

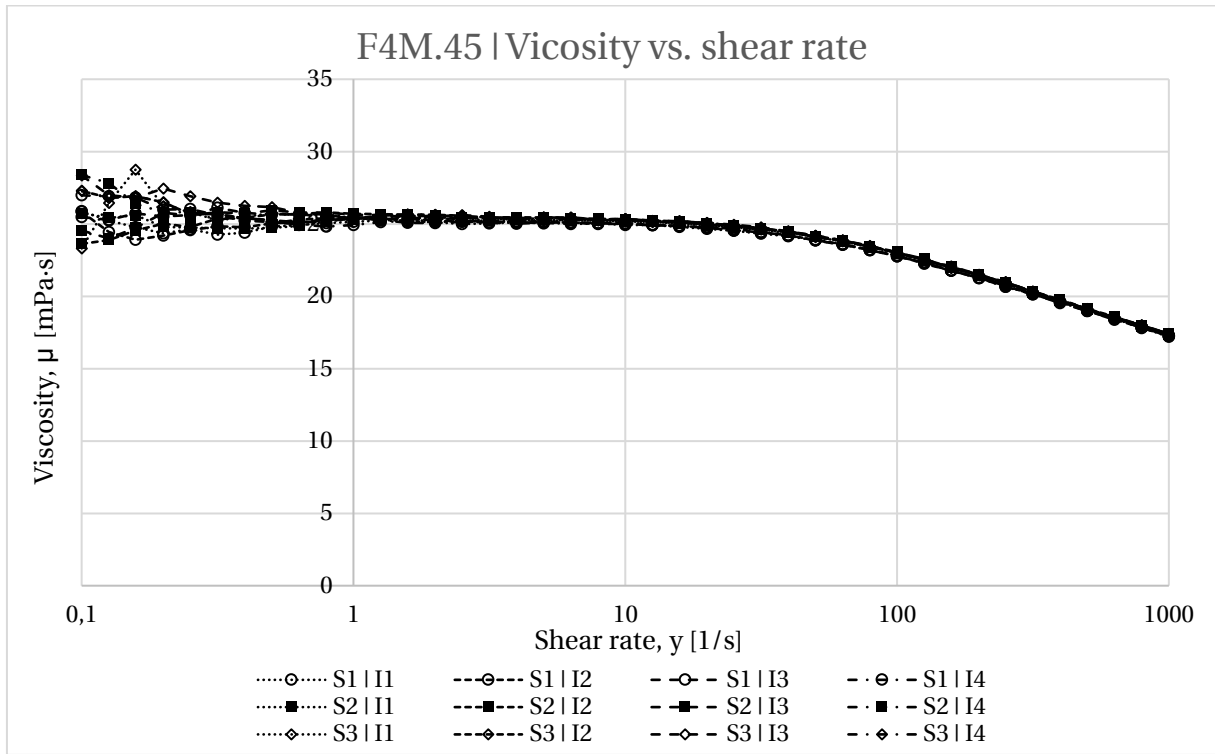


Figure I-3: Flow curves corresponding to batch F4M.45. Legend entries are presented in the format SX | IY, where X codes for the specimen number (1 - not agitated, not deaired; 2 - agitated, not deaired; 3 - agitated, deaired) and Y corresponds to the shear interval (1-4)

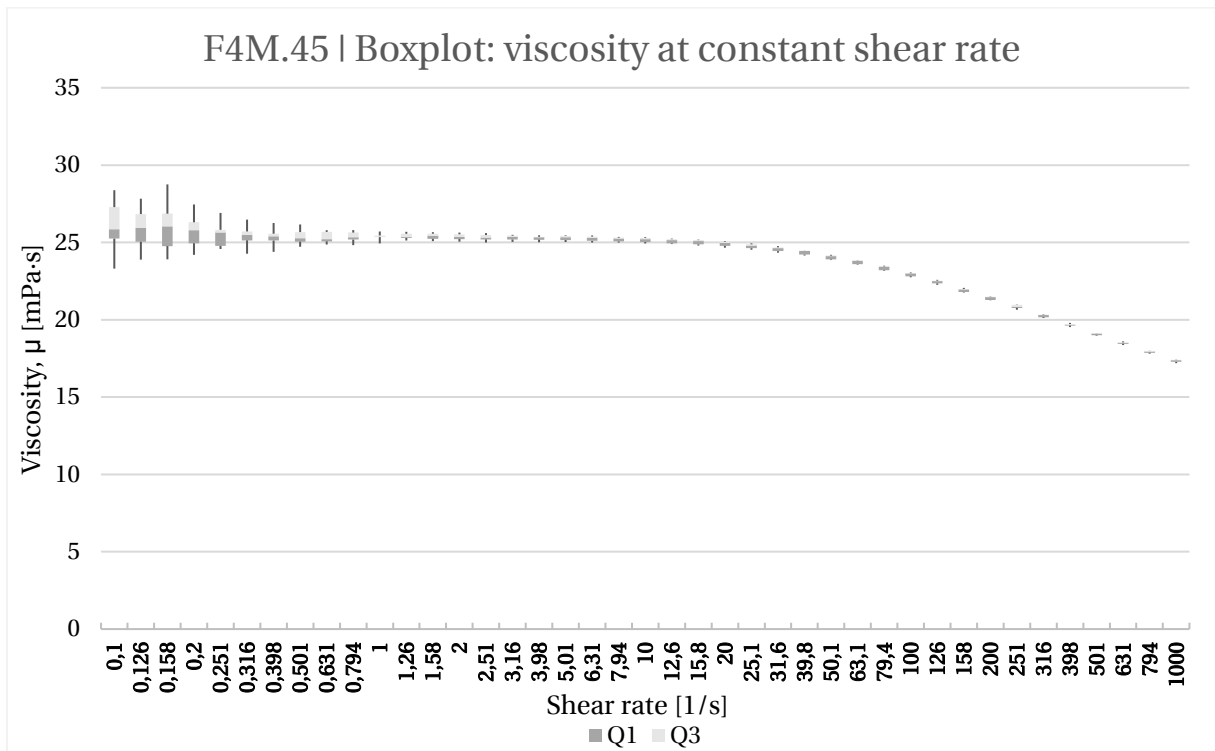


Figure I-4: Variability of viscosity readings for batch F4M.45 per shear rate

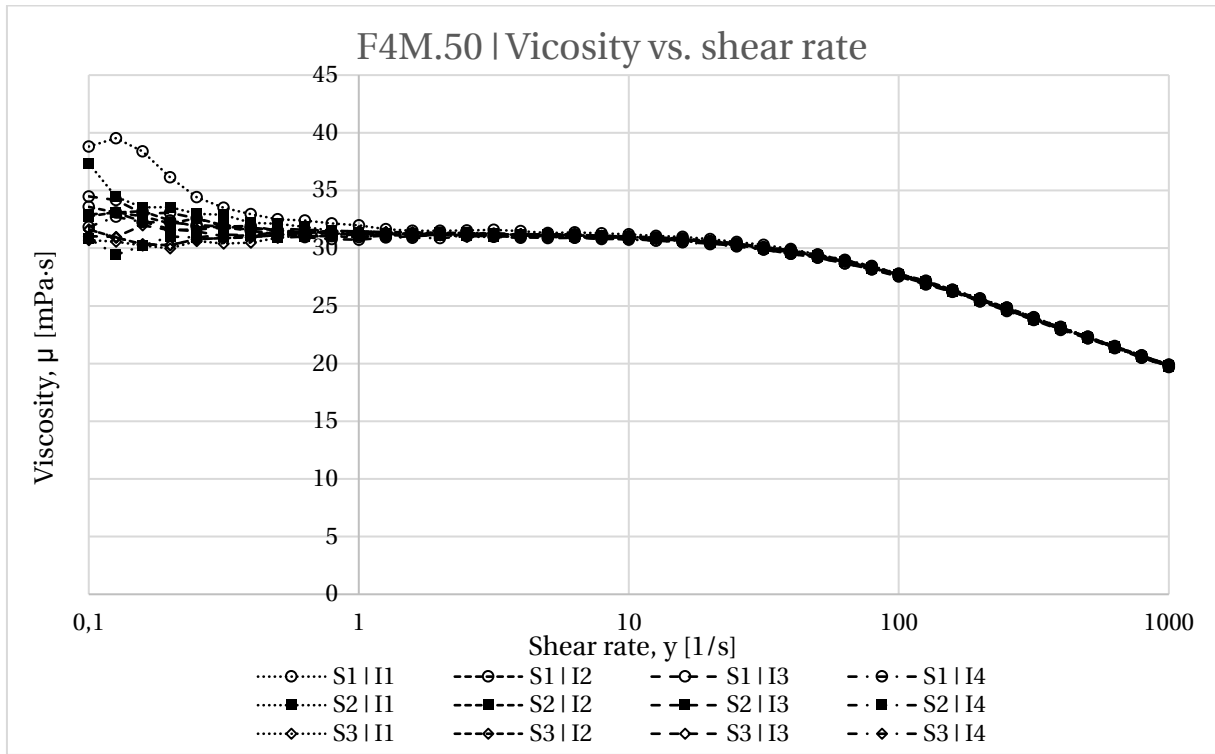


Figure I-5: Flow curves corresponding to batch F4M.50. Legend entries are presented in the format SX | IY, where X codes for the specimen number (1 - not agitated, not deaired; 2 - agitated, not deaired; 3 - agitated, deaired) and Y corresponds to the shear interval (1-4)

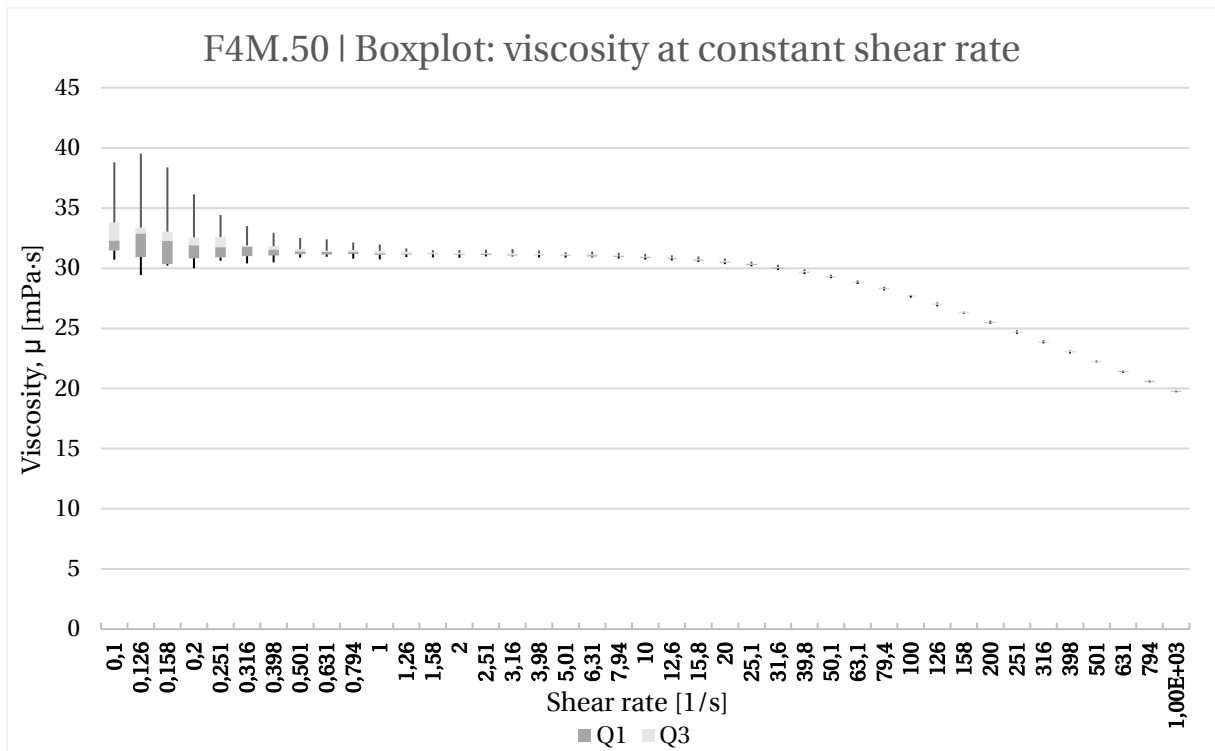


Figure I-6: Variability of viscosity readings for batch F4M.50 per shear rate

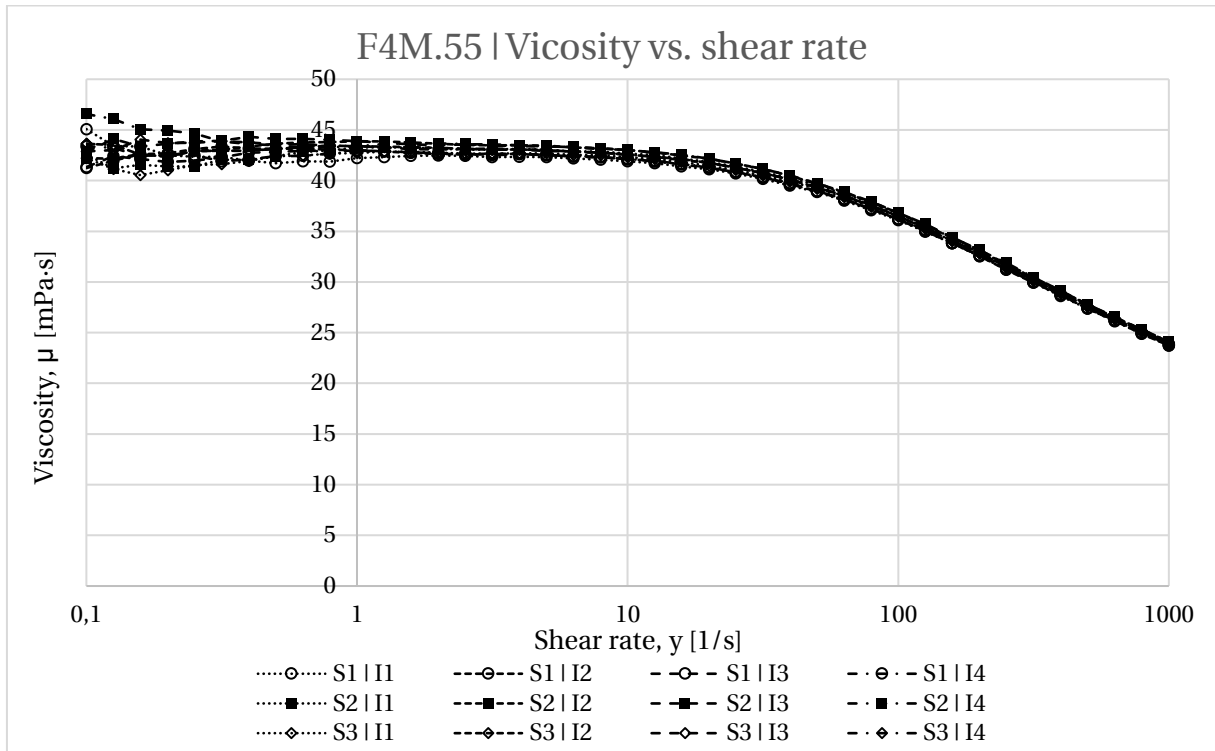


Figure I-7: Flow curves corresponding to batch F4M.55. Legend entries are presented in the format SX | IY, where X codes for the specimen number (1 - not agitated, not deaired; 2 - agitated, not deaired; 3 - agitated, deaired) and Y corresponds to the shear interval (1-4)

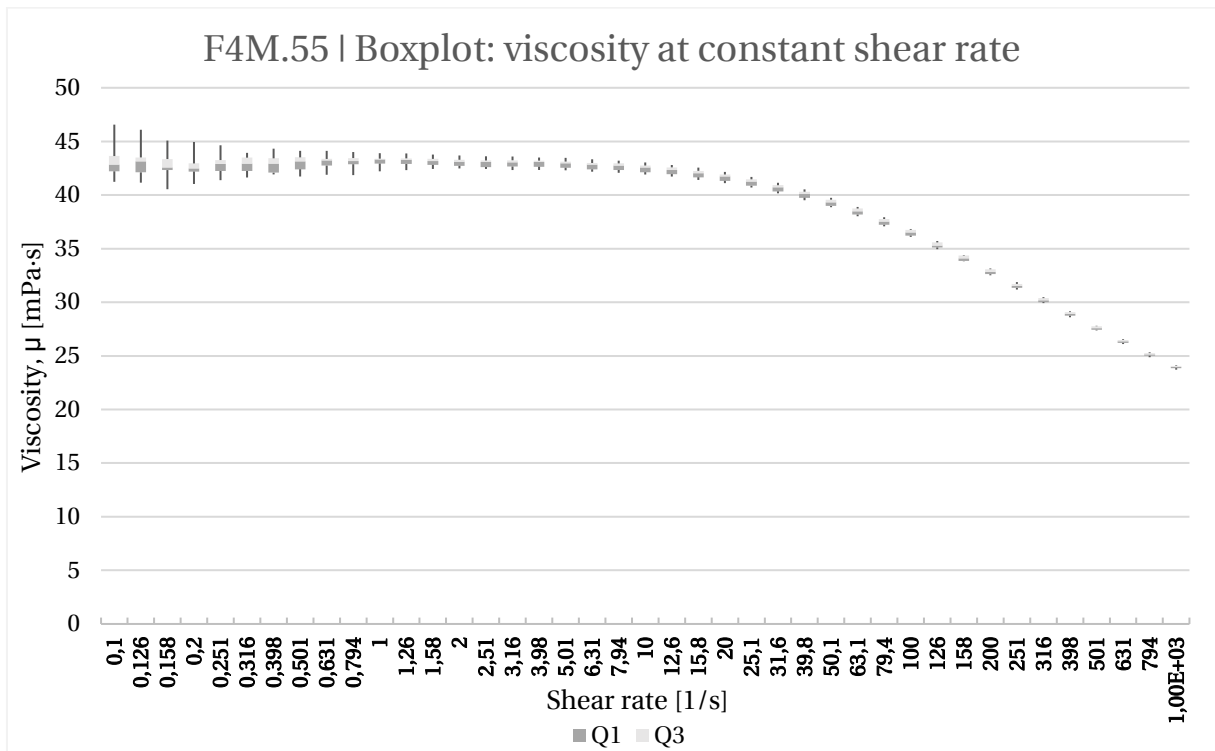


Figure I-8: Variability of viscosity readings for batch F4M.55 per shear rate

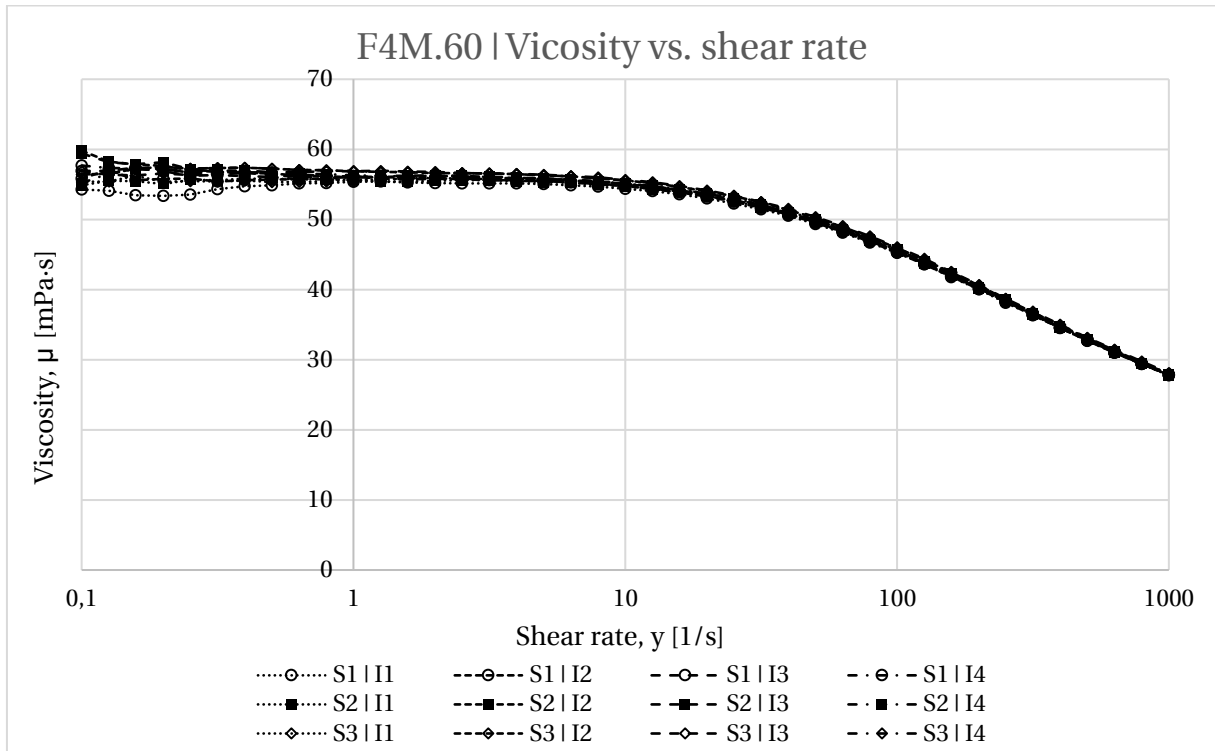


Figure I-9: Flow curves corresponding to batch F4M.60. Legend entries are presented in the format SX | IY, where X codes for the specimen number (1 - not agitated, not deaired; 2 - agitated, not deaired; 3 - agitated, deaired) and Y corresponds to the shear interval (1-4)

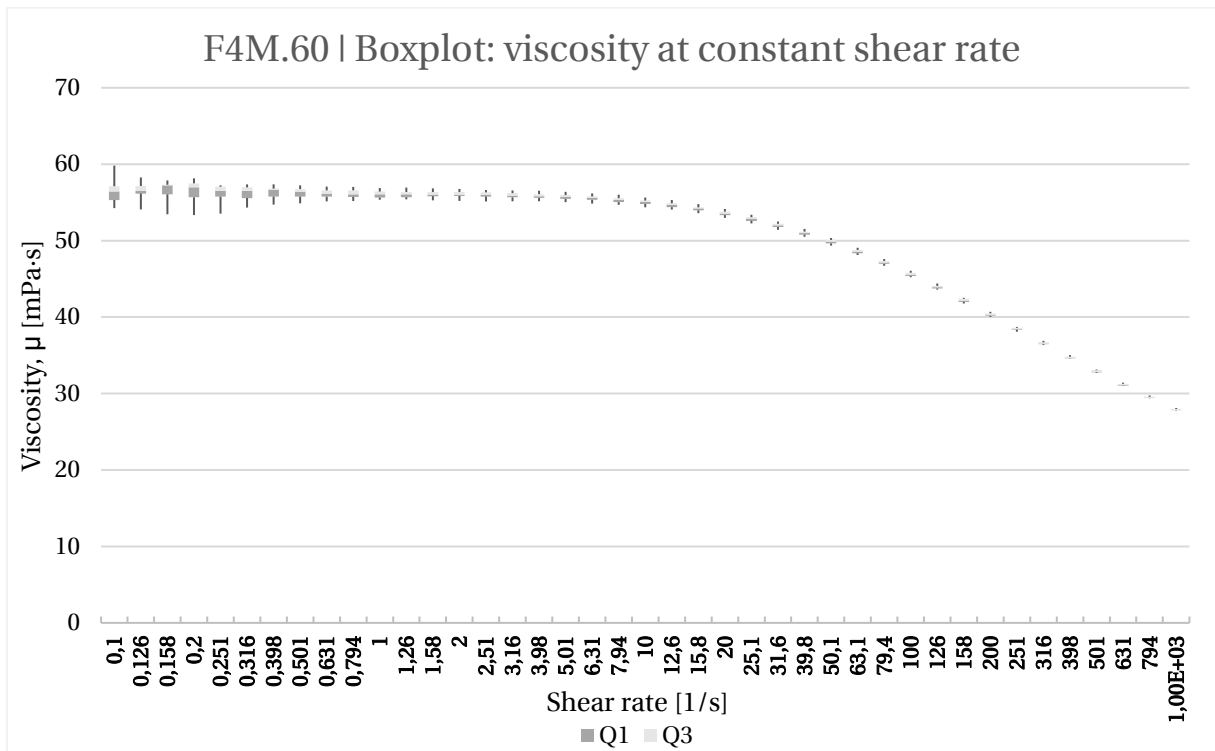


Figure I-10: Variability of viscosity readings for batch F4M.60 per shear rate

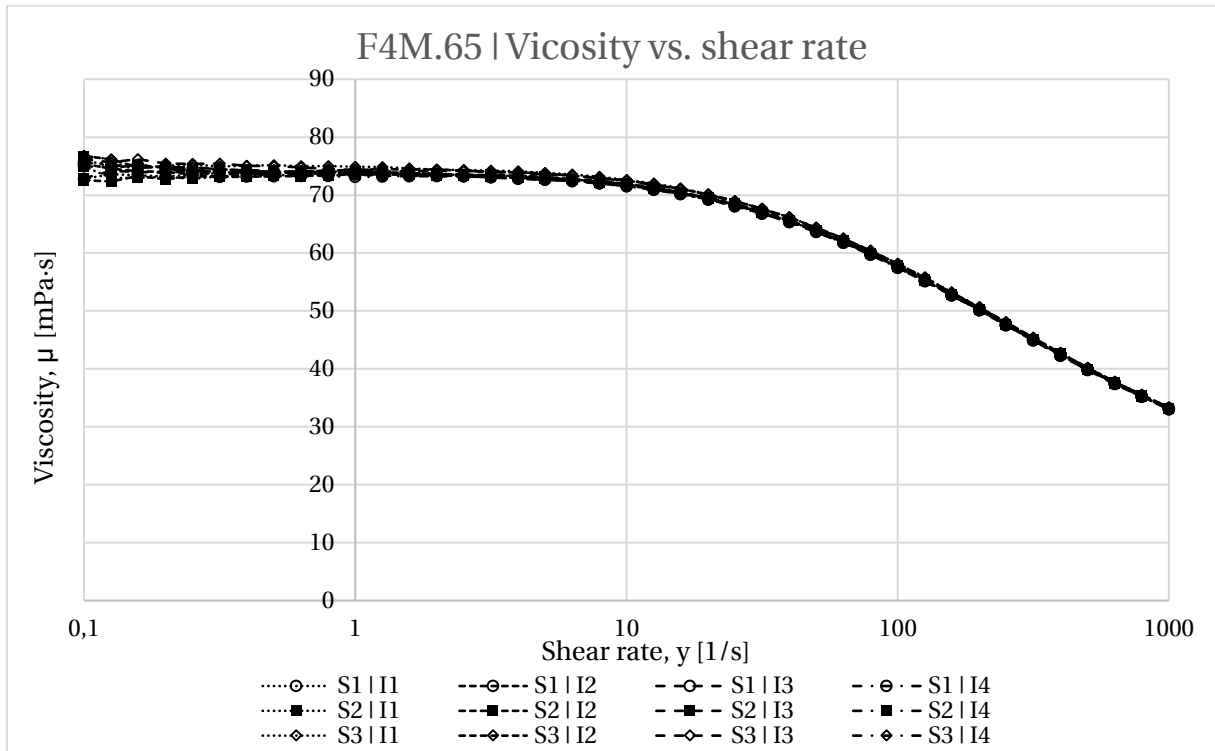


Figure I-11: Flow curves corresponding to batch F4M.65. Legend entries are presented in the format SX | IY, where X codes for the specimen number (1 - not agitated, not deaired; 2 - agitated, not deaired; 3 - agitated, deaired) and Y corresponds to the shear interval (1-4)

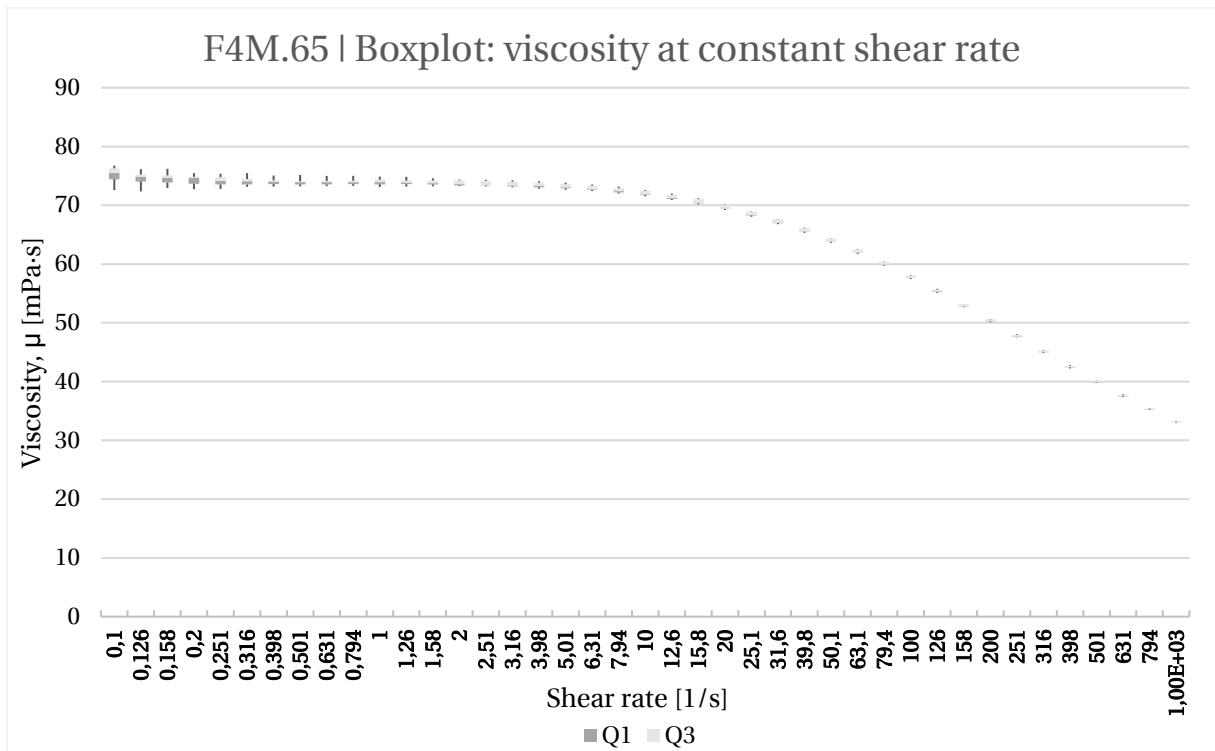


Figure I-12: Variability of viscosity readings for batch F4M.65 per shear rate

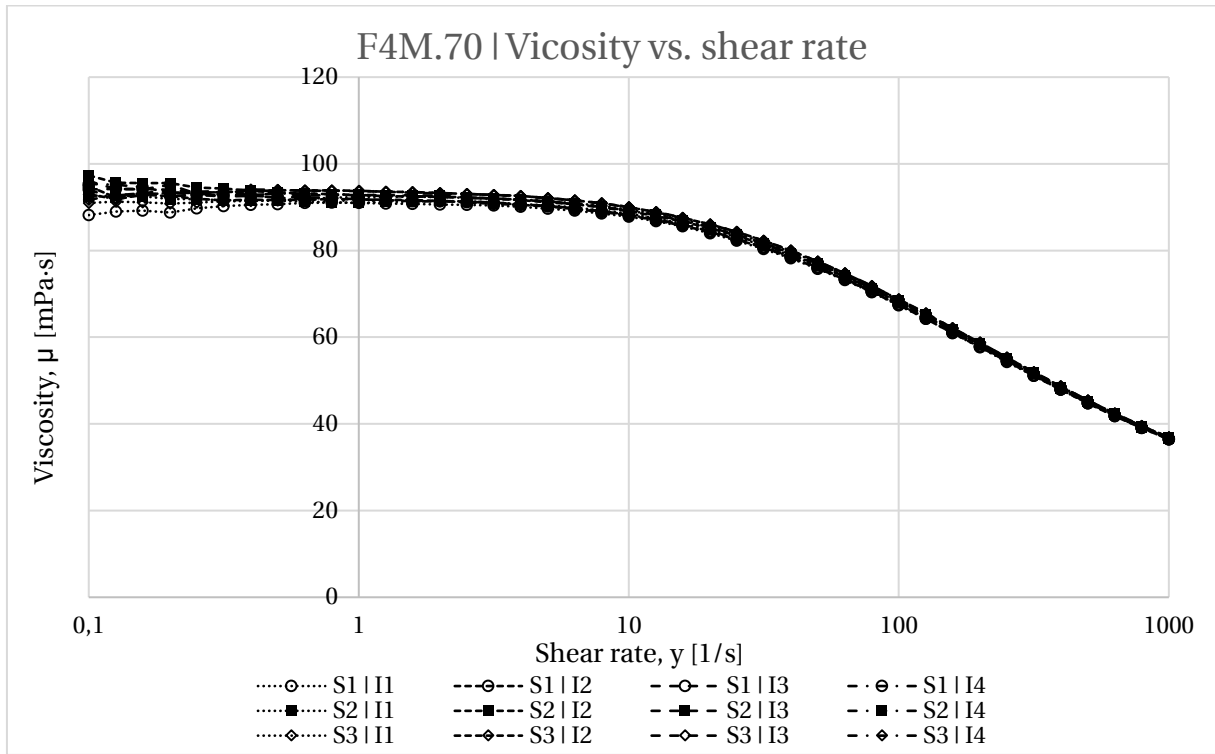


Figure I-13: Flow curves corresponding to batch F4M.70. Legend entries are presented in the format SX | IY, where X codes for the specimen number (1 - not agitated, not deaired; 2 - agitated, not deaired; 3 - agitated, deaired) and Y corresponds to the shear interval (1-4)

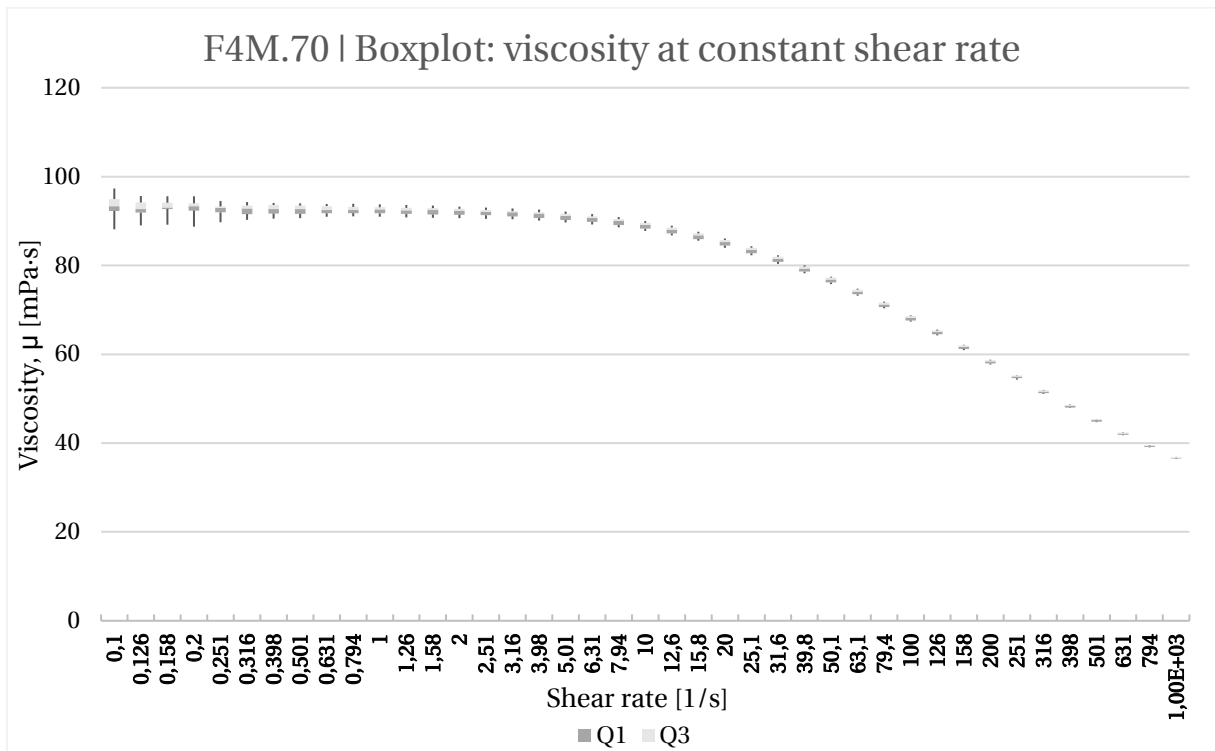


Figure I-14: Variability of viscosity readings for batch F4M.70 per shear rate

## II Histograms and normal distribution functions

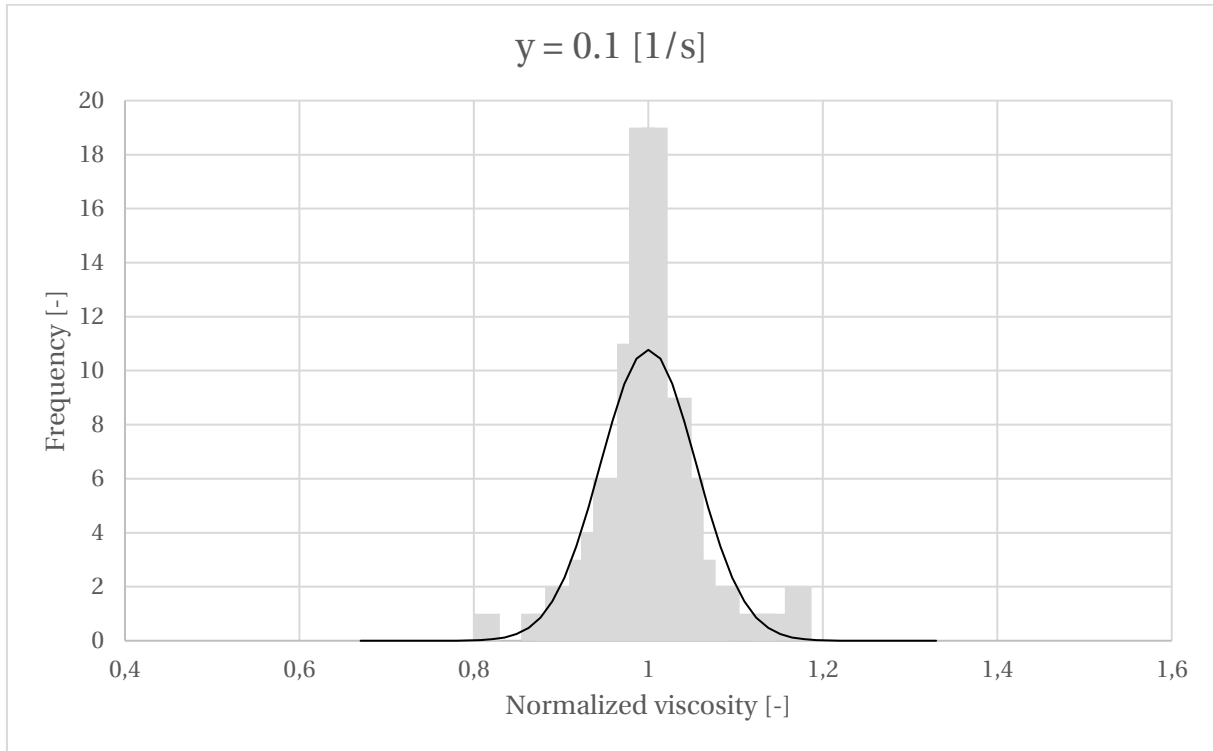


Figure II-1: Histogram of normalized viscosity readings at  $\dot{\gamma} = 0.1$  1/s for the ensemble of all seven batches. Binwidth corresponds to  $\sigma_p/4$ , where  $\sigma_p$  is the standard deviation of the aforementioned population of 84 normalized measurements.

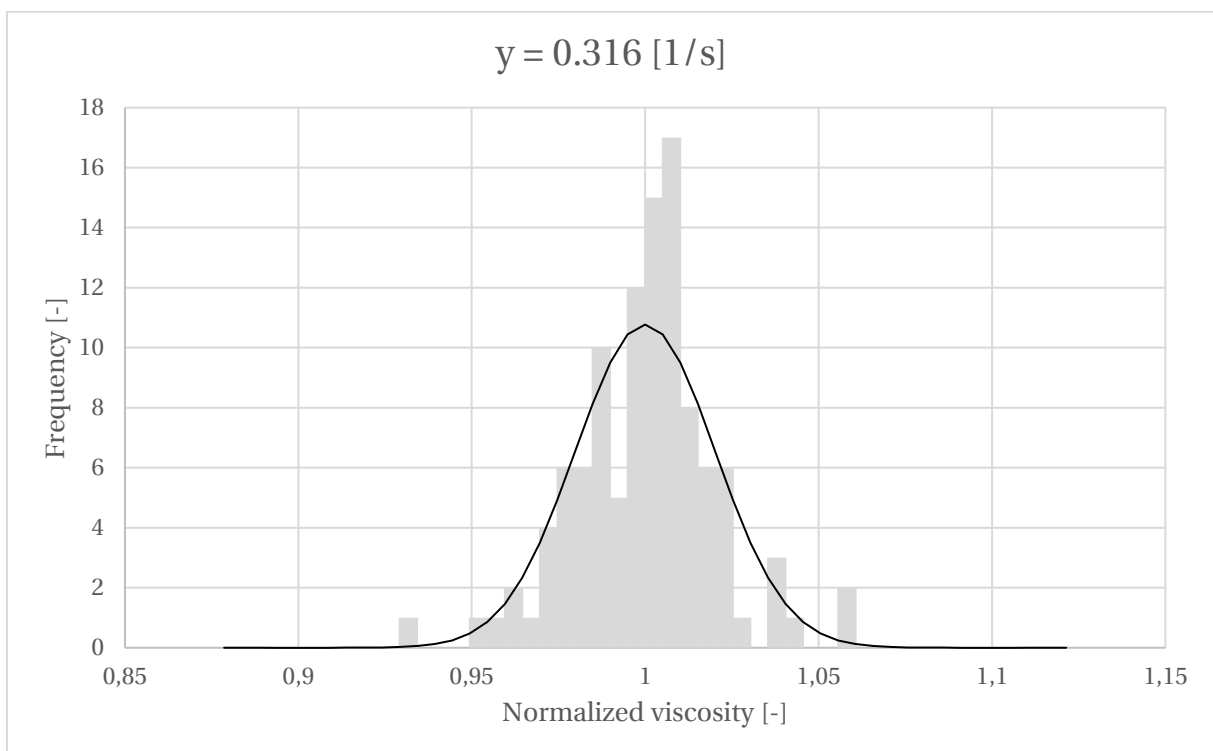


Figure II-2: Histogram of normalized viscosity readings at  $\dot{\gamma} = 0.316$  1/s for the ensemble of all seven batches. Binwidth corresponds to  $\sigma_p/4$ , where  $\sigma_p$  is the standard deviation of the aforementioned population of 84 normalized measurements.

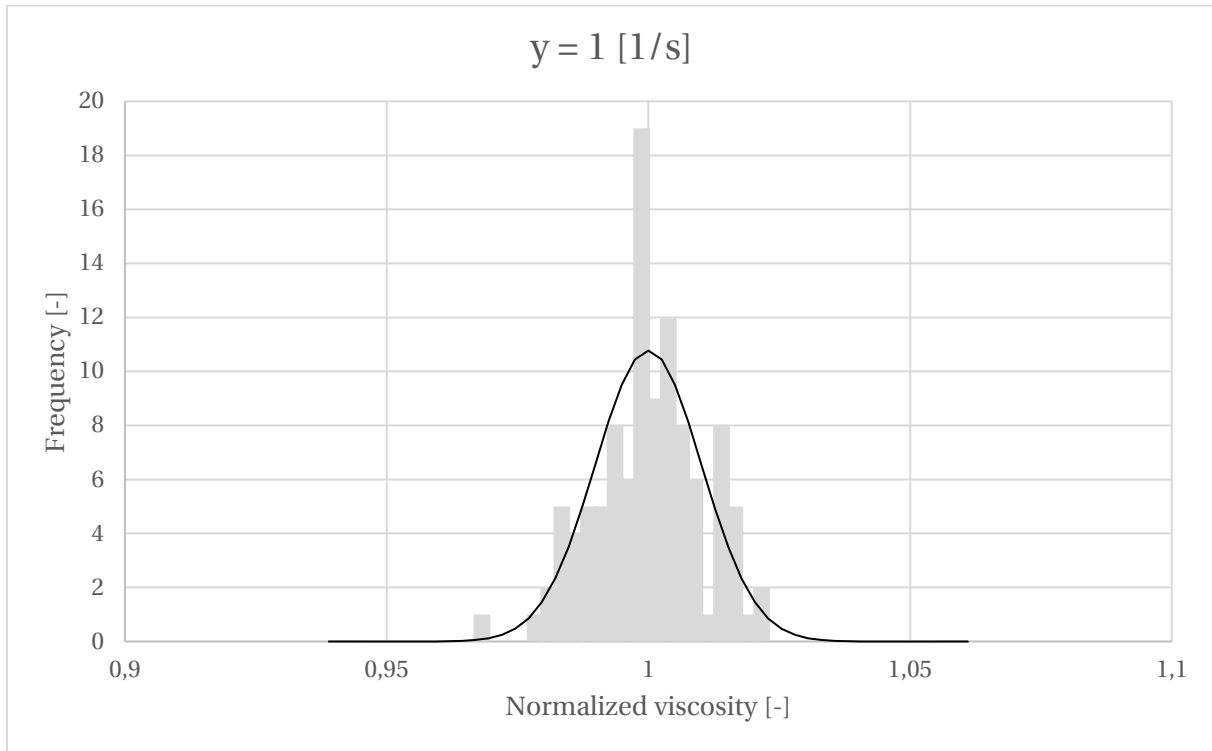


Figure II-3: Histogram of normalized viscosity readings at  $\dot{\gamma} = 1$  1/s for the ensemble of all seven batches. Binwidth corresponds to  $\sigma_p/4$ , where  $\sigma_p$  is the standard deviation of the aforementioned population of 84 normalized measurements.

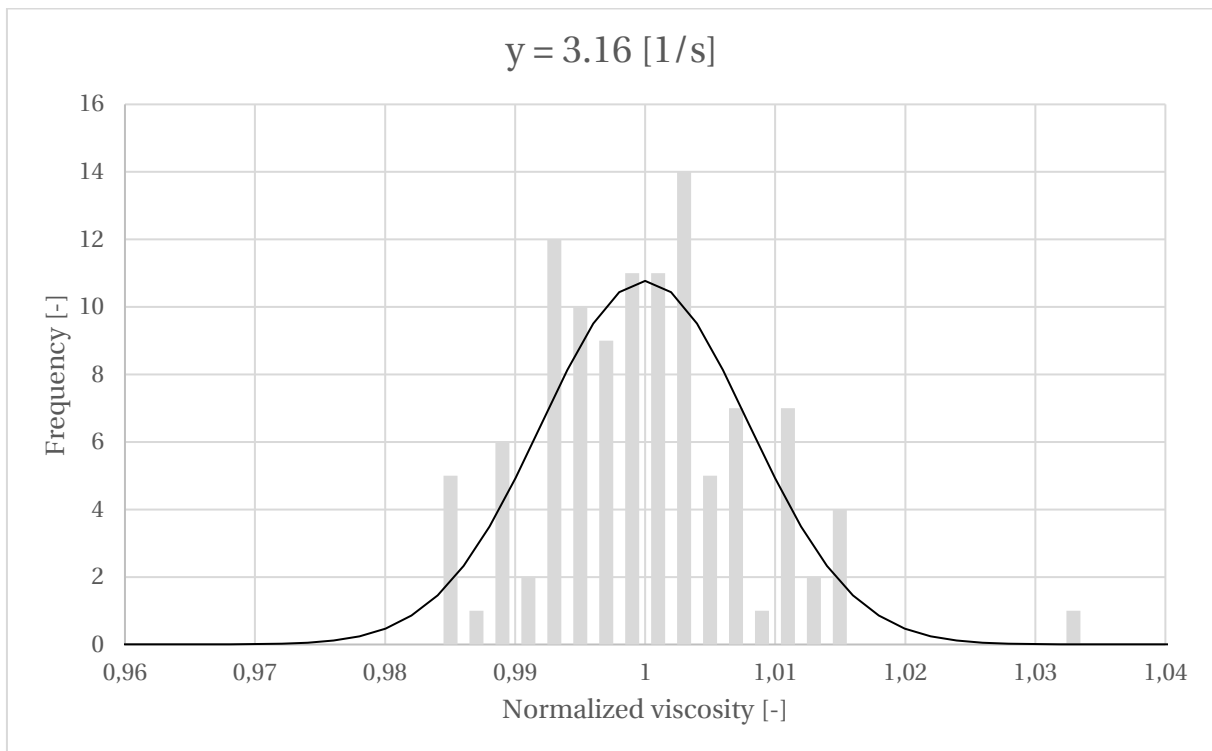


Figure II-4: Histogram of normalized viscosity readings at  $\dot{\gamma} = 3.16$  1/s for the ensemble of all seven batches. Binwidth corresponds to  $\sigma_p/4$ , where  $\sigma_p$  is the standard deviation of the aforementioned population of 84 normalized measurements.

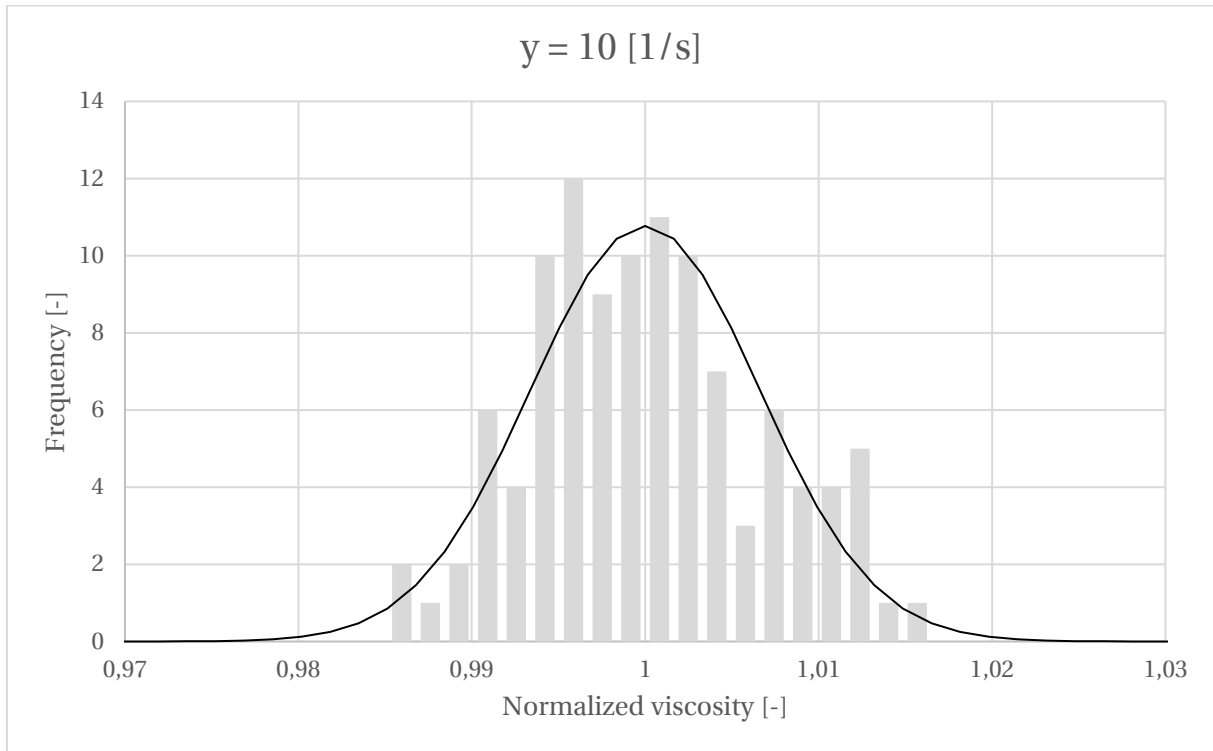


Figure II-5: Histogram of normalized viscosity readings at  $\dot{\gamma} = 10$  1/s for the ensemble of all seven batches. Binwidth corresponds to  $\sigma_p/4$ , where  $\sigma_p$  is the standard deviation of the aforementioned population of 84 normalized measurements.

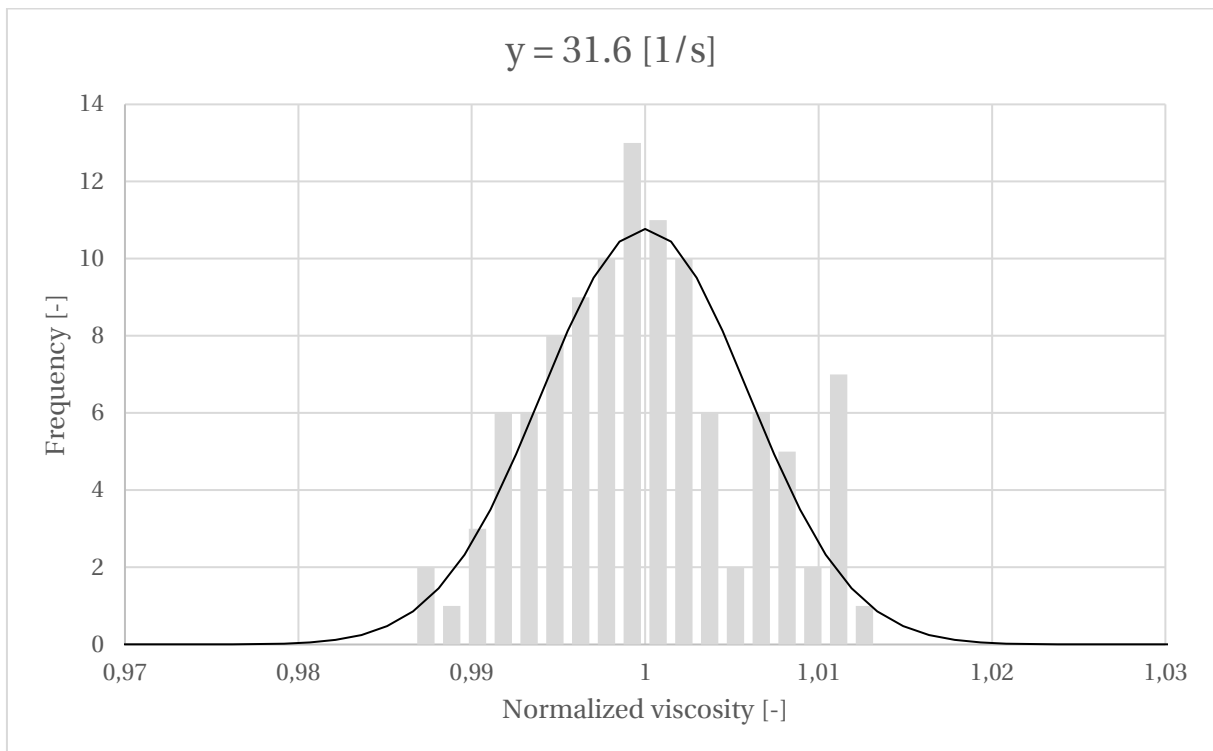


Figure II-6: Histogram of normalized viscosity readings at  $\dot{\gamma} = 31.6$  1/s for the ensemble of all seven batches. Binwidth corresponds to  $\sigma_p/4$ , where  $\sigma_p$  is the standard deviation of the aforementioned population of 84 normalized measurements.

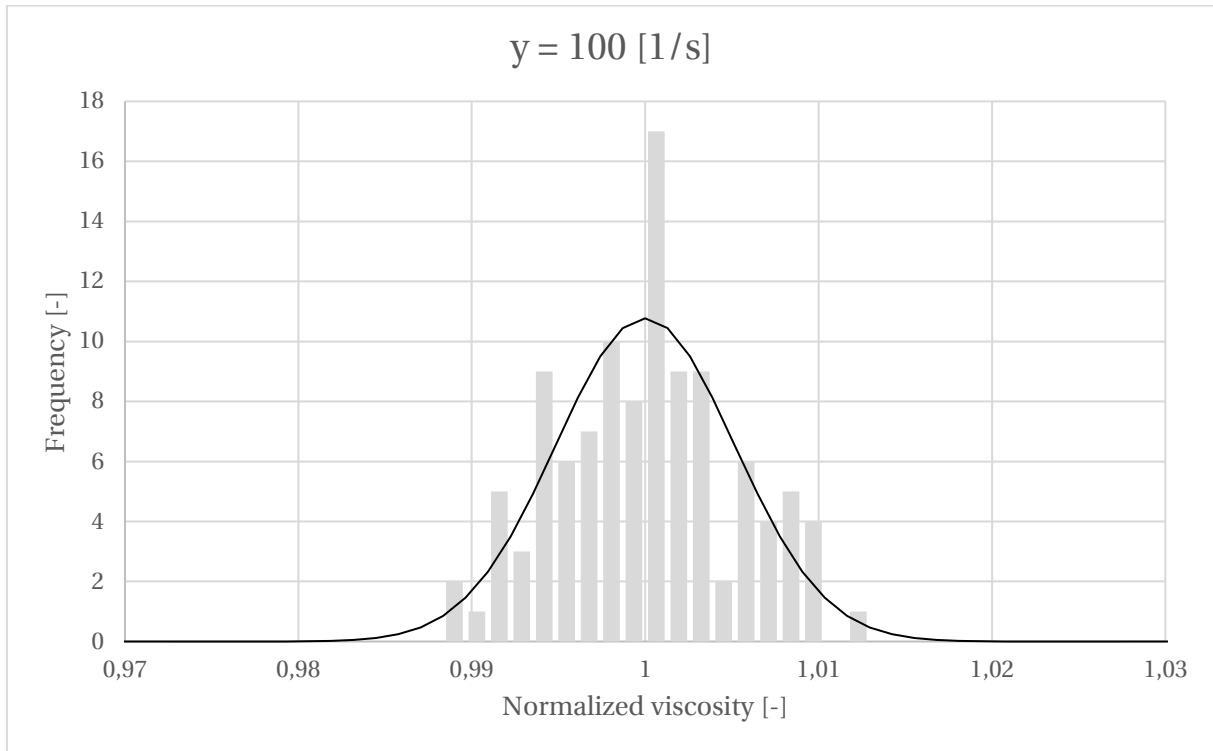


Figure II-7: Histogram of normalized viscosity readings at  $\dot{\gamma} = 100 \text{ 1/s}$  for the ensemble of all seven batches. Binwidth corresponds to  $\sigma_p/4$ , where  $\sigma_p$  is the standard deviation of the aforementioned population of 84 normalized measurements.

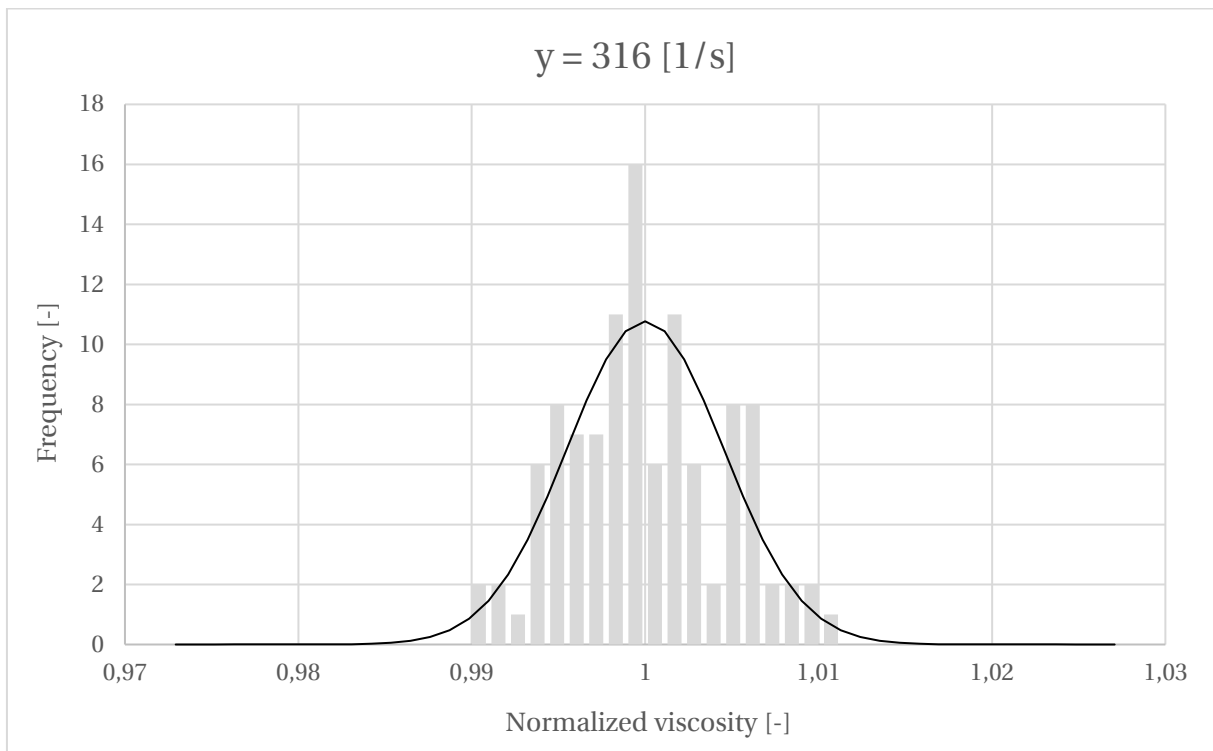


Figure II-8: Histogram of normalized viscosity readings at  $\dot{\gamma} = 316 \text{ 1/s}$  for the ensemble of all seven batches. Binwidth corresponds to  $\sigma_p/4$ , where  $\sigma_p$  is the standard deviation of the aforementioned population of 84 normalized measurements.

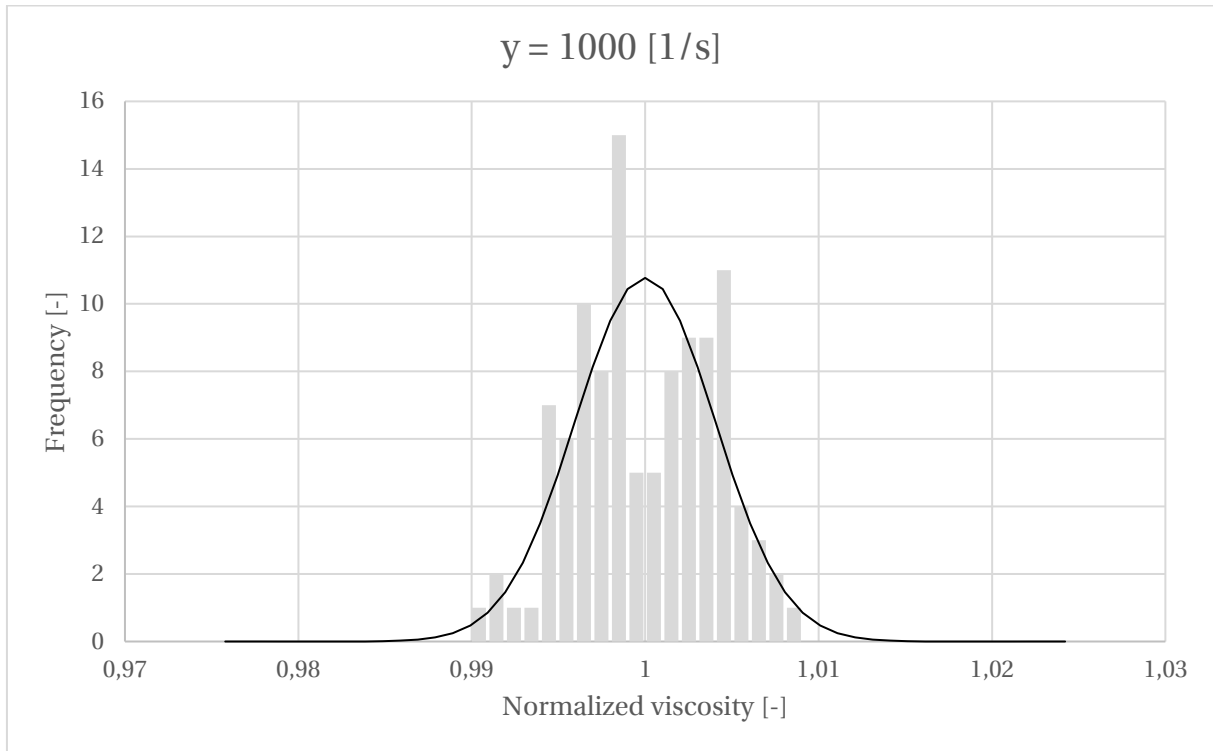


Figure II-9: Histogram of normalized viscosity readings at  $\dot{\gamma} = 1000 \text{ 1/s}$  for the ensemble of all seven batches. Binwidth corresponds to  $\sigma_p/4$ , where  $\sigma_p$  is the standard deviation of the aforementioned population of 84 normalized measurements.

## III 95% confidence intervals for rheological measurements

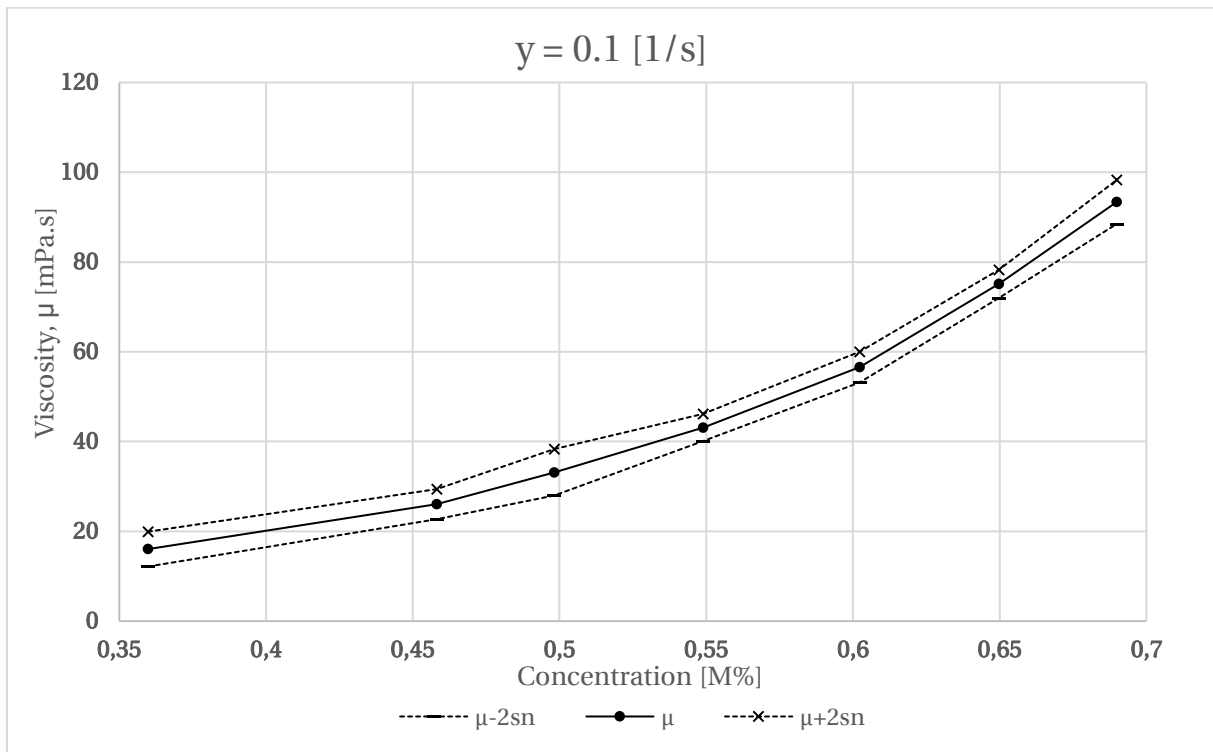


Figure III-1: Mean viscosity as a function of concentration for  $\dot{\gamma} = 0.1$  1/s and 95% confidence bounds following from the normal distribution of viscosity readings.

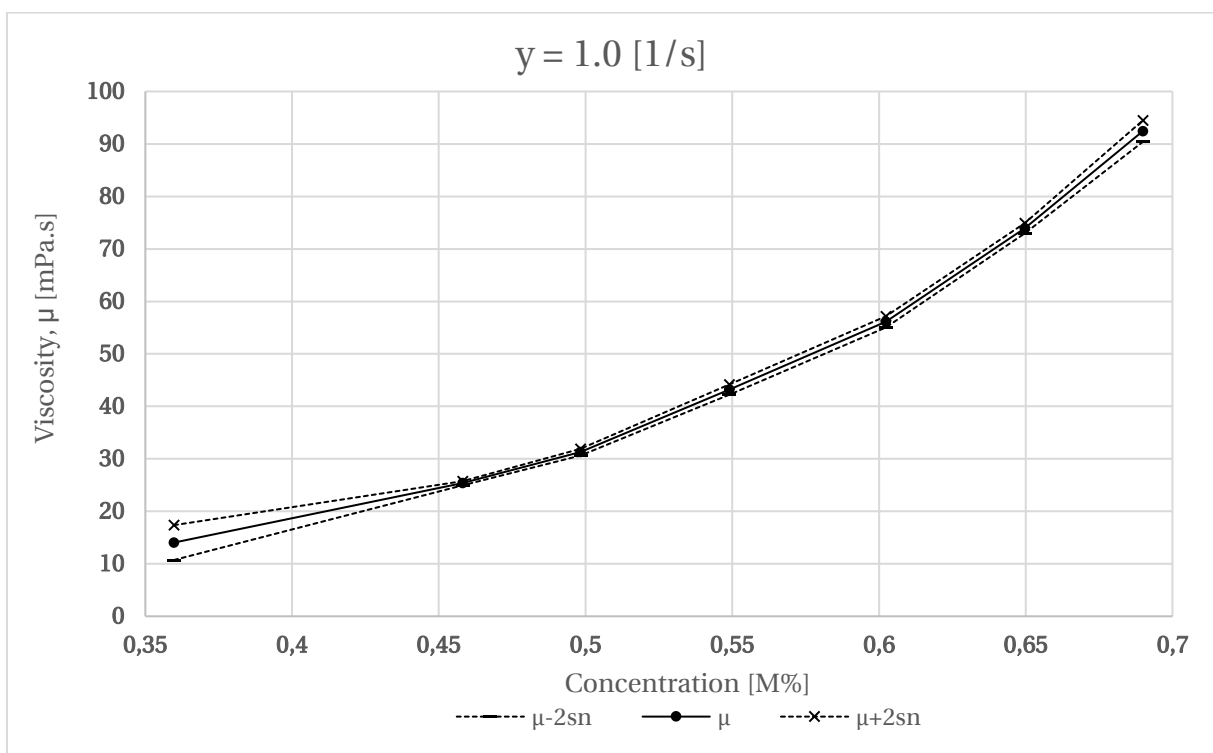


Figure III-2: Mean viscosity as a function of concentration for  $\dot{\gamma} = 1$  1/s and 95% confidence bounds following from the normal distribution of viscosity readings.

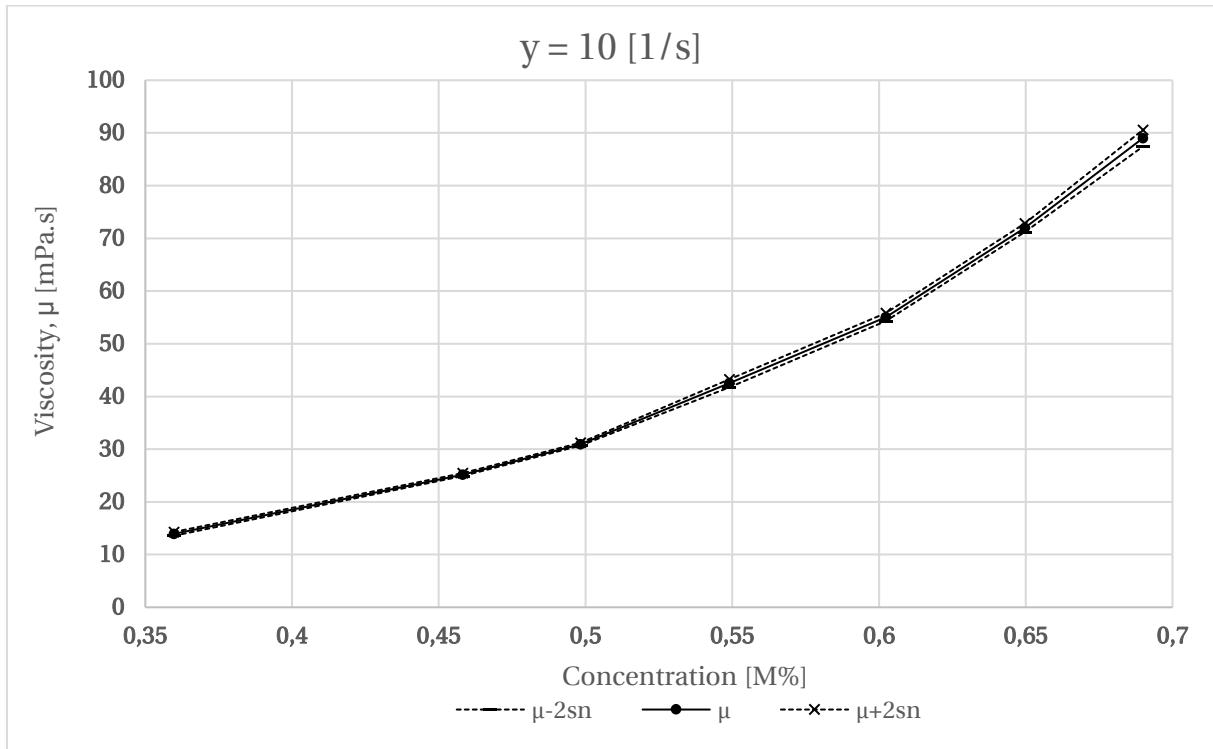


Figure III-3: Mean viscosity as a function of concentration for  $\dot{\gamma} = 10$  1/s and 95% confidence bounds following from the normal distribution of viscosity readings.

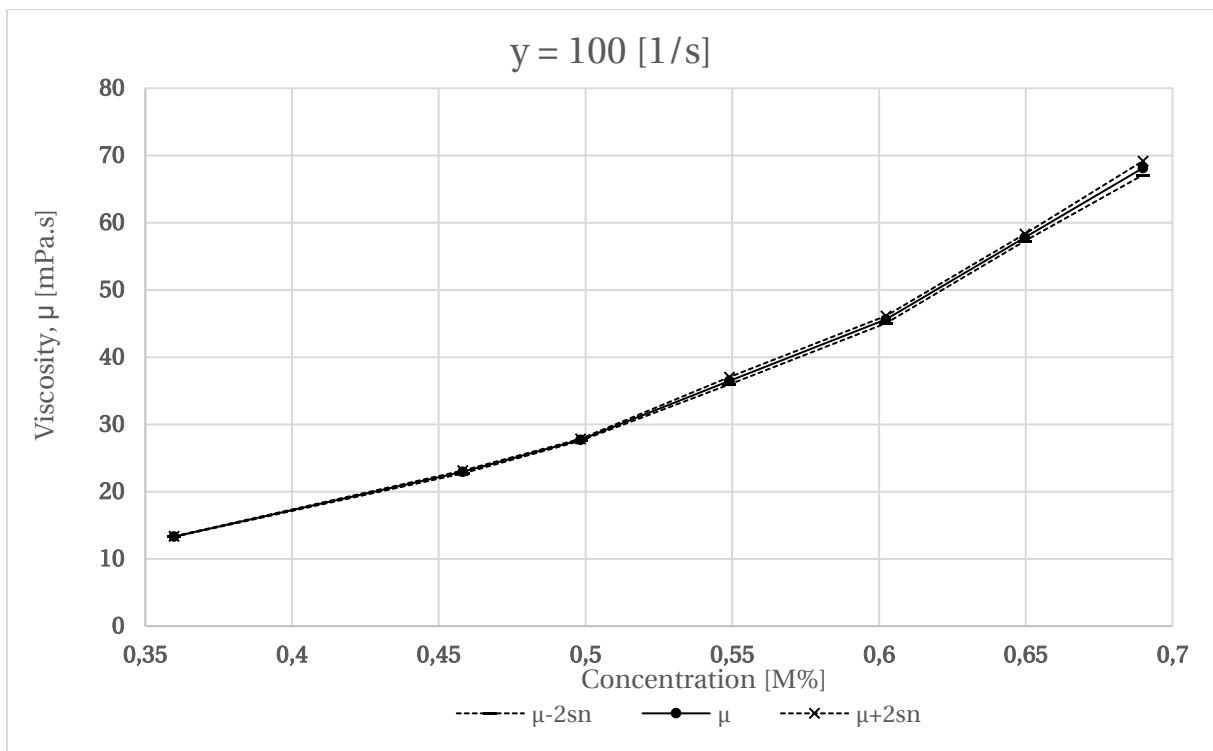


Figure III-4: Mean viscosity as a function of concentration for  $\dot{\gamma} = 100$  1/s and 95% confidence bounds following from the normal distribution of viscosity readings.

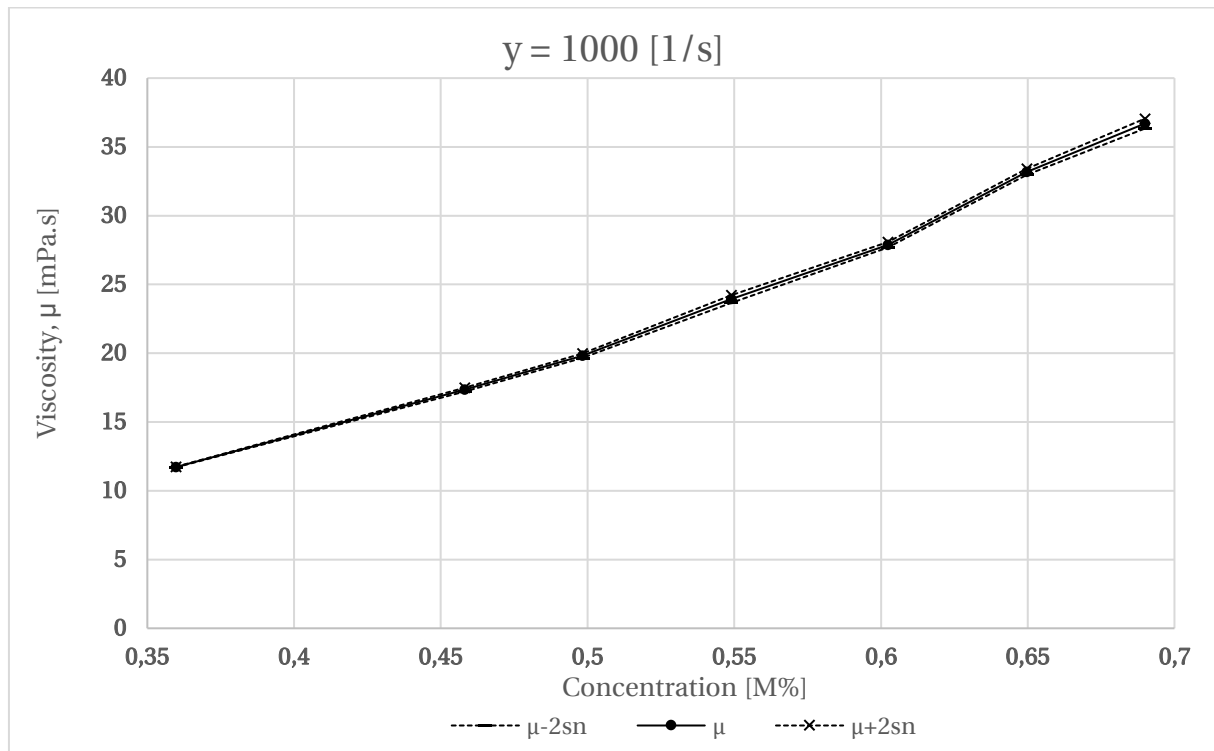


Figure III-5: Mean viscosity as a function of concentration for  $\dot{\gamma} = 1000 \text{ 1/s}$  and 95% confidence bounds following from the normal distribution of viscosity readings.

#### IV Rheological measurements plotted alongside least square approximation (power law) and generic fit

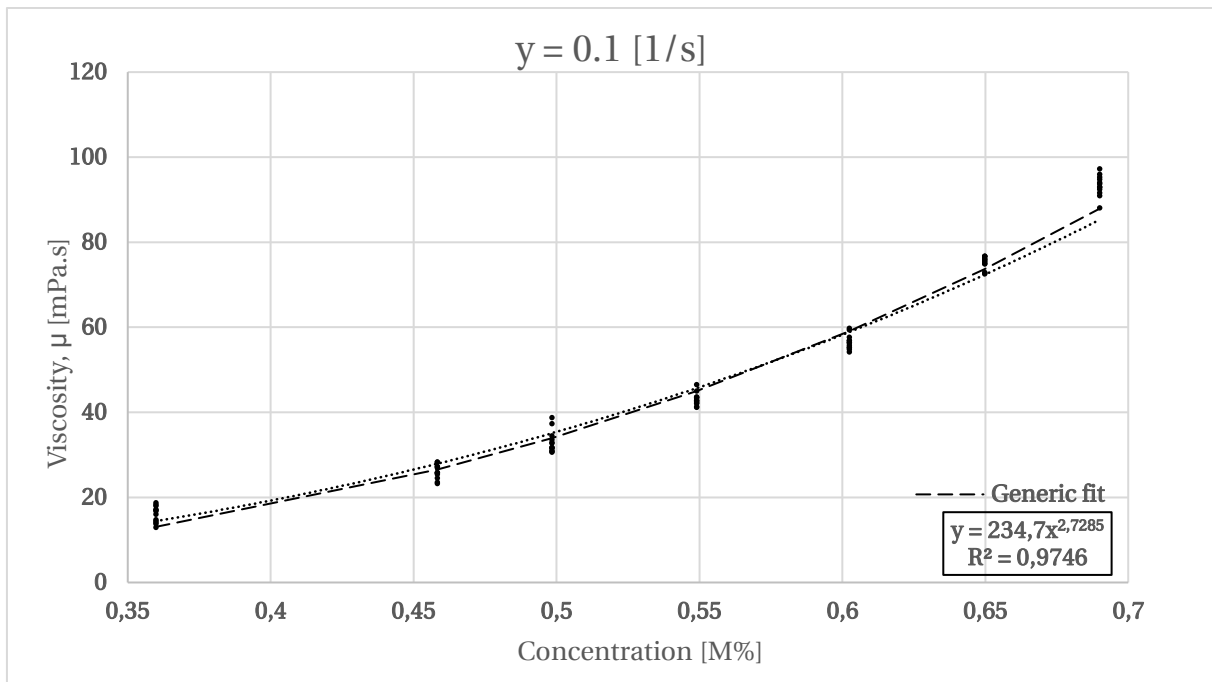


Figure IV-1: Rheological measurements at different concentrations for  $\dot{\gamma} = 0.1$  1/s , accompanied generic and least square power fit ( $y=Ax^B$ ). For the latter of the two approximations, the corresponding equation and  $R^2$  is depicted in the bottom left corner.

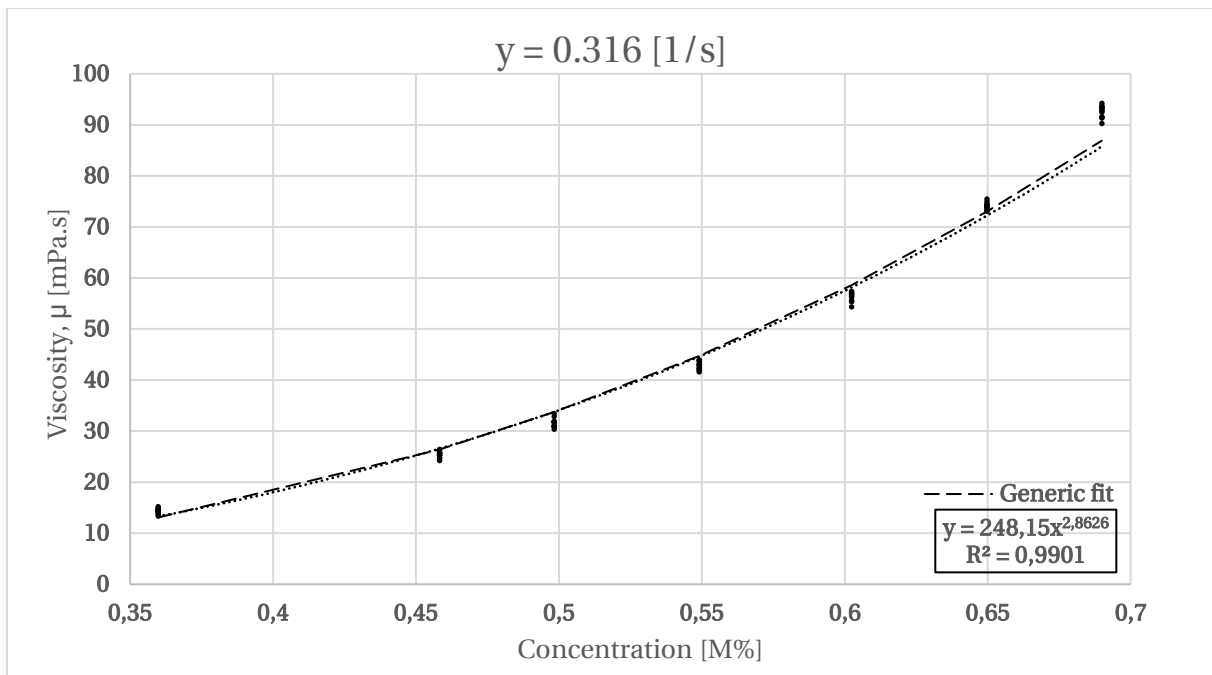


Figure IV-2: Rheological measurements at different concentrations for  $\dot{\gamma} = 0.316$  1/s , accompanied generic and least square power fit ( $y=Ax^B$ ). For the latter of the two approximations, the corresponding equation and  $R^2$  is depicted in the bottom left corner.

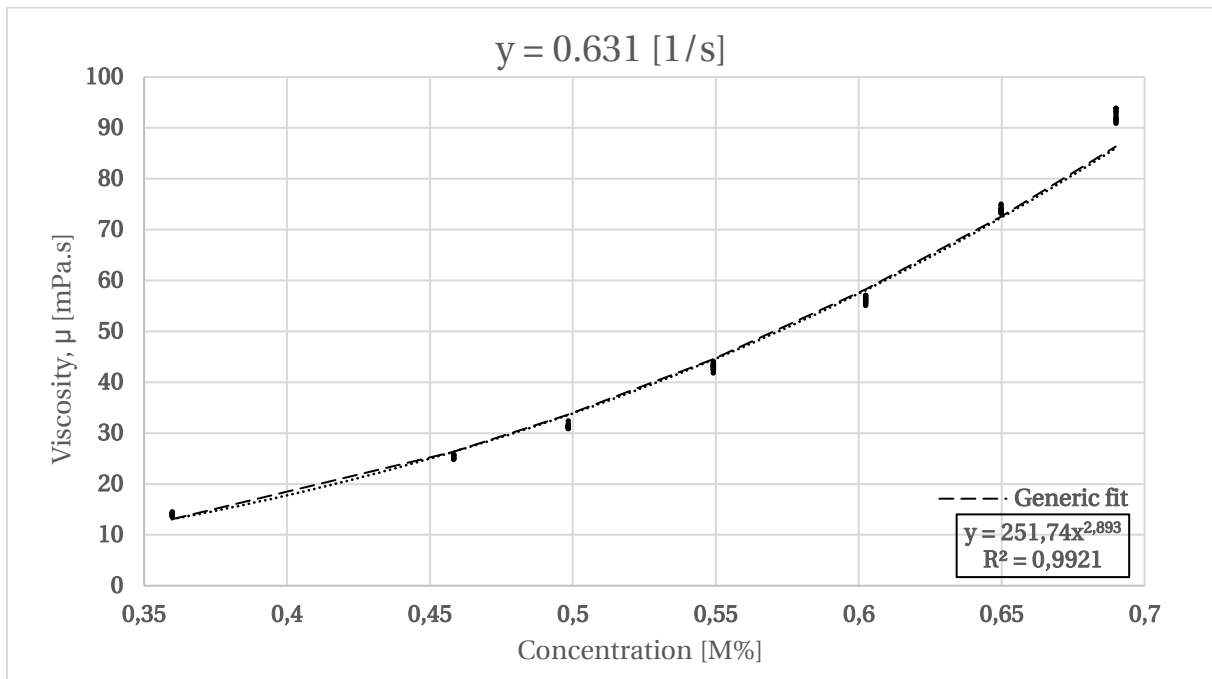


Figure IV-3: Rheological measurements at different concentrations for  $\dot{\gamma} = 0.631$  1/s , accompanied generic and least square power fit ( $y=Ax^b$ ). For the latter of the two approximations, the corresponding equation and  $R^2$  is depicted in the bottom left corner.

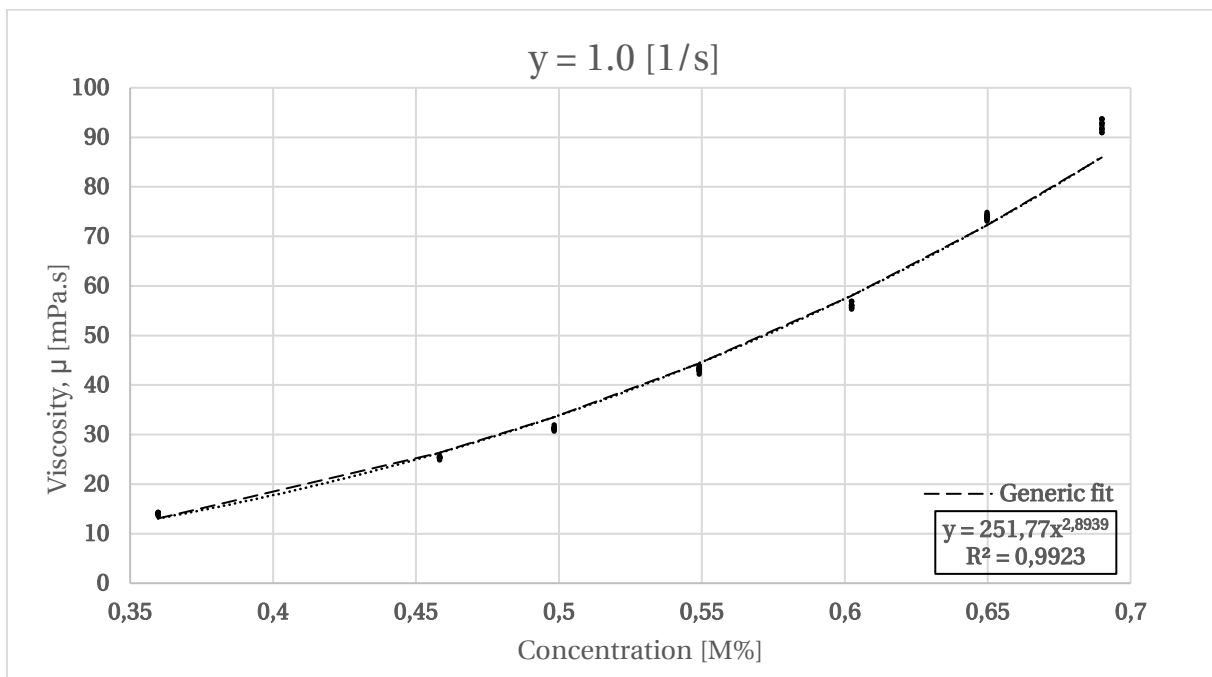


Figure IV-4: Rheological measurements at different concentrations for  $\dot{\gamma} = 1$  1/s , accompanied generic and least square power fit ( $y=Ax^b$ ). For the latter of the two approximations, the corresponding equation and  $R^2$  is depicted in the bottom left corner.

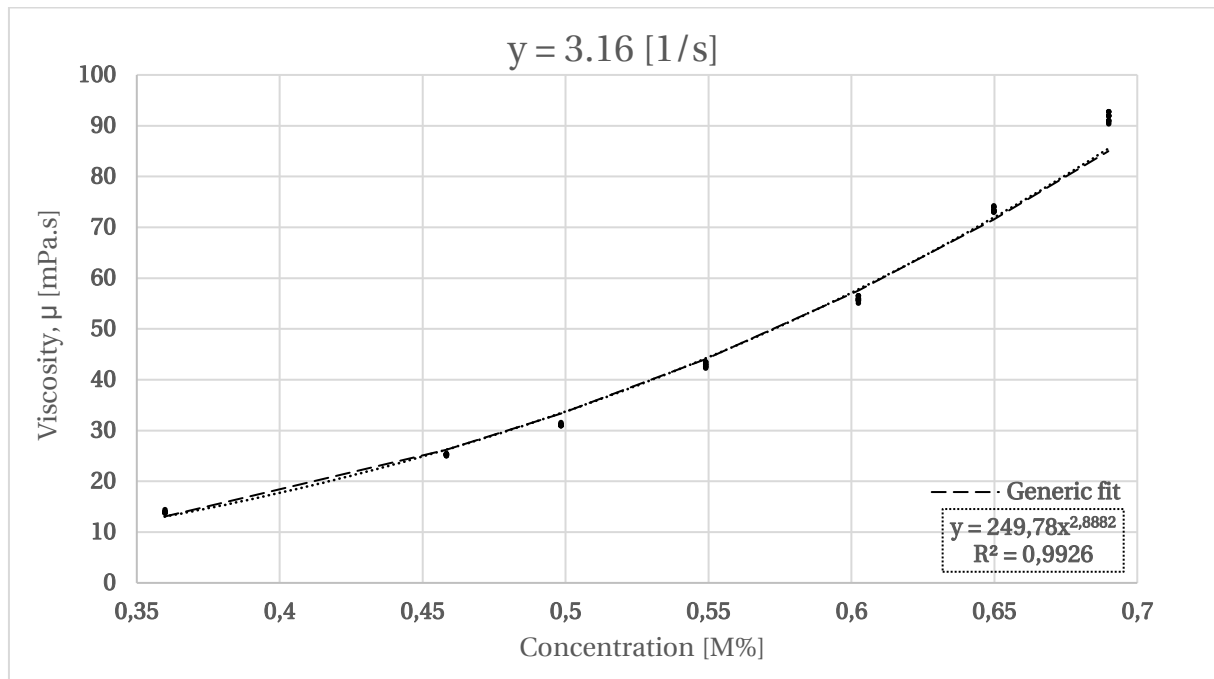


Figure IV-5: Rheological measurements at different concentrations for  $\dot{\gamma} = 3.16 \text{ 1/s}$ , accompanied generic and least square power fit ( $y=Ax^B$ ). For the latter of the two approximations, the corresponding equation and  $R^2$  is depicted in the bottom left corner.

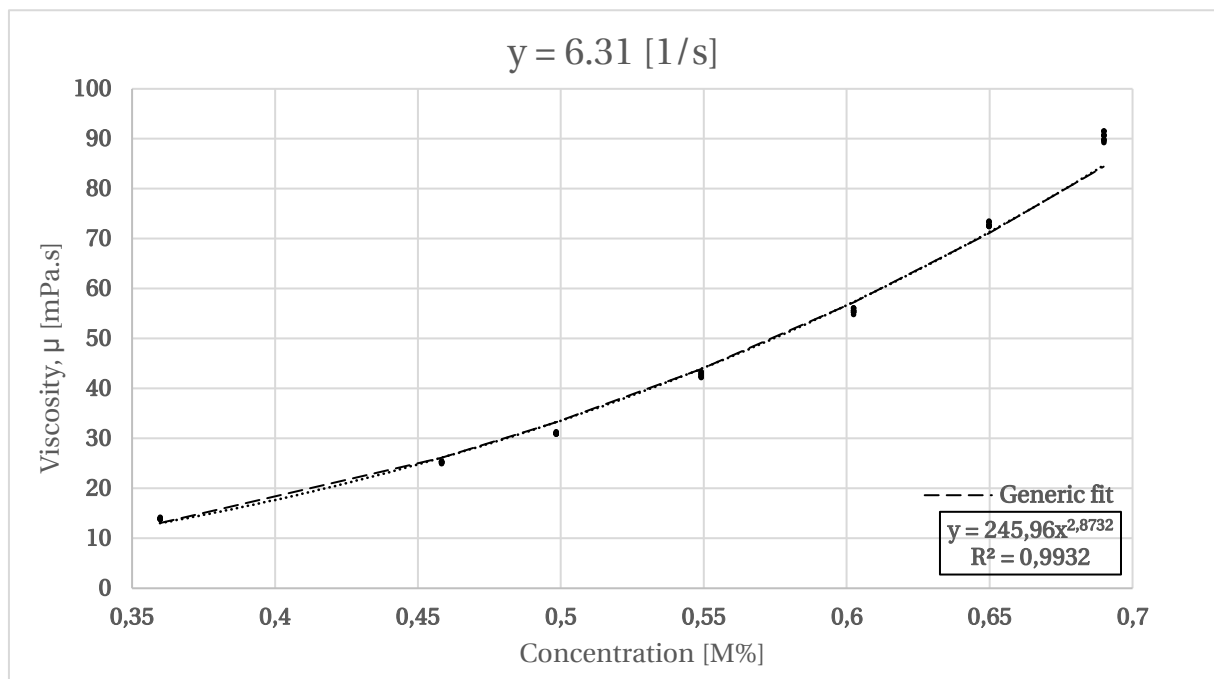


Figure IV-6: Rheological measurements at different concentrations for  $\dot{\gamma} = 6.31 \text{ 1/s}$ , accompanied generic and least square power fit ( $y=Ax^B$ ). For the latter of the two approximations, the corresponding equation and  $R^2$  is depicted in the bottom left corner.

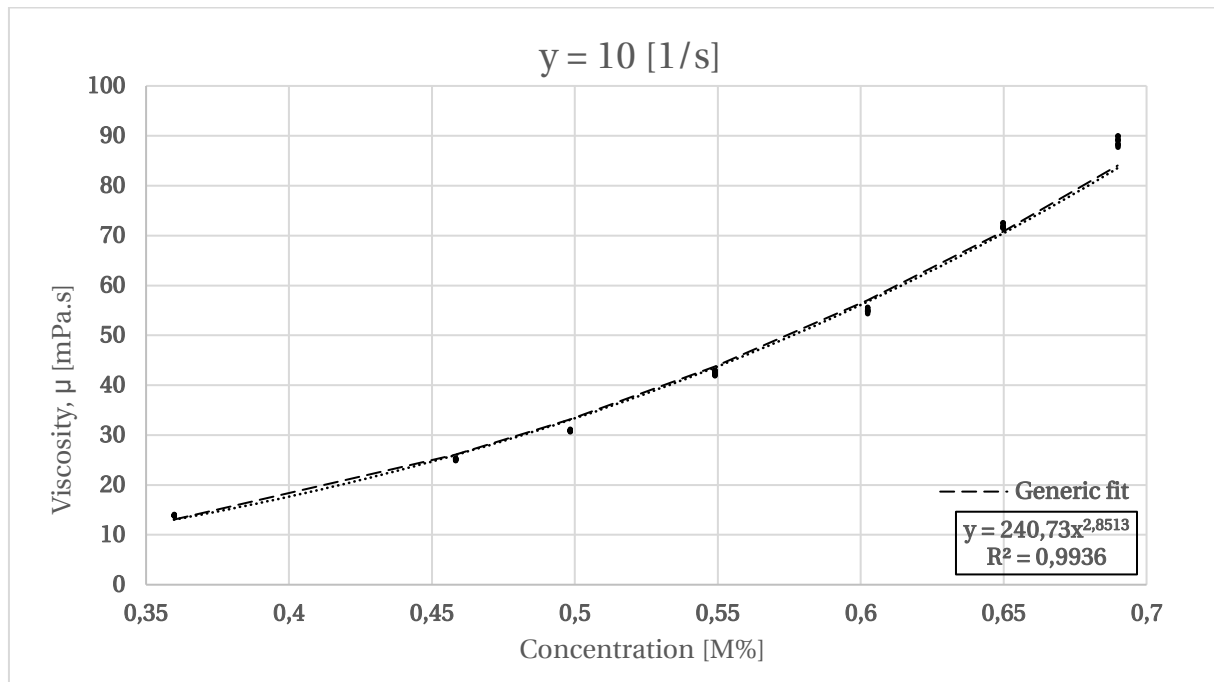


Figure IV-7: Rheological measurements at different concentrations for  $\dot{\gamma} = 10 \text{ 1/s}$ , accompanied generic and least square power fit ( $y=Ax^B$ ). For the latter of the two approximations, the corresponding equation and  $R^2$  is depicted in the bottom left corner.

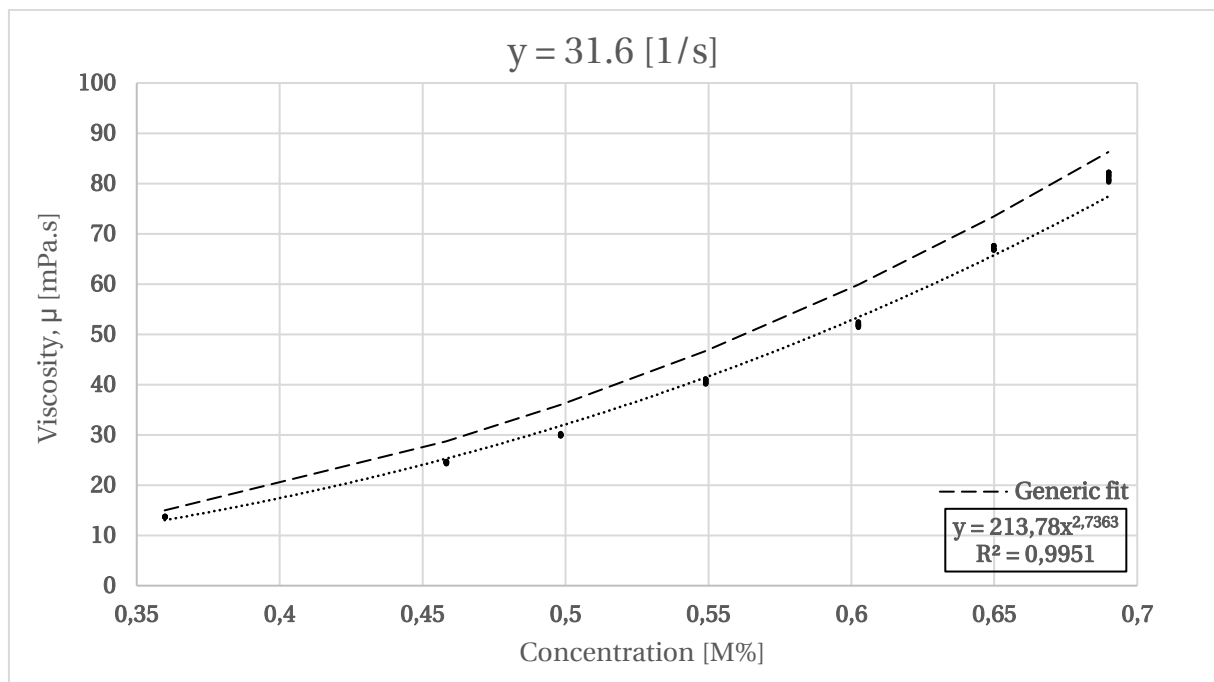


Figure IV-8: Rheological measurements at different concentrations for  $\dot{\gamma} = 31.6 \text{ 1/s}$ , accompanied generic and least square power fit ( $y=Ax^B$ ). For the latter of the two approximations, the corresponding equation and  $R^2$  is depicted in the bottom left corner.

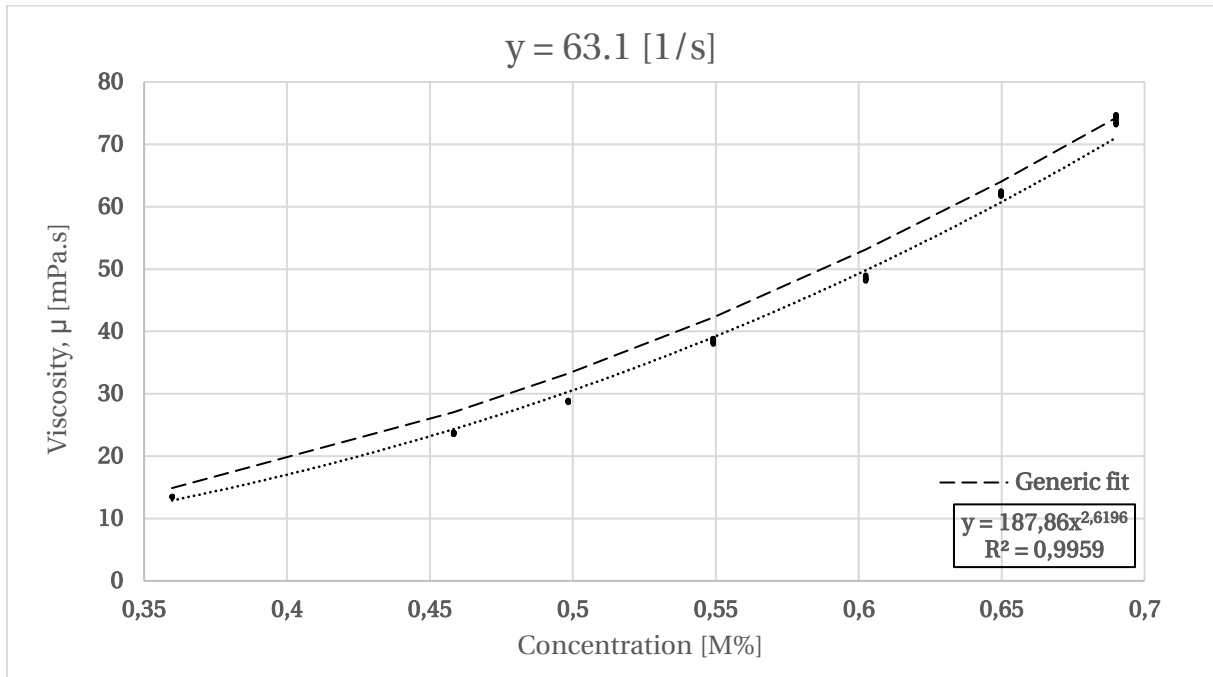


Figure IV-9: Rheological measurements at different concentrations for  $\dot{\gamma} = 63.1 1/s$ , accompanied generic and least square power fit ( $y=Ax^B$ ). For the latter of the two approximations, the corresponding equation and  $R^2$  is depicted in the bottom left corner.

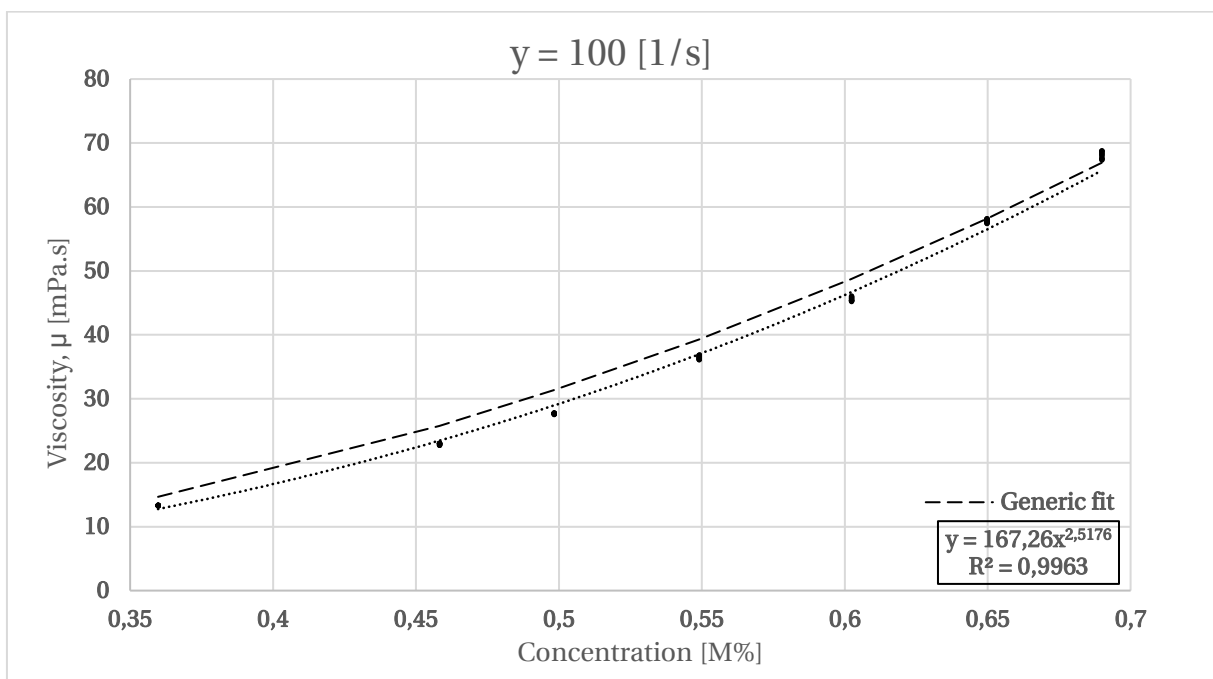


Figure IV-10: Rheological measurements at different concentrations for  $\dot{\gamma} = 100 1/s$ , accompanied generic and least square power fit ( $y=Ax^B$ ). For the latter of the two approximations, the corresponding equation and  $R^2$  is depicted in the bottom left corner.

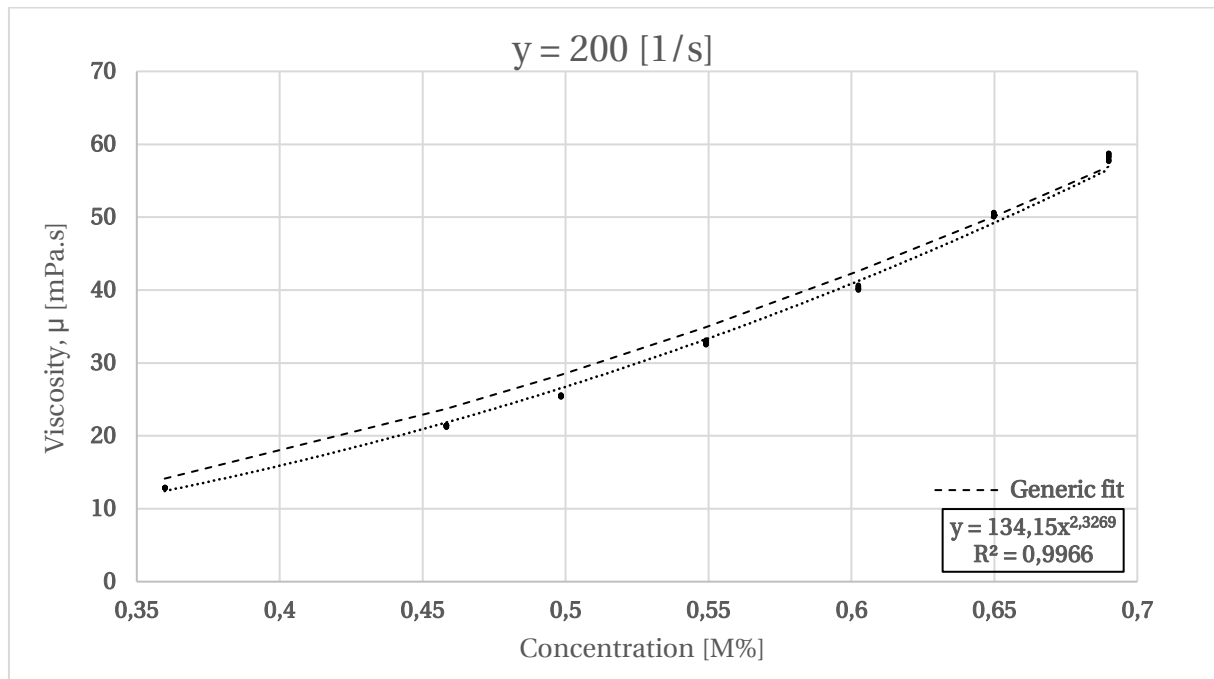


Figure IV-11: Rheological measurements at different concentrations for  $\dot{\gamma} = 200 \text{ 1/s}$ , accompanied generic and least square power fit ( $y=Ax^b$ ). For the latter of the two approximations, the corresponding equation and  $R^2$  is depicted in the bottom left corner.

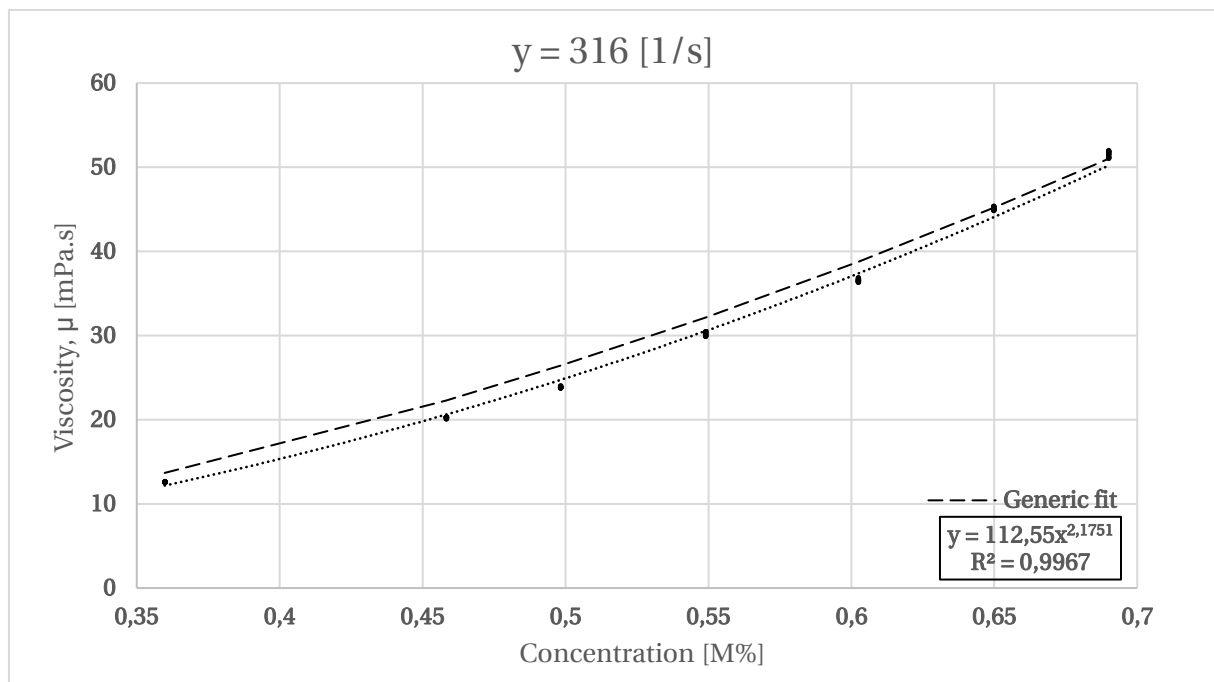


Figure IV-12: Rheological measurements at different concentrations for  $\dot{\gamma} = 316 \text{ 1/s}$ , accompanied generic and least square power fit ( $y=Ax^b$ ). For the latter of the two approximations, the corresponding equation and  $R^2$  is depicted in the bottom left corner.

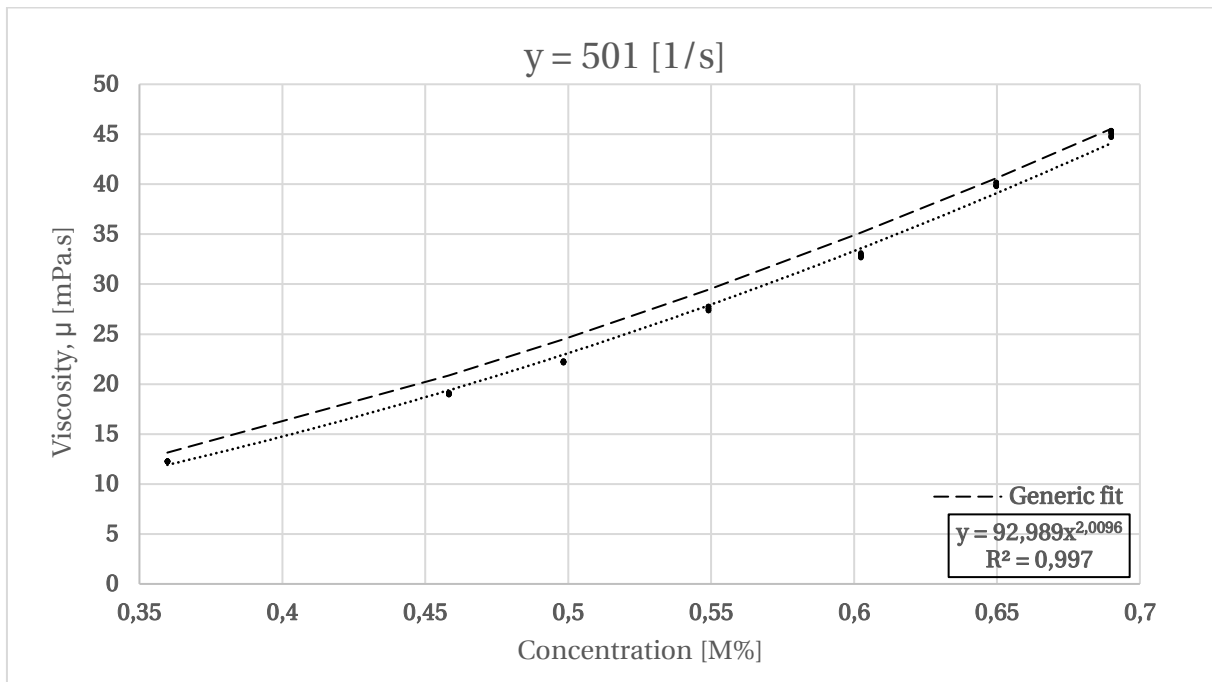


Figure IV-13: Rheological measurements at different concentrations for  $\dot{\gamma} = 501 \text{ 1/s}$ , accompanied generic and least square power fit ( $y=Ax^b$ ). For the latter of the two approximations, the corresponding equation and  $R^2$  is depicted in the bottom left corner.

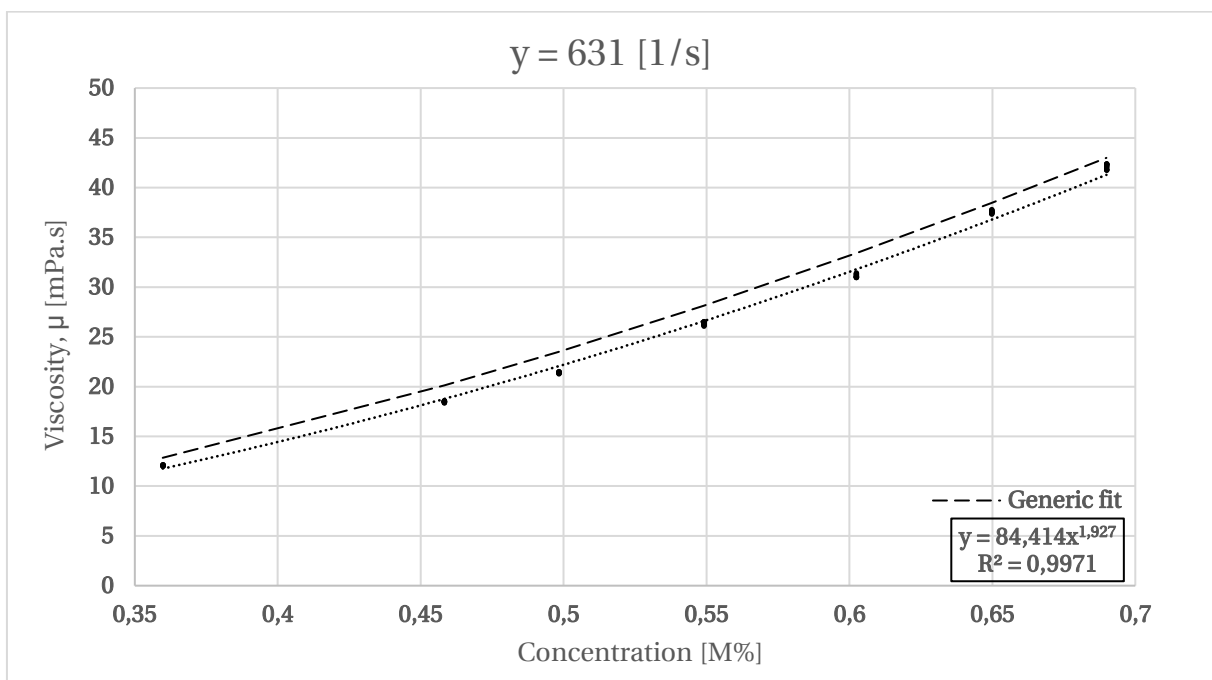


Figure IV-14: Rheological measurements at different concentrations for  $\dot{\gamma} = 631 \text{ 1/s}$ , accompanied generic and least square power fit ( $y=Ax^b$ ). For the latter of the two approximations, the corresponding equation and  $R^2$  is depicted in the bottom left corner.

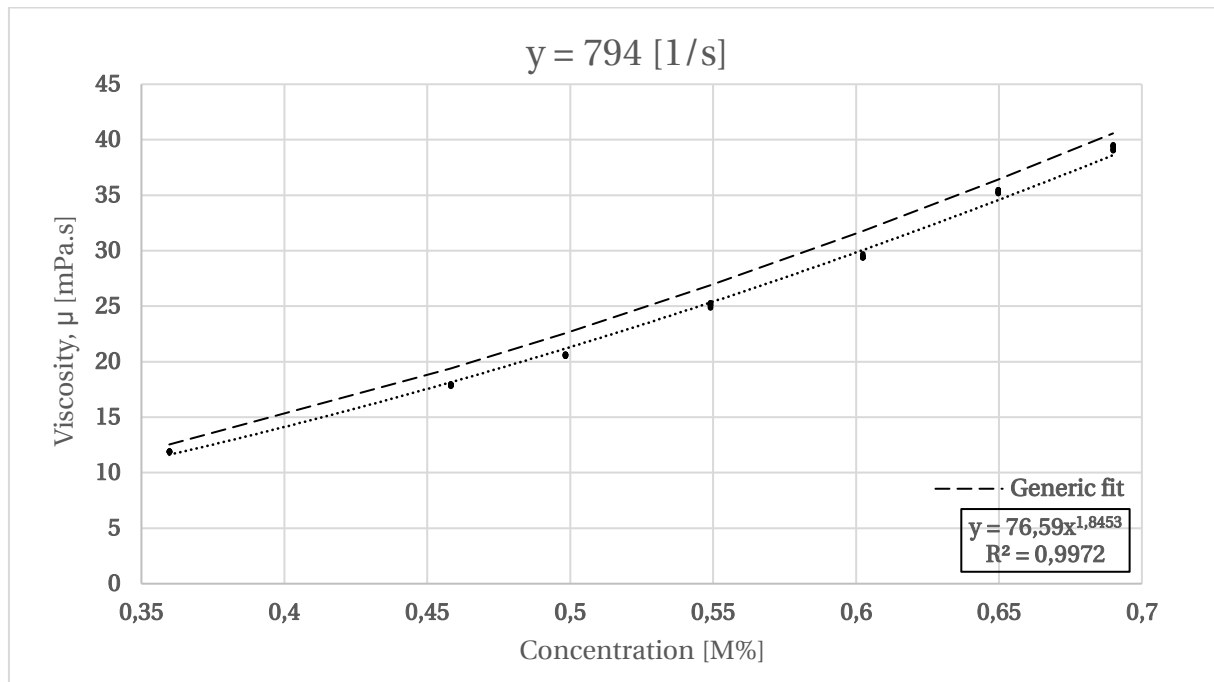


Figure IV-15: Rheological measurements at different concentrations for  $\dot{\gamma} = 794 \text{ 1/s}$ , accompanied generic and least square power fit ( $y=Ax^b$ ). For the latter of the two approximations, the corresponding equation and  $R^2$  is depicted in the bottom left corner.

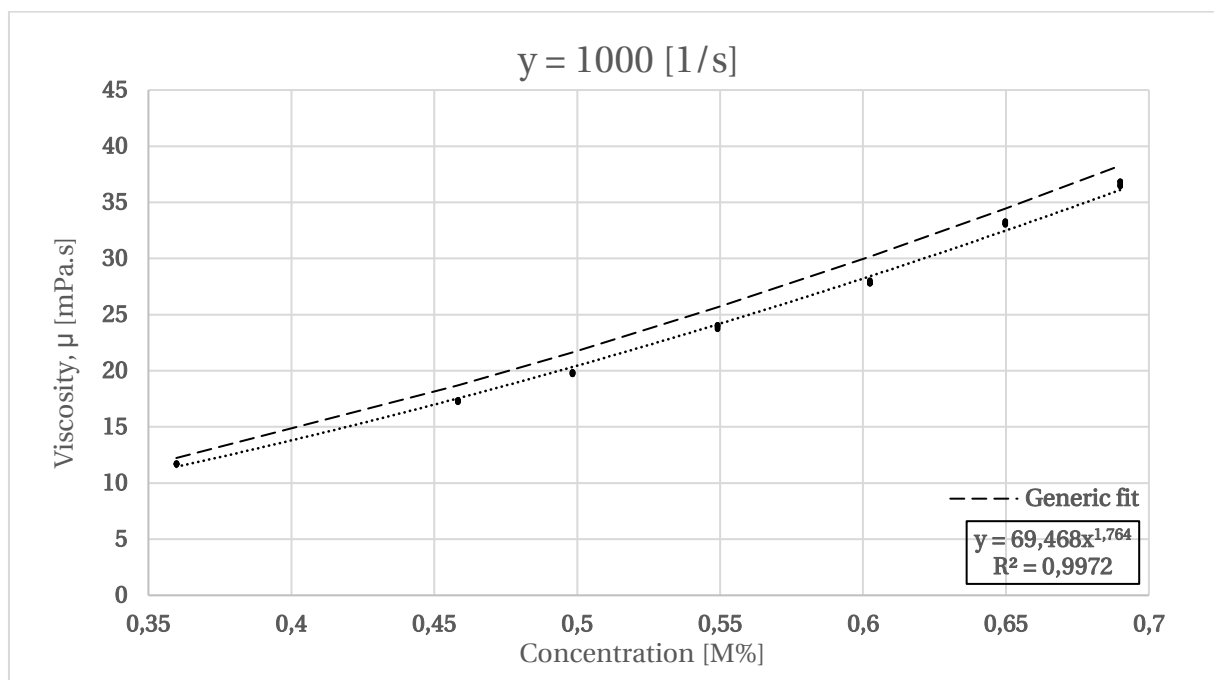


Figure IV-16: Rheological measurements at different concentrations for  $\dot{\gamma} = 1000 \text{ 1/s}$ , accompanied generic and least square power fit ( $y=Ax^b$ ). For the latter of the two approximations, the corresponding equation and  $R^2$  is depicted in the bottom left corner.